CRANFIELD UNIVERSITY

JONATHAN ANING

CRITIQUE OF FOURIER TRANSFORM INFRARED MICROSPECTROSCOPY APPLICATIONS TO PROSTATE PATHOLOGY DIAGNOSIS

CRANFIELD HEALTH

DM THESIS

CRANFIELD UNIVERSITY

CRANFIELD HEALTH

DM THESIS

Academic Year 2009-2010

Mr Jonathan Aning

Critique of Fourier Transform Infrared microspectroscopy applications to prostate pathology diagnosis

Supervisor: Dr. Nick Stone

January 2010

Declaration

I declare that the work in this dissertation is the result of my own work, none of which has been submitted in support of an application for another degree or qualification at any other university, or other institution of learning.

Jonathan Aning January 2010

"Making your mark on the world is hard. If it were easy, everybody would do it. But it's not. It takes patience, it takes commitment, and it comes with plenty of failure along the way. The real test is not whether you avoid this failure, because you won't. It's whether you let it harden or shame you into inaction, or whether you learn from it; whether you choose to persevere."

Barack Obama 2009

I dedicate this thesis to my parents and those who inspire me

Acknowledgements

I would like to thank first and foremost my supervisors Dr Nick Stone and Mr Hugh Gilbert for their patience, guidance and support throughout this project. I would like to express my particular appreciation for Nick, both for his expertise in vibrational spectroscopy and his role in developing my scientific potential. Professor Hugh Barr, I am grateful for your endless enthusiasm, ceaseless commitment to the biophotonics team and unfaltering belief in my abilities. I also sincerely thank Mr Alastair Ritchie, the complete urologist and my scientific role model, whose brief but observant and constructive comments always focused my mind.

This project would not have been possible without many people generously giving their time, many thanks to: the patients for contributing specimens, Joanne Motte for preparing my specimens and Dr Jeremy Uff for providing the histological diagnoses, Mr Aloy Okeke who with Mr Hugh Gilbert facilitated specimen collection and Dr Martin Isabelle for sharing thoughts on spectroscopy and strong coffee during the long days in the laboratory. I am grateful for the friendship and support of all the members of the biophotonics research group during my time in Gloucester. I thank COBALT and the Isle of Man Anti Cancer Association for contributing financial support to the project.

Finally I would like to thank my friends and family who have endured both my emotions and my focus. I am and always will be indebted to my parents for my education and their support throughout my life. I thank my sister Rebecca and Joanna for their unconditional love throughout the hardest times of my academic journey.

Abstract

Prostate cancer is a biologically heterogenous disease with considerable variation in clinical aggressiveness. Gleason grade, the universally accepted method for classification of prostate cancer, is subjective and gives limited predictive information regarding prostate cancer progression. There is a clinical need for an objective, reliable tool to help pathologists improve current prostate tissue analysis methods and better assess the malignant potential of prostate tumours. Fourier Transform Infrared (FTIR) microspectroscopy is a powerful bioanalytical technique that uses infrared light to interrogate biological tissue. The studies detailed in this thesis examine the ability of FTIR combined with multivariate analysis to discriminate between benign, premalignant and malignant prostate pathology in snap frozen, paraffinated and deparaffinated tissue.

Prostate tissue was collected during and after urological procedures performed between 2005 and 2008. The tissue was analysed utilising a bench top FTIR system in point and image mapping modes. The histology under interrogation was identified by a uro-pathologist. Multivariate analysis was applied to the spectral dataset obtained. FTIR performance was evaluated.

FTIR was able to reproducibly discriminate between benign and malignant prostate tissue in a pilot study. Cross validated diagnostic algorithms, constructed from the spectral dataset in this experiment, achieved sensitivities and specificities of 95% and 89% respectively.

FTIR analysis of transverse paraffinated and deparaffinated radical prostatectomy sections achieved good differentiation of the benign, premalignant and malignant

pathology groups. However the performance of diagnostic algorithms constructed from this dataset under cross validation was poor.

The work in this thesis illustrates the potential of FTIR to provide an objective method to assist the pathologist in the assessment of prostate samples. The limitations of the technique and directions for future work are presented.

Contents

Chapter Four: Discussion 158

Figures

Chapter One: Introduction

Chapter Two: Materials and Methods

Chapter Three: Results

Chapter Four: Discussion

Tables

Chapter One: Introduction

Chapter Two: Materials and Methods

Chapter Three: Results

Chapter Four: Discussion

" I had prostate cancer. It was rather painful and, in many ways, life changing "

Sir Roger Moore 1927-

1 Introduction

Prostate cancer is the most common cancer in men in the United Kingdom and the second most common male cancer in the world[1]. Despite a dramatic rise in prostate cancer incidence over the last decade, its aetiology and natural history remain poorly understood. Currently, histopathological analysis of prostate tissue obtained at transrectal ultrasound (TRUS) guided biopsy is the gold standard for diagnosis of prostate cancer and contributes to treatment strategy. Pathological interpretation of prostate specimens is time consuming and subjective. Although its current place as a standard is undisputed, it has an inherent weakness: - inter observer variation, which has been demonstrated repeatedly[2,3,4,5]. There is a need for alternative innovations to improve the cost, speed and accuracy of prostate cancer diagnosis. Progress in this field would improve patient management in addition to gaining a better understanding of the disease.

Fourier Transform Infrared Spectroscopy (FTIR) is an optical technology capable of interrogating materials and objectively determining biochemical composition. FTIR is in widespread use in industry however its' potential biomedical applications have only recently been evaluated. The studies which are detailed in this thesis investigate the ability of FTIR to discriminate between common prostate pathologies and identify where FTIR may create a niche in clinical practice.

This chapter describes the normal anatomy and function of the prostate in addition to common pathological variants. The pathway to a prostate cancer diagnosis is outlined in addition to current management controversies. To conclude the literature regarding the biomedical applications of FTIR is reviewed and the aims and objectives of this thesis are stated.

1.1 The Prostate Gland

1.1.1 The Anatomy of the Normal Prostate

The prostate gland was first described anatomically in 1538 by Vesalius and was named "the prostate" in 1611 by Casper Bartholin[6]. The prostate is an exocrine gland which forms part of the male reproductive system. The gland secretes an alkaline fluid that makes up a significant component of seminal fluid. The gland is inversely conical in shape and situated in the true pelvis (see Figure 1.1). The base of the prostate is in continuity with the bladder neck, the gland surrounds the first part of the urethra and the apex opposes the urogenital diaphragm. The anterior and posterior relations of the gland are the symphysis pubis and the rectum respectively[7]. The seminal vesicles which also contribute fluid towards the ejaculate are attached to the base of the prostate. The vesicles are separated from the rectum by the rectovesical pouch. The glands of the seminal vesicles merge and join the ductus deferens to form the ejaculatory duct[7].

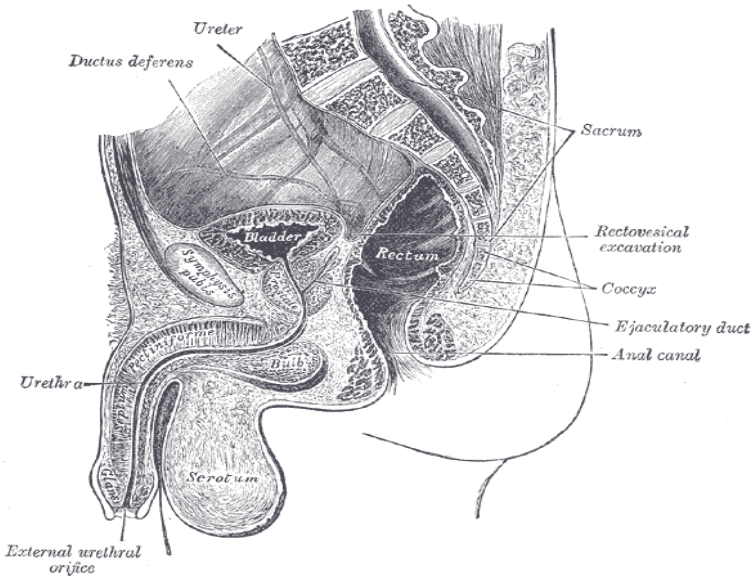

Figure 1.1 Median sagittal section of the male pelvis[8]

The arterial supply to the prostate is derived from the internal iliac artery entering through neurovascular pedicles on the superolateral aspect of the gland bilaterally.

Venous drainage is into the prostatic plexus, in the pericapsular region, and subsequently into the internal iliac veins[9].

The lymphatic drainage of the prostate is primarily into the internal iliac nodes. The external and sacral nodes also receive drainage. These nodes are usually the first site of extraprostatic lymphatic spread from prostate cancer.

The prostate is supplied by a rich neural plexus. The acini receive parasympathetic (cholinergic) innervation from the pelvic splanchnic nerves. The stroma which contract to empty the gland during ejaculation receive sympathetic innervation (adrenergic) from the inferior hypogastric plexus. The nerves penetrate the gland and may provide a route for intra or extraprostatic cancer spread. One theory is that this spread occurs because the nerves offer the path of least resistance. When seen as a pathological entity it is termed perineural invasion[10].

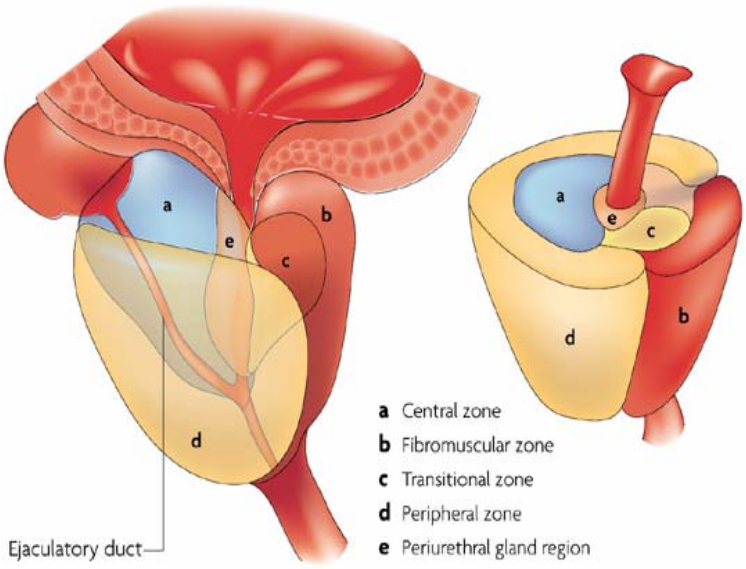

Figure 1.2 Sagittal and transverse prostate views illustrating McNeal's zonal anatomy[11]

The currently accepted anatomy of the prostate gland was first described by McNeal in 1968. In his model, illustrated in figure 1.2, the prostate is divided into three main glandular zones (central, transitional, peripheral) orientated around the prostatic urethra. The key reference point is the 35^{o} angle at the midpoint of the prostatic urethra which

separates the prostate into proximal and distal segments. The bulge of the verumontanum located on the posterior wall of the distal segment, defines the point of separation. The ejaculatory ducts and greater than 90% of the glands of the prostate empty into the distal urethra[12,13,14] .

Each zone has a different glandular organisation and proclivity for disease:-

The central zone (CZ) encircles the ejaculatory ducts and is cone shaped, extending from the prostate base to the verumontanum. The CZ accounts for approximately 25% of normal prostatic volume. Approximately 10% of prostate cancers arise in the CZ[14].

The transitional zone (TZ) forms two pear shaped lobes on either side of the proximal urethra and accounts for 5% of normal prostate volume. The glands in the transitional zone are the primary site of benign prostatic hyperplasia (BPH). Approximately 15-20% of prostate cancers arise in the TZ[14].

The peripheral zone (PZ) surrounds the central and transitional zones in the basal portion of the gland and the distal prostatic urethra. The PZ constitutes the majority of normal prostate volume (70%). 70-75% of carcinomas arise in the PZ and it is a common site of prostatic intraepithelial neoplasia (PIN), inflammation, atrophy and occasionally hyperplasia[14].

The periurethral zone is composed of small glands around the proximal urethra lying within the confines of the preprostatic sphincter[14].

Important non glandular elements complete the model. Fibromuscular stroma, composed of compact collagen and smooth muscle bundles, surrounds the prostate and is sometimes described as a ‘capsule’. This is not a true capsule but is clinically important in defining and evaluating extraprostatic extension of carcinoma. The preprostatic sphincter forms a sleeve of smooth muscle fibres around the proximal urethra. The sphincter prevents retrograde flow of seminal fluid when it contracts during ejaculation. Striated muscle fibres are present inferior to the prostate apex. These are continuous with the external urethral sphincter and are responsible for urinary continence[14].

1.1.2 Relevance of Prostate Anatomy in Current Clinical Practice

The investigation and management of disorders of the prostate requires sound knowledge and application of anatomy. For example, the verumontanum is a key landmark for endoscopic procedures of the lower urinary tract. When performing endoscopic surgery to relieve bladder outflow obstruction (transurethral resection of the prostate (TURP) or bladder neck incision (BNI)), resection is not pursued distal to the verumontanum to avoid damage to the external urethral sphincter and preserve continence after surgery (Illustrated in figure 1.3). Pelvic lymph nodes (usually the obturator nodes) may be sampled during radical prostatectomy (surgery to remove the prostate in patients with prostate cancer) this may provide useful tumour staging information. The obturator nodes are usually the first to be involved in metastatic spread.

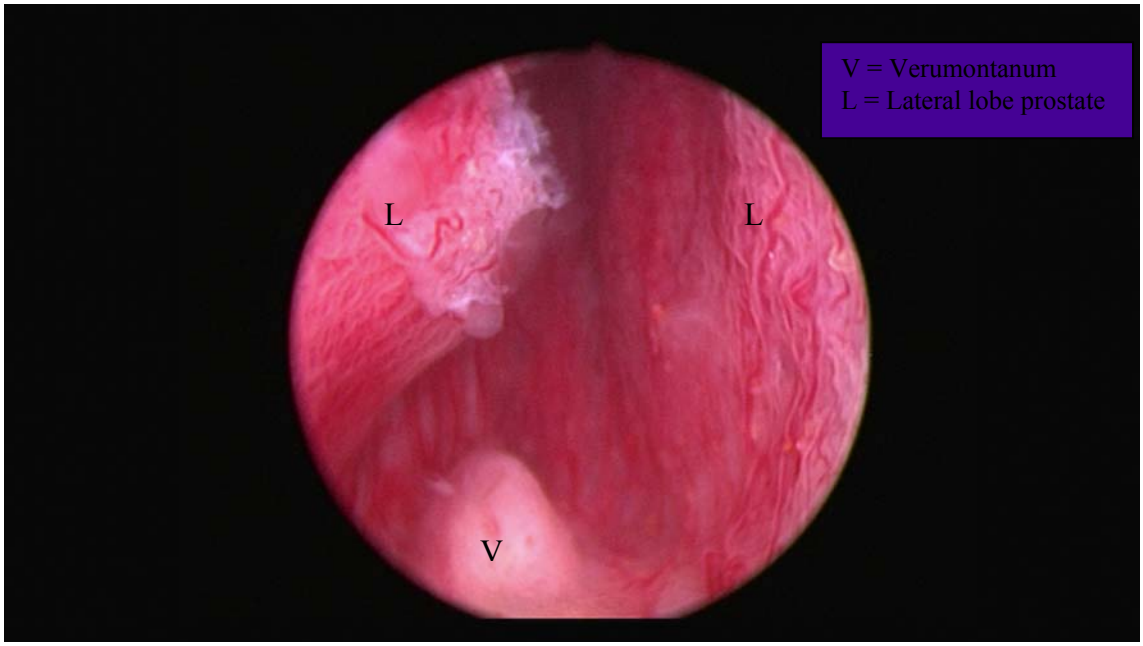

Figure 1.3 The internal anatomy of the prostate viewed at TURP

The regions of the prostate sampled by core biopsy and transurethral resection of the prostate are likely to be quite different. Transrectal ultrasound guided core biopsies will mostly consist of tissue from the peripheral zone, seldom the central or transitional zones. TURP specimens are more likely to consist of tissue from the urethra, bladder neck, periurethral zone, transitional zone and anterior fibromuscular stroma[14]. Well

differentiated carcinoma found incidentally in TURP specimens is more likely to represent carcinoma which has arisen in the transitional zone. Poorly differentiated carcinoma in TURP specimens may represent tumour originating in the peripheral zone that invades the transitional zone[15]. In this thesis FTIR has been used to interrogate core biopsy tissue, TURP specimens and prostate sections in their entirety to establish spectroscopic parameters for all prostate tissue.

1.1.3 The Histology of the Normal Prostate

The prostate gland has a tubulo-alveolar organisation; the main zones (CZ, TZ, and PZ) all contain ducts and glands. The typical gland is lined by a basement membrane (BM), which is composed of type IV collagen, fibronectin, laminin, heparin sulphate and entactin[16]. The BM is separated from the secretory epithelial cells by a layer of basal cells lying parallel to the BM. These basal cells have little discernable cytoplasm and darkly stained nuclei[12]. Although basal cell function is poorly understood, histologically basal cells are important as their presence differentiates between benign disease and adenocarcinoma when they are not present. The epithelium consists of columnar shaped cells that secrete proteins such as prostate specific antigen (PSA) and prostatic acid phosphatase (PAP) into the seminal plasma[17]. The glands secrete mucins and produce lipofuscin[18]. Biochemical products including citric acid and acid phosphatase are also secreted[19]. The glands empty into prostatic ducts and in turn the prostatic urethra. Ducts are lined by transitional cell epithelium just before they enter the urethra.

1.1.4 Variation in Zonal Histology and Biochemistry

Variation in normal histology exists between zones. The glands of the peripheral and transitional zones have rounded contours. Central zone glands are larger, more complex and often located in lobules around central ducts, ridges and arches. Central zone architecture may be mistaken for hyperplasia or prostatic intraepithelial neoplasia.

Peripheral zone stroma is loosely woven with randomly arranged smooth muscle. Transitional zone stroma contains more compact, interlacing smooth muscle bundles. The stroma in the central zone is less abundant but contains compact smooth muscle fibres.

Biochemically, the central zone is the only zone which produces pepsinogen II and tissue plasminogen activator[20,21]. Lectin binding patterns have been found to reflect selective binding to specific cellular glycoconjugates which differ between the central and peripheral zone[22].

1.2 Pathology of the Prostate

The focus of pathological analysis of prostate tissue in routine clinical practice is primarily to identify whether and to what extent prostate cancer is present. The lay term cancer is frequently used to equate with malignant neoplasm. The term neoplasm (also known as tumour) is defined as an abnormal, poorly controlled proliferation of cells. A benign neoplasm remains localised in its tissue of origin with no propensity to spread. A malignant tumour comprises cells with the ability to invade adjacent tissues and spread to distant sites in the body, a process known as metastasis. Knowledge of benign pathologies of the prostate in addition to possible premalignant lesions is essential to enable differentiation between benign and malignant pathologies. This section will concentrate on common pathologies of the prostate that will be interrogated by FTIR in this thesis.

1.2.1 Benign Prostatic Hyperplasia

Benign prostatic hyperplasia (BPH) is common. The term is often used in relation to the symptom complex that is associated with it. Clinically, BPH is characterised by voiding and storage symptoms of variable severity[23]. Progression of the disease may lead to recurrent urinary tract infections, bladder calculi or urinary retention. BPH is however a pathological diagnosis and therefore can only accurately be made after prostate tissue analysis.

Histologically, BPH represents specific deviations in architecture rather than simply an increase in cell population. Macroscopically the identification of hyperplastic glandular acini separated by fibrous stroma in a nodular pattern confirms the pathological diagnosis. In the transitional zone medium and large BPH glands may display architectural complexity and papillary infolding. Some nodules are cystically dilated and may contain a milky fluid. Other nodules contain calcified concretion '*corpora amylacea*' – well circumscribed round structures with concentric lamellar rings.

Periurethral nodules have an abundance of pale ground material and a few collagen fibres. Microscopically the acini are tightly packed, lined by tall columnar epithelial cells with small basal nuclei[24], as seen in Figure 1.4.

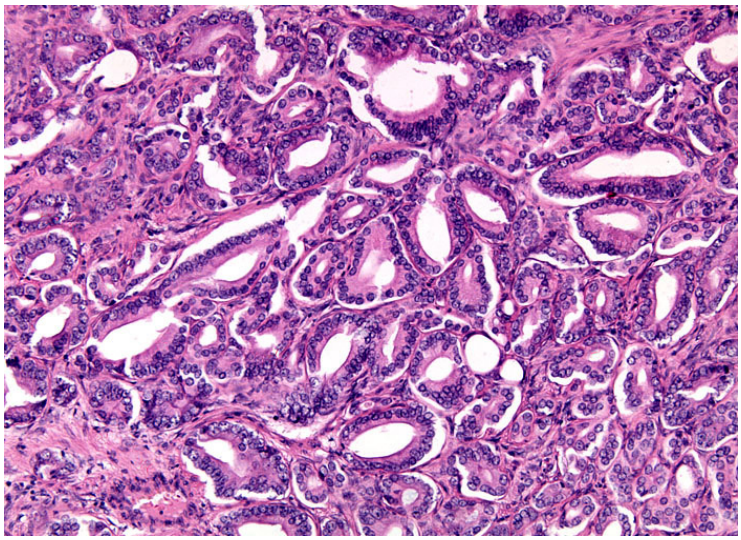

Figure 1.4 Photomicrograph of Benign Prostatic Hyperplasia[25]

The epithelium usually has a distinct double layer of secretory and basal cells. BPH cells are often thrown into folds however the nuclei remain aligned in a single row, which differs from PIN where the nuclei are irregularly arranged. The cytoplasm in BPH is abundant and clear.

BPH is intimately related to ageing[26], its presence in autopsy studies rises from approximately 20% in men aged 41-50, to 50% in men aged 51-60 and to over 90% in men older than 80[27]. Although BPH is not life threatening, the effect of the lower urinary tract symptoms resulting from bladder outflow obstruction on patient quality of life can be significant[28]. Lifestyle modifications and medication[29] form the mainstay of conservative treatments for BPH. Surgical treatments range from insertion of prostatic stents which maintain prostatic urethral patency to enucleation of prostate tissue by either open or endoscopic techniques. TURP is a commonly performed endoscopic operation to relive bladder outflow obstruction in men[30], and is one of the sources of prostate tissue obtained in this project.

1.2.2 Prostatitis

Inflammation of the prostate is termed prostatitis. The condition usually follows infection of the bladder or urethra, is benign, may be acute or chronic and have either definitive (for example: surgical instrumentation) or idiopathic precipitants. Acute bacterial prostatitis is the most common urologic diagnosis in men younger than 50 years old[31]. Common causative organisms include E. Coli, Proteus and Chlamydia. Clinically patients may report a number of symptoms: fever, urinary frequency and urgency, dysuria, haematospermia and pain in the lower back, rectum and perineum. Acute bacterial prostatitis may culminate in abscess formation and the condition requires prompt medical treatment. The diagnosis of acute prostatitis is made from assessment of the clinical presentation, positive urine or blood cultures and the examination finding of a tender prostate at digital rectal examination. Chronic prostatitis may be asymptomatic or present with chronic pelvic pain. Men with chronic prostatitis may present solely with an elevated PSA and an abnormal digital rectal examination. In these men prostatitis may be diagnosed histologically from a prostate biopsy whilst being investigated for a suspected prostate cancer.

The peripheral zone of the prostate is reported to be the most susceptible to prostatitis. The transitional zone is less predisposed but may display features of secondary inflammation in the presence of prostatic hyperplasia. The central zone is considered resistant to inflammation. Microscopically in acute prostatitis sheets of neutrophils are visualised in and around prostatic ducts and acini, in addition to desquamated epithelium and debris (see Figure 1.5). The stroma is oedematous, haemorrhagic and microabscesses may be observed. Granulomas, lymphocytes, plasma cells and macrophages may also be found in the prostate stroma in the presence of chronic disease[32].

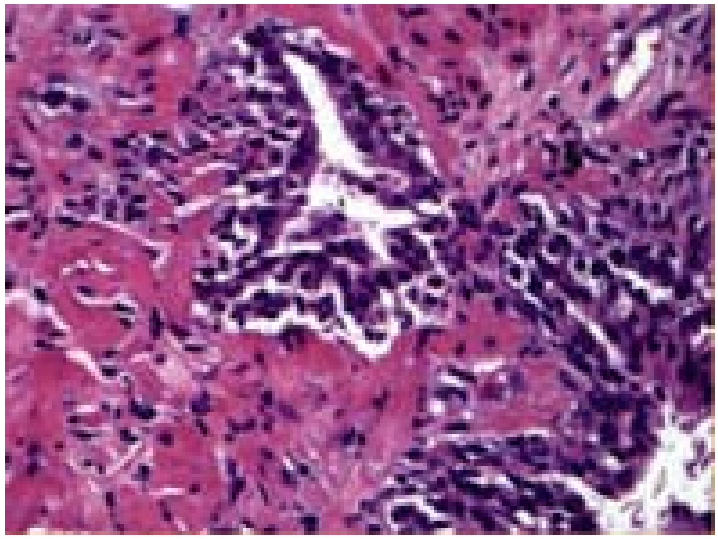

Figure 1.5 Photomicrograph of acute bacterial prostatitis

1.2.3 Atrophy of the Prostate

Atrophy is a benign process generally associated with ageing but may occur as an end result of inflammation. It is characterised by shrinkage of distal ductules, glands and stroma. Atrophy affects predominantly the peripheral zone. Clinically atrophy may be seen as a hyperechoic lesion on transrectal ultrasound which may be suspicious for carcinoma. It is important to be aware of atrophy as an entity because a lobular glandular organisation may not be apparent causing it to be mistaken for carcinoma of the prostate[32].

1.2.4 Prostatic Intraepithelial Neoplasia

Prostatic intraepithelial neoplasia (PIN) may be a precursor of invasive cancer[33,34,35] . The term was first adopted by Bostwick and Brawer to describe all forms of atypical and malignant lesions of epithelial cells confined to the lumens of ducts and acini[36]. PIN is characterised by an intraluminal proliferation of secretory epithelium that demonstrates a spectrum of cytological changes. High grade PIN may strongly resemble carcinoma. Although initially described in three grades, the majority of pathologists now only report high grade PIN due to difficulties in consistency distinguishing the features of early PIN and the clinical significance of high grade PIN due to its strong association with invasive carcinoma[37]. PIN has been demonstrated to be more prevalent

with age[38,39], and its presence is more common in prostatectomy specimens with carcinoma present[36,39,40] . In core biopsies the incidence of isolated high grade PIN (without cancer) has been reported to be between 0.7 and 16.5% (mean 4%)[41]. PIN may predate the diagnosis of cancer by five years[38,39]. The identification of isolated high grade PIN within a specimen clinically may result in a higher index of suspicion for the presence of malignancy.

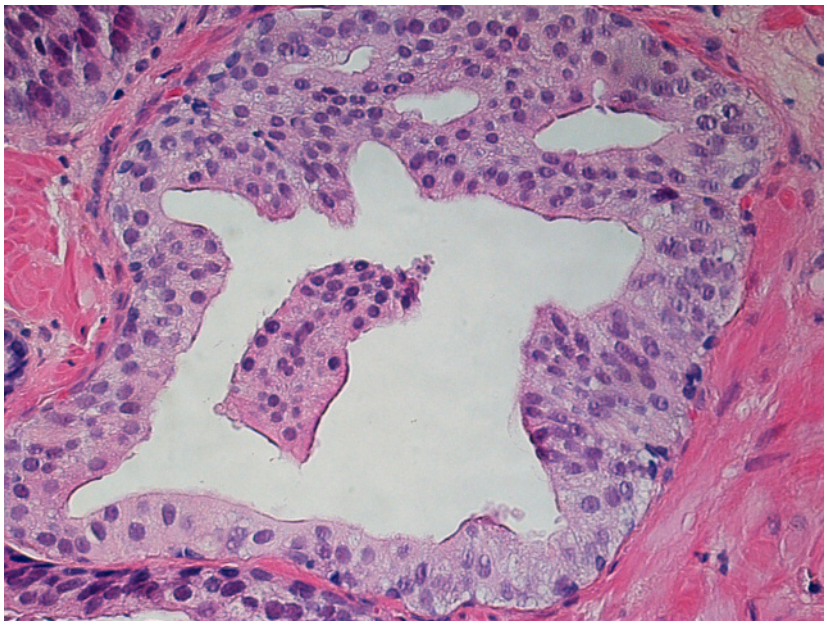

Figure 1.6 Photomicrograph of High Grade Prostatic Intraepithelial Neoplasia[42]

Microscopic features of high grade PIN are large prominent nucleoli, hyperchromasia and cytoplasmic eosinophilia, as seen in Figure 1.6. PIN glands stand out from normal ones because of their basophilic appearance. There may be partial loss of the basal cell layer. Four major architectural patterns have been described: tufted, micropapillary, cribriform and flat. PIN shares many similarities with prostate adenocarcinoma: it is predominantly identified in the peripheral zone, often adjacent to carcinoma[43,44,45] and it demonstrates similar patterns of spread. The first pattern is the replacement of normal luminal secretory epithelium by neoplastic cells. The second is pagetoid spread along ducts, characterised by invagination of neoplastic cells between the basal layer and the

columnar secretory cell layer. The third pattern is direct microinvasion through the ductal or acinar wall, disrupting the basal cell layer and basement membrane[36,46,47] .

1.2.5 Atypical Small Acinar Proliferation

Atypical small acinar proliferation (ASAP) describes a small focus of prostate glands that is suspicious but not diagnostic of Adenocarcinoma. ASAP is present in 2% of prostate core biopsies[48]. Microscopically ASAP has small acini lined with cytologically abnormal epithelial cells. The columnar cells have prominent nuclei containing nucleoli; the basal layer may be absent but the basement membrane is intact. Difficulties in diagnosing ASAP are acknowledged as it may only be present in small foci. Isolated ASAP in a biopsy raises the suspicion that cancer focus may have been missed. Studies have demonstrated cancer presence at subsequent biopsy in over 40% of cases[49].

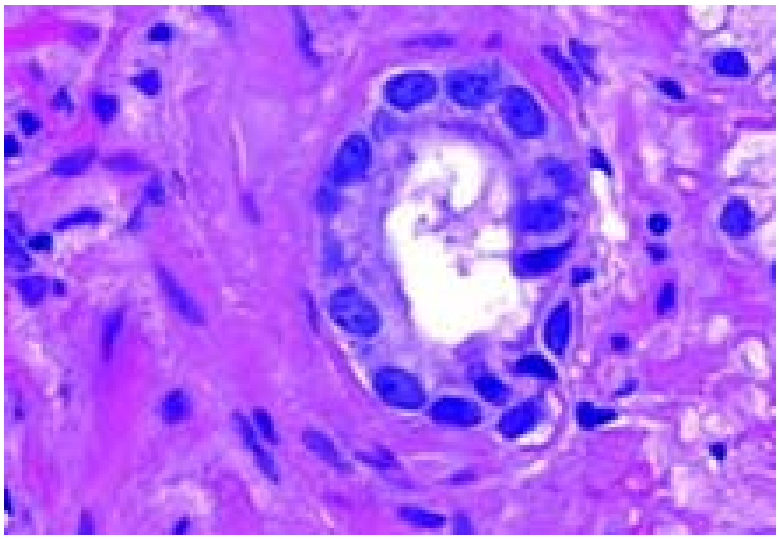

Figure 1.7 Photomicrograph of atypical small acinar proliferation

1.2.6 Adenocarcinoma of the Prostate

Prostate adenocarcinoma (CaP) is an invasive malignant epithelial tumour consisting of secretory cells. The epidemiology and relevant clinical aspects of the disease will be outlined later in this thesis. Macroscopically on section grossly evident tumours appear firm and solid. Tumours usually extend microscopically beyond their macroscopic border. Subtle tumours may be recognised by structural asymmetry expanding and

obscuring boundaries of prostate zones. Anterior and apical tumours may be difficult to identify because of mixed stromal and nodular hyperplasia[50].

Microscopically, adenocarcinomas of the prostate range from well differentiated (difficult to distinguish from benign prostate glands) to poorly differentiated tumours (which may be devoid of features of prostatic origin). Common to virtually all cancers is the absence of a basal cell layer. Identification of basal cell absence may be difficult as certain cancers will have cells that mimic basal cells, therefore the use of special stains may be necessary to determine basal cell presence.

When studying prostate tissue to determine whether cancer is present histopathologists focus on gland architectural, nuclear, cytoplasmic and intraluminal features in addition to searching for malignant specific features. Adenocarcinoma of the prostate is not recognised to elicit a stromal response therefore the stroma is not considered useful in prostate cancer diagnosis.

Architectural features: Benign prostatic glands generally maintain a degree of order and are evenly dispersed. In contrast adenocarcinoma glands grow in a haphazard fashion. Features of infiltration include glands irregularly separated from each other by bundles of smooth muscle and the presence of small atypical glands situated between larger benign glands. More obvious features of malignancy are evident when there is loss of gland differentiation with the formation of cribriform structures, fused glands and poorly formed glands. Undifferentiated tumours may be composed of solid sheets, cords of cells or isolated individual cells. These above features are key components of the Gleason grading system (described in the next section).

Nuclear features: The extent of nuclear atypia typically correlates with the architectural degree of differentiation. Nuclear enlargement with prominent nucleoli is a common feature in cancer cells but not diagnostic in isolation. In high grade cancer nuclear pleomorphism and mitotic figures may be seen.

Cytoplasmic features: Prostate cancer glands tend to have a sharp luminal border in contrast with benign glands. Although cytoplasmic features of low grade prostate cancer glands are often not distinctive; tumour glands may have amphophilic cytoplasm. The

cytoplasm in all grades of prostate cancer generally lacks lipofuscin which is present in some benign prostate glands[51].

Intraluminal features: Crystalloids, eosinophilic crystal like structures may be seen frequently in low grade prostate cancer[52]. These structures may also be seen in benign glands but less frequently. Intraluminal pink acellular dense secretions or blue tinged mucinous secretions are findings seen preferentially in cancer[53]. In contrast corpora amylacea are common in benign glands and rarely seen in prostate cancer[52].

Malignant specific features: Perineural invasion, mucinous fibroplasia and glomerulations have not been described in benign tissue and are diagnostic of prostate cancer. Perineural invasion describes the presence of cancer cells circumferentially within the perineural space. Mucinous fibroplasia describes loose fibrous tissue with an ingrowth of fibroblasts. Glomerulations refers to gland with a cribriform pattern that is not transluminal. The cribriform structure may attach to only one edge of the gland thus resembling a glomerulus.

1.2.7 The Gleason Grading System

The Gleason grading system, named after Donald F Gleason, is the most widely used histopathological grading system for adenocarcinoma of the prostate. It was recommended by the World Health Organisation at a consensus conference in 1993[54]. The Gleason grading system is based on glandular architecture; nuclear atypia is not evaluated[55]. Although other systems adopted nuclear atypia in their grading systems there has been no evidence that this added to the prognostic information obtained from glandular morphology[56]. The Gleason grading system describes five histological patterns or grades ranging from well differentiated to poorly differentiated (illustrated in figures 1.8-1.12, table 1.1). Prostate cancer is heterogeneous so more than one pattern may exist within a specimen. The most prevalent pattern and the second most prevalent pattern are combined to obtain a Gleason score between 2 and 10. Although the original classification did not account for patterns occupying less than 5% of the tumour or tertiary patterns, it is now recommended that the worst grade present should also be reported irrespective of its percentage present in radical prostatectomy specimens, because its presence is associated with a poorer prognosis[57]. In radical prostatectomy

specimens a higher Gleason pattern is reported as a tertiary grade if it occupies <5% of the tumour. In core biopsies the highest Gleason pattern is incorporated in the Gleason score irrespective of its percentage (higher Gleason grade is not applicable to core biopsies under current recommendations)[58]. Crush artefacts and evidence of hormone and radiation treatments within samples should not be Gleason graded.

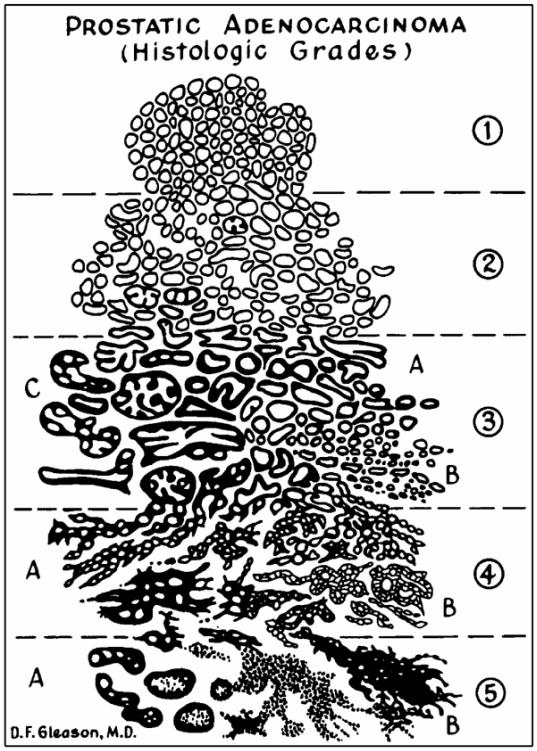

Figure 1.8 Original schematic of the Gleason system [55]

Gleason Grade	Histological Criteria	Differentiation
1	Single, separate, uniform glands closely packed, with definite edge	Well differentiated
2	Single, separate uniform glands loosely packed, with irregular edge	
3A	Single, separate uniform glands, scattered	
3B	Single, separate, very small glands, scattered	
3C	Papillary/cribriform masses, smoothly circumscribed	
4A	Fused glands, raggedly infiltrating	
4B	Same, with large pale cells ("hypernephroid")	
5A	Almost solid, rounded masses, necrosis ("comedocarcinoma")	
5B	Anaplastic, raggedly infiltrating	Poorly differentiated

Table 1.1 The histological criteria of Gleason 1-5 in the original wording[55]

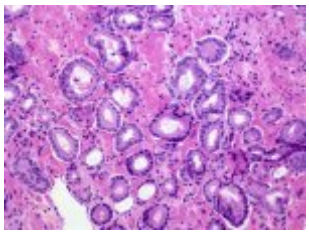

Figure 1.9 Photomicrograph of Gleason pattern 2

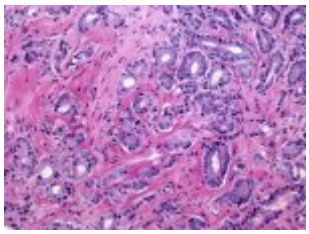

Figure 1.10 Photomicrograph of Gleason pattern 3

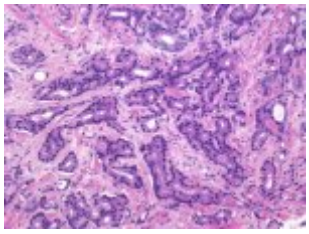

Figure 1.11 Photomicrograph of Gleason pattern 4

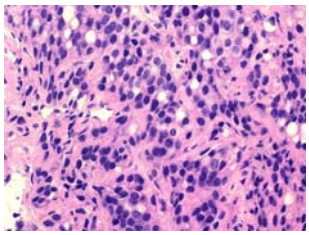

Figure 1.12 Photomicrograph of Gleason pattern 5

1.2.8 Current Additional Cancer Molecular Profiling Techniques

Immunohistochemistry currently plays a significant role in determining the presence of prostate cancer in samples which are difficult to classify; most commonly prostatic

biopsies. High molecular weight basal cell-specific cytokeratin, preferentially stains basal cells, confirmation of the presence of basal cells presence or absence is useful in the diagnosis of small acinar carcinoma[59]. Prostate specific markers such as PSA and PAP have limited role in identifying prostate tumours because antibodies of one or both are acknowledged to be present in both primary and secondary lesions, however benign glands may also be positive for these markers[59]. Neuroendocrine markers when used in well prepared prostate tissue are focally expressed in many adenocarcinomas although their role in carcinoma is unknown. There are a plethora of papers on genetic alterations present in prostate cancer: some appear to be random while others seem to be consistently present. Examples of markers which are being investigated include the proliferation markers: Ki-67, MIB-1 and PCNA[60,61]. However the role of all these markers as providers of predictive or prognostic information has been limited by the heterogeneity of prostate tissue and conflicting results.

DNA micro array technology has been used to quantitatively elucidate genes expressed by prostate cancer cells. The role of these genes in carcinogenesis can be further explored using micro array technology in combination with more complex statistical methods. The aim is to identify genes which could act as biomarkers for prostate cancer. However as one recently attempted meta-analysis of several microarray experiments has shown the comparison of genes from cells obtained from different laboratories is difficult because there are differences in preparation and experimental conditions[62]. Micro array technology has recently been used in combination with FTIR; this is discussed later in section 1.6.7.

1.2.9 Limitations of Conventional Histopathology

Prostate cancer diagnosis is dependent on obtaining prostate tissue specimens with the disease present. However because prostate cancers are often multifocal and heterogeneous in pathology, even if prostate biopsy targeting protocols are adhered to, negative biopsies do not exclude the possibility of prostate cancer. Similarly, positive biopsies may not contain or reflect the degree and severity of prostate cancer present within the prostate.

Pathology is the gold standard for prostate cancer diagnosis. Prostate core biopsies may contain limited carcinoma within the sample and cancer diagnoses can then be missed on account of human error. Several studies have demonstrated that when prostate cancer is present there is inter-observer variation in applying Gleason grade[3,4,5,6,63]. Uro-pathologists achieve the best reproducibility in their assessment of Gleason grade (kappa 0.61-0.80). General pathologists have moderate inter-observer agreement (kappa 0.41-0.60). These studies illustrate that variability in interpretation is a global phenomena[63,64], under diagnosis of Gleason grade is the main problem. Specific difficulties include recognising the border areas between Gleason patterns and that microscopic foci of carcinoma do not necessarily represent low grade carcinoma. A criticism of these studies might be that they contain a small number of observers, however this is likely to represent current practice. Significant improvements in Gleason grading have been achieved by online tutorials[65,66] and regular refresher courses may be beneficial for non specialist pathologists covering a urological workload. Egevad et al. performed an international survey of current Gleason grade practice and found that 77 genitourinary pathologists demonstrated varying opinions on the actual criteria themselves[64]. The subjectivity in interpretation of the Gleason grade is a concern because the pathological assessment guides treatment. Innovations to make pathological analysis more robust would be welcomed by all involved in ensuring the delivery of high quality patient care.

1.3 Prostate Cancer Epidemiology

1.3.1 International Prostate Cancer Epidemiology

Worldwide 670,000 men were diagnosed with prostate cancer in 2002, accounting for one in nine of all new male cancers. Three quarters of new diagnoses are made in the developed world with the highest rates in North America and the lowest rates in Asia[1]. An ageing population, increased surgery for benign prostatic hyperplasia, increased health awareness and screening for prostate cancer using the Prostate Specific Antigen (PSA) blood test are thought to account for the increasing incidence of the disease[67].

1.3.2 United Kingdom Prostate Cancer Epidemiology

In 2006, 35,515 new cases were diagnosed in the UK, accounting for 24% of all new male cancer diagnoses. The current lifetime risk of being diagnosed with prostate cancer is one in ten[68]. The majority of men found to have prostate cancer are diagnosed over the age of 65 with the largest number of cases diagnosed in those aged between 70 and 74[69,70,71,72]. Post mortem studies estimate that 50% of men over 50 will have histological evidence of prostate cancer, this percentage rises to 80% by the age of 80. However only one in 26 (3.8%) will die of the disease[73]. McGregor *et al* determined that of patients with detectable prostate cancer that would prove lethal by the age of 85 only 16% would actually die from prostate cancer, the rest would die from other causes[74]. This data may be interpreted to conclude that 'men are more likely to die with rather than from prostate cancer'.

There were 10,239 deaths from prostate cancer in the UK in 2007, accounting for 13% of male deaths[69,71,75] . Prostate cancer remains second to lung cancer as the leading cause of male cancer death in the UK, a situation mirrored in worldwide statistics. Despite a dramatic rise in the incidence of prostate cancer over the last twenty years, mortality rates only rose marginally until 2003/2004. Rates have fallen slightly since 2003 but it is not possible to elicit whether this is attributable to improved cancer treatments, changes in cancer registry coding[76], the attribution of death to prostate cancer[77] or the effects of PSA testing. This is illustrated in Figure 1.13.

Survival rates in the UK have improved over the last twenty years. The relative five year survival rate from prostate cancer for diagnoses made in 2000 - 2001 in England and Wales was 71% compared with 31% for men with diagnoses made between 1971 – 1975[78,79].

Interpretation of these trends is difficult however because the case mix of patients diagnosed has changed. The statistical anomaly called 'Will Rodgers phenomenon' is well documented and may account for improved patient survival from prostate cancer. Between 1992 and 2002, interpretation of the Gleason grading system was amended to stop the diagnosis of Gleason 2 adenocarcinoma of the prostate. The lowest Gleason grade allocated to prostate specimens became 3+3=6. This had the effect of causing migration in Gleason grade i.e. Gleason 2 disease became Gleason 3 and an associated tendency for pathologists to promote higher Gleason grades accordingly. Gleason grade and stage are used to produce standardised disease outcome data. Therefore if contemporary Gleason grades are higher, survival from prostate cancer by Gleason grade may not actually have changed over time. Thus what has been represented in survival trends is purely the reclassification of Gleason grade[80].

The recent emphasis on early prostate cancer detection has led to increasing numbers of young patients being diagnosed with early cancers. Although some improvement in survival will be due to early diagnosis and improved prostate cancer treatment, urologists are aware that increasing numbers of early cancers which may have been clinically insignificant may be being identified, thereby causing lead–time bias (earlier diagnosis of disease with no lengthening of life).

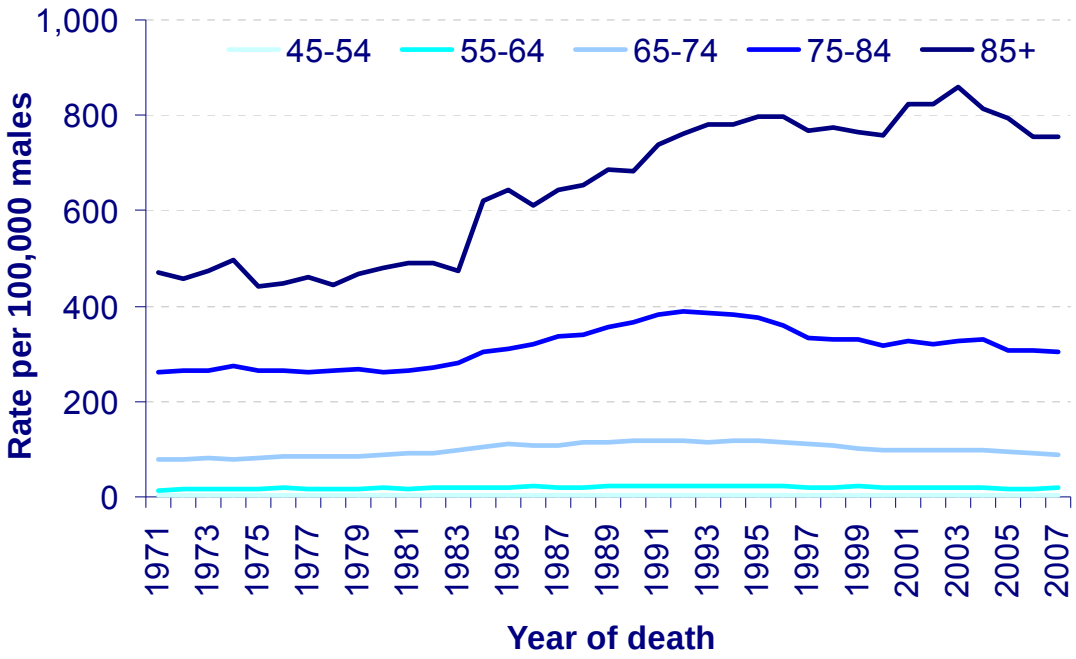

Figure 1.13 Age specific mortality rates, prostate cancer, UK, 1971-2007[81]

1.3.3 Aetiology of Prostate Cancer

Increasing age[73], family history[82] and ethnicity[83] are currently the only established risk factors for prostate cancer. Despite a keen interest in establishing potentially modifiable factors, no definitive evidence to support a change in treatment strategy exists. Diet[84], lifestyle[85,86] , endogenous hormones[87], and medical conditions[88] / interventions[89,90] have been and continue to be investigated. The difficulty of performing such epidemiological studies is firstly the confounding multifactorial influences affecting the development of prostate cancer and secondly the fact that we are in a PSA era (the PSA test will be discussed in detail in the following section) and variable thresholds for performing the investigation means a PSA detection bias exists[91].

1.4 Diagnostic Modalities of Prostate Cancer

Prostate cancer may cause prostate gland enlargement leading men to present with symptoms, however localised prostate cancer is often asymptomatic. Men commonly present now for investigation of their prostate because of concerns raised by increasingly prominent public health campaigns about prostate cancer or because relatives, friends or celebrities have been diagnosed with the disease. This section describes current clinical diagnostic modalities and practice.

1.4.1 Clinical Signs and Symptoms

The majority of prostate cancers arise in the peripheral zone, therefore it is unusual that sufficient enlargement will occur in the PZ to cause urinary symptoms in the form of urinary frequency and difficulty in passing urine. Although transitional zone tumours and large PZ tumours may cause urinary outflow symptoms; it is likely that coexisting transitional zone enlargement secondary to hyperplasia contributes towards most men presenting for investigation in this way. Haematuria, haematospermia and perineal discomfort may also cause men to present for investigation.

Locally advanced prostate cancer may present with all the above features in addition to pelvic pain, rectal bleeding, or renal failure secondary to ureteric obstruction. Malignant priapism and rectal obstruction are rarely seen possible presenting symptoms.

Metastatic prostate cancer is often occult however activity at sites of spread may cause symptoms. Bone pain, pathological fractures or spinal cord compression may result from bone metastasis. Lymphadenopathy may cause lower limb swelling due to the blockage of lymph channels. Other presentations may occur due to the generalised systemic effects of malignancy.

1.4.2 Digital Rectal Examination

Digital rectal examination (DRE) is performed to assess the external contour of the prostate gland. Most prostate cancers originate in the peripheral zone and may be detected by DRE when the volume is 0.2ml or larger. An abnormal DRE is not specific

for cancer; both prostatitis and benign prostatic hypertrophy may cause an abnormal examination. The risk of a positive DRE turning out to be a prostate cancer is closely related to the PSA value: the higher the PSA value the more likely the DRE assessment will be positive. An abnormal DRE in the presence of a normal PSA, < 4.0ng/ml, has a 30% chance of predicting a prostate cancer, for this reason DRE is a vital part of the diagnostic process[92]. DRE is also important for the clinical staging of disease as described in the next section.

1.4.3 Prostate Specific Antigen

Prostate specific antigen (PSA) was discovered in 1979 by Wang *et al*[93]. PSA is a kallikrein-like serine protease produced almost exclusively by the epithelial cells of the prostate and secreted into the ductal system. The normal mode of existence in serum is in complex with α-1-anti-chymotrypsin and α-2-macroglobulin, only a small percentage of serum PSA is in its free form. Serum PSA is determined by immunoassay techniques. Currently there are many different commercial kits but no common international standard exists[94]. Monoclonal antibodies have been designed to detect the free form of PSA, the complex of PSA and α-1-anti-chymotrypsin and the total PSA.

Total PSA has been found to correlate well with advancing age and it has been advocated that these values are taken into account with respect to PSA related diagnostic strategies[95]. There is no universally accepted cut off point or upper limit of a normal PSA; values over an arbitrary cut off point of 4.0ng/ml are inferred to be abnormal in manufacturers' reference ranges; however many men may harbour prostate cancer with a low serum PSA. This is illustrated in table 1.2 which shows the rates of prostate cancer in relation to serum PSA, in men deemed to have normal PSA values, in the placebo arm of a US prevention study[96].

PSA level ng/ml	Risk of Prostate Cancer (%)
0-0.5	6.6
0.6-1	10.1
1.1-2	17
2.1-3	23.9
3.1-4	26.9

Table 1.2 The risk of prostate cancer in relation to low PSA values[96]

In the decade that followed PSA's discovery, studies demonstrated that PSA could be detected in human serum and that there was a positive correlation between an elevated serum PSA and prostate tumour volume and stage[97,98]. Based on the assumption that most adenocarcinomas secrete more PSA than normal or hyperplastic glands the PSA blood test gained widespread acceptance as a prostate cancer screening tool in clinical practice in the developed world. The original author Stamey, who identified the link between blood PSA levels and prostate cancer, recently questioned the validity of PSA in its current role. He presented evidence to support a significant body of opinion in the urological community that the majority of cancers picked up by PSA screening are clinically insignificant[99]. PSA is useful to detect recurrence and monitor response in patients with prostate cancer who have undergone therapy. The limitations of the PSA test are primarily that it is organ specific but not cancer specific and therefore may be raised in benign pathologies including urinary tract infection, BPH and prostatitis. PSA is a poor predictor of prostate cancer volume and severity especially at low levels (<10ng/ml) where the PSA value more accurately reflects the size of the gland[99]. Intertumoural variation in PSA secretion also limits the diagnostic sensitivity of the test as certain subtypes of prostate cancer for example small cell neuroendocrine carcinoma are associated with low PSA concentrations[100].

Improving the characteristics modifications of the PSA has been considered; PSA velocity (rate of change over time) and PSA density (PSA ratio to prostate volume) have not demonstrated a greater value than PSA alone in prostate cancer diagnosis[96,101]. Free PSA, the free form of PSA, is present in a greater proportion of men without

cancer. The concept of the free / total PSA ratio (f/t PSA) has been extensively investigated to attempt to differentiate between BPH and prostate cancer in men with PSA levels between 4 and 10ng/ml and a negative DRE. In a prospective multicentre trial, prostate cancer was found in 56% of men with a f/t PSA ratio of <0.10 but in 8% of men with a f/t PSA > 0.25[102]. Free PSA is however unstable at room temperature and at 4°C and assays are not standardised as there are many inactive isoforms of free PSA including pro-PSA and BPSA, therefore caution in clinical application of these results is necessary.

1.4.4 Prostate Specific Antigen and Prostate Cancer Screening

Wilson and Jungner established the criteria that should be upheld in a gold standard screening assessment[103]. Prostate cancer screening and specifically the PSA test do not fulfil most of these criteria. Controversy exists about whether with changing public healthcare expectations and advances in technology the Wilson and Jungner screening criteria should be modified. In the case of prostate cancer the debate ranges: from the advocates who say the relatively inexpensive test detects clinically significant disease, to the opponents of screening who highlight the low specificity, over diagnosis and morbidity and cost of further investigation and treatment of prostate cancer. Two large population based randomized trials were designed to evaluate the efficacy of screening using DRE and the PSA test and have recently reported their early findings.

The Prostate, Lung, Colorectal and Ovary trial (PLCO) randomly assigned 76,693 men in the United States to receive either annual screening or usual care. The subjects were aged between 55 and 74 and a PSA of over 4.0ng/ml was deemed to be positive for prostate cancer. After seven to ten years of follow up although the screened group was associated with a 22% increase in the rate of prostate cancer detection and good compliance there was no difference in prostate cancer mortality between the two groups[104]. One of the limitations of this study is that in US healthcare is privately funded and the majority of men within this trial are likely to already have had a serum PSA prior to inclusion in the trial[105]. Men with significant tumours who were young and may have benefited from screening would not have been entered into the trial as they

would have been undergoing treatment. This may account for the lack of survival benefit of screening.

The European Randomized Study of Screening for Prostate Cancer (ERSPC) randomized 182,000 men between the ages of 50 and 74 years to PSA screening at an average of once every four years and a control group receiving no screening. During a median follow up of nine years, this study found a higher proportion of prostate cancers in the screened group but concluded the rate of death from prostate cancer was reduced by 20%. However they also highlighted 1410 men would need to be screened and 48 additional cases of prostate cancer would have to be treated to prevent one death from prostate cancer[106]. The ERSPC also has limitations: the study was conducted in several different countries and therefore variability regarding the men included and strategies for screening and follow up occurred. The PSA threshold for prostate biopsy was also lower at 3.0ng/ml when compared to the PLCO trial.

Further analyses of these trials will undoubtedly be reported in the future however both highlight the risks of over diagnosis and over treatment associated with PSA screening. Clinicians will evaluate the data in different ways but a shared decision making approach to PSA screening is currently more appropriate than ever.

1.4.5 Biomarkers for Prostate Cancer Detection

Biomarkers which can both identify prostate cancer and accurately differentiate indolent from aggressive cancers are being investigated. A brief summary of emerging markers is described below.

Prostate Cancer Gene 3 (PCA3) is a biomarker that is being used in clinical practice albeit only in certain institutions in the United Kingdom. PCA3 is present in urine, expressed prostatic secretions, semen and prostate tissue. The marker usually is measured in urine after DRE and prostatic massage which allows shedding of prostate epithelial cells. The marker is evaluated using reverse transcriptase polymerase chain reaction (PCR). PCA3 is over expressed in 95% of prostate cancers and in studies to date a sensitivity and specificity of 66% and 89% respectively have been achieved. The sensitivity of PCA3 is increased in the subgroup of patients with a PSA less than

4.0ng/ml[107,108]. Although the results to date have been encouraging there is need for further refinement of this test before it would replace PSA in routine practice for screening. Currently the investigation is particularly useful for determining who to re-biopsy in men with an elevated PSA level and no prostate cancer on initial biopsy, men who are found to have cancer with normal PSA levels, men with PSA levels elevated secondary to prostatitis and in active surveillance of men with suspected multifocal disease.

Translocation or gene fusion markers are genes found in cancerous tissue, which are not expressed in benign tissue. ERG and ETV1 are two examples of genes that have been identified to be present specifically in prostate cancer[109].

Proteonomics is the large scale study of proteins. Proteins are the end product of gene expression and are the functional mediators of cellular changes in cancer. In the search for protein biomarkers, surface enhanced laser desorption/ionization time of flight (SELDI-TOF) and matrix assisted laser desorption/ionization-TOF mass spectrometry are currently the most common techniques used however reproducibility is currently a concern. Trials to establish the reproducibility of the technique have been commenced[110,111].

Autoantibodies directed against prostate cancer tumour specific antigens have also been discovered using high throughput proteonomic techniques. Multiple autoantibody signatures have been identified in serum and when used as a panel together have demonstrated a better specificity and sensitivity performance for prostate cancer detection than serum PSA[112]. However further studies are required in to develop this technology.

Prostate stem cell antigen (PSCA) is a prostate specific glycoprotein that is expressed on surface of prostate cancer cells. This can be detected by immunohistochemistry and PSCA RNA in blood. Increased PSCA expression has been related to increased prostate cancer risk[113,114].

Prostate specific proteins GSTP-1[115,116], EPCA[117], HK2[118], Hepsin[119] have all demonstrated promise as possible biomarkers however refinements in detection and further study is required to confirm their usefulness.

High throughput technologies, like genomic microarrays, have facilitated biomarker discovery in different specimens including serum, urine and prostatic tissue however rigorous scientific investigation is necessary before any are introduced into routine practice. Researchers and clinicians are mindful of the legacy of the PSA test; which took more than 10 years to reach clinical practice after its discovery but took approximately the same amount of time to understand its limitations.

1.4.6 Transrectal Ultrasonography and Prostatic Biopsies

Transrectal ultrasonography (TRUS) enables the operator to measure gland volume and delineate obvious focal lesions. Although some prostate cancers may be visualised as a hypoechoic lesion in the peripheral zone the appearance is non specific[120]. The primary application remains the image guidance of transrectal or perineal biopsies. TRUS guided 18G core biopsy has become the standard way to obtain prostate tissue for pathological examination in patients suspected of having prostate cancer. Multiple cores may be taken with low complications if antibiotic prophylaxis is used[121,122]. Sampling sites should be as far posterior and lateral in the gland as possible. At least eight biopsy cores should be taken, more than twelve cores are not significantly more conclusive[123]. The British Prostate Testing for Cancer and Treatment Study has recommended ten core biopsies[124]. Current indications for re-biopsy are rising or persistently high PSA, a suspicious DRE, or findings of ASAP or extensive PIN[125]. The quantification of the amount of cancer on the needle biopsy, number of positive cores and core location give clinicians valuable information about individual tumour characteristics[126].

1.4.7 Magnetic Resonance Imaging, Computed Tomography and Nuclear Medicine

Cross sectional imaging techniques such as magnetic resonance imaging (MRI) and computed tomography (CT) are used for disease staging of patients with prostate cancer (see section 1.4.6). Studies in the past have demonstrated low sensitivity to detect prostate cancer. MRI spectroscopy is being evaluated in a diagnostic role however its

ultimate role is also likely to be in staging prostate cancer (see section 1.7.2) and is currently predominantly a research technique. Radionucleotide bone scans provide a sensitive method for diagnosing bone metastases and play an important role in prostate cancer staging. Elderly patients or patients with multiple co-morbidities who present with a significantly elevated PSA and abnormal DRE may only have a bone scan to confirm their diagnosis. If the bone scan demonstrates bone metastases then the assumption may be made that prostate cancer is the primary however this is not routine clinical practice and a histological diagnosis is preferred.

1.4.8 TNM Staging of the Prostate

Staging is a method of describing the extent of local and distant spread of any tumour. Staging may be either clinical (based on examination and radiological findings) or pathological (based on pathology specimen analysis). Staging is important in clinical practice because it enables an assessment of prognosis and thus guides patient management. The Tumour Node Metastases (TNM) staging system is adopted by most urologists for prostate cancer[127]. T-stage describes the extent of local spread and is assessed by DRE and imaging. N-stage is assessed by imaging or biopsy of suspicious lymph nodes. M-stage is assessed by examination, imaging and biochemical investigations. The definitions of each stage are described in Table 1.3.

T – Primary tumour	
Tx	Primary tumour cannot be assessed
T0	Evidence of primary tumour
T1	Clinically inapparent tumour not visible by imaging
T1a	Tumour incidental histological finding 5% or less of tissue resected
T1b	Tumour incidental histological finding in more than 5% of tissue resected
T1c	Tumour identified by needle biopsy (e.g. because of elevated prostate specific antigen [PSA] level)
T2	Tumour confined within the prostate
T2a	Tumour involves one half of one lobe or less
T2b	Tumour involves more than half of one lobe, but not both lobes
T2c	Tumour involves both lobes
T3	Tumour extends through the prostatic capsule
T3a	Extracapsular extension (unilateral or bilateral) including microscopic bladder neck involvement
T3b	Tumour invades the seminal vesicle(s)
T4	Tumour is fixed or invades adjacent structures other than seminal vesicles: external sphincter, rectum, levator muscles, and/or pelvic wall
N – Regional lymph nodes	
Nx	Regional lymph nodes cannot assessed
N0	No regional lymph node metastasis
N1	Regional lymph node metastasis
M – Distant metastasis	
Mx	Distant metastasis cannot be assessed
M0	No distant metastasis
M1a	Non-regional lymph node(s)
M1b	Bone(s)
M1c	Other site(s)

Table 1.3 TNM (2009) staging of adenocarcinoma of the prostate[127]

1.5 Management of Patients with Prostate Cancer

The studies in this thesis focus on prostate cancer diagnosis. The management of patients with prostate cancer is a huge subject area; for the purpose of understanding some of the treatment options available for patients with prostate cancer, a brief discussion of treatment modalities follows.

1.5.1 Management of Patients with Localised Prostate Cancer

Men diagnosed with prostate cancer who have no obvious evidence of spread of their disease outside of the prostate are eligible for all radical (curative) treatment options. The National Institute for Health and Clinical Excellence (NICE) has recently published clear guidelines about how patients should be risk stratified and managed. This is illustrated in table 1.4.

Watchful Waiting: This refers to the avoidance of treatment unless there is disease progression. Those who progress may be offered hormone therapy or palliation. This is usually offered to older men or those with multiple co-morbidities who are more likely to die from something other than prostate cancer.

- Should be treatment of choice in low-risk men who are suitable for radical treatment
- Include at least 1 re-biopsy
- If evidence of disease progression men should be offered radical treatment

- Use 3D conformal radiotherapy
- Minimum dose 74 Gy (maximum 2 Gy per fraction)

	Low-risk men (PSA ≤ 10 ng/ml and Gleason score ≤ 6 and T1-T2a)	Intermediate risk men (PSA 10-20 ng/ml or Gleason score 7 or T2b-2c)	High-risk men (PSA ≥20 ng/ml or Gleason score ≥8 or T3-T4)
Watchful waiting	◇	◇	◇
Active surveillance	✓	◇	X
Brachytherapy	◇	◇	X
Prostatectomy	◇	✓	✓
Radiotherapy	◇	✓	✓
Cryotherapy	X*	X*	X*
HIFU	X*	X*	X*

✓	Preferred treatment
◇	Treatment option
X	Not recommended
X*	Not recommended other than in the context of clinical trials

Table 1.4 NICE guidance on the management of men with localised prostate cancer[128]

Active Surveillance: Active surveillance aims to avoid the unnecessary treatment of early prostate cancers which may prove to be indolent. These men are kept under regular surveillance using the PSA blood test, DRE and if appropriate repeat prostatic biopsy. If their disease demonstrates any evidence of early progression the patients are offered radical treatment. This treatment has recently been advocated to avoid inflicting unnecessary morbidity on patients who have had a low risk early cancer diagnosed.

Radical Prostatectomy: This is the surgical removal of the entire prostate gland and seminal vesicles. The approach can be open via either the retropubic or perineal approach or use the minimally invasive techniques of laparoscopy or robotic surgery. The risks of surgery are significant and include incontinence, erectile dysfunction and the possibility of surgically positive margins (failure to remove all cancer cells).

External beam Radiotherapy: This is usually preceded by hormonal treatments such as *Zoladex* (goserelin) injections. Doses are delivered in fractions over a four to eight week period. Radiotherapy also has significant associated risks: disease recurrence, altered urinary and bowel activity and erectile dysfunction. Adjuvant hormone therapy may be continued post treatment.

Brachytherapy: This is a form of radiotherapy in which the radiation is given through radioactive sources either permanently implanted seeds (low dose) or temporarily inserted wires (high dose). Brachytherapy may not be possible in a large prostate gland. Relative contraindications include men with bladder outflow obstruction symptoms. Brachytherapy shares similar risks with radiotherapy.

HIFU and Cryotherapy: These techniques use technology to either heat or freeze the prostate. The objective is destruction of the prostate cancer; these techniques are currently in the early phases of rigorous scientific investigation.

1.5.2 Management of Patients with Advanced Prostate Cancer

The mainstay of treatment for patients who have metastatic prostate cancer is hormone therapy. Cytotoxic chemotherapy may be considered in patients with good performance

status should the prostate cancer become androgen independent. Palliative care approaches are the mainstay of treatment in the terminal phase of the illness.

1.5.3 The Practical Challenges of Prostate Cancer in Clinical Practice

PSA screening irrespective of the evidence base to support it is for the moment commonplace in clinical practice. The PSA test has undoubtedly contributed not only to the increased incidence of known prostate cancer[129], but also to the increased number of men presenting for urological review and prostate biopsy as a result of a raised PSA. Over diagnosis of prostate cancer is an accepted consequence of current practice. The concept of active surveillance was introduced to counter the unnecessary treatment of clinically insignificant prostate tumours[130]. Unfortunately though we can attribute tumour risk by analysis of its characteristics we do not yet have a test that can accurately differentiate clinically aggressive (significant) tumours from those that will be clinically insignificant. For this reason men diagnosed with localised prostate cancer have to deal with uncertainty and anxiety in addition to potential morbidity whether they have active surveillance or active intervention. There is a need for a marker to determine severity of disease.

The management and follow up of patients with both suspected and confirmed prostate cancer accounts for a significant proportion of Urology and Oncology departments' workloads and budgets. The publication of the NHS cancer plan in 2000[131] has added external pressure from the Department of Health on minimising patients' waiting time before they are seen in clinic. Currently patients in the UK with suspected prostate cancer should be seen within 2 weeks of referral[132] and should not have to wait longer than 18 weeks from GP referral to treatment[133]. The burden on the histopathology service has increased exponentially as a result of the number of biopsies resulting from abnormal PSA tests. Pathology manpower shortages are rarely reported however anecdotally their existence is recognised and evident in clinical practice[134]. Novel approaches to speed up the diagnostic pathway will benefit both clinicians and their patients.

The cost burden of prostate cancer treatment and management is significant. Wilson *et al*. compared the cost of prostate cancer treatments over 5.5 years in 4553 newly

diagnosed patients in America. The individual cost in the first six months including treatment and follow up ranged from 2586 dollars (for a patient undergoing watchful waiting) to 24,204 dollars (for a patient undergoing external beam radiation). The average annual cost of follow up after the first year was 7740 dollars[135]. Cost savings in the current recession are necessary and prostate cancer management is no exception.

1.6 Fourier Transform Infrared Spectroscopy

Isaac Newton (1642-1727) discovered that white light directed at a prism could be separated into its component colours, a *spectrum*, in 1704. Newton's law of the composition of light was published in *Optiks* in 1704 and formed the origin of the science of spectroscopy – the study of spectra.

Bunsen and Kirchoff invented the first spectroscope capable of analysing chemical composition in 1859. This device comprised a prism with a combination of lens and slits. Technological advances and refinements of the integral components have led to modern day spectrometers. The work in this thesis concentrates on infrared spectroscopy and the theory which follows is relevant to this field.

1.6.1 The Theory of Molecular Spectroscopy

Electromagnetic radiation, of which visible light forms a small part, is composed of a magnetic and electric field positioned perpendicular to each other. The propagation of light from a source through space can be considered as a sinusoidal wave as illustrated in figure 1.14. Light will travel in a straight line unless interrupted by molecules or matter in its path. When the electric component of light interacts with matter it may absorbed, scattered or pass through it, producing a spectrum. Molecular spectroscopy is the quantitative and qualitative analysis of the spectra produced by this interaction.

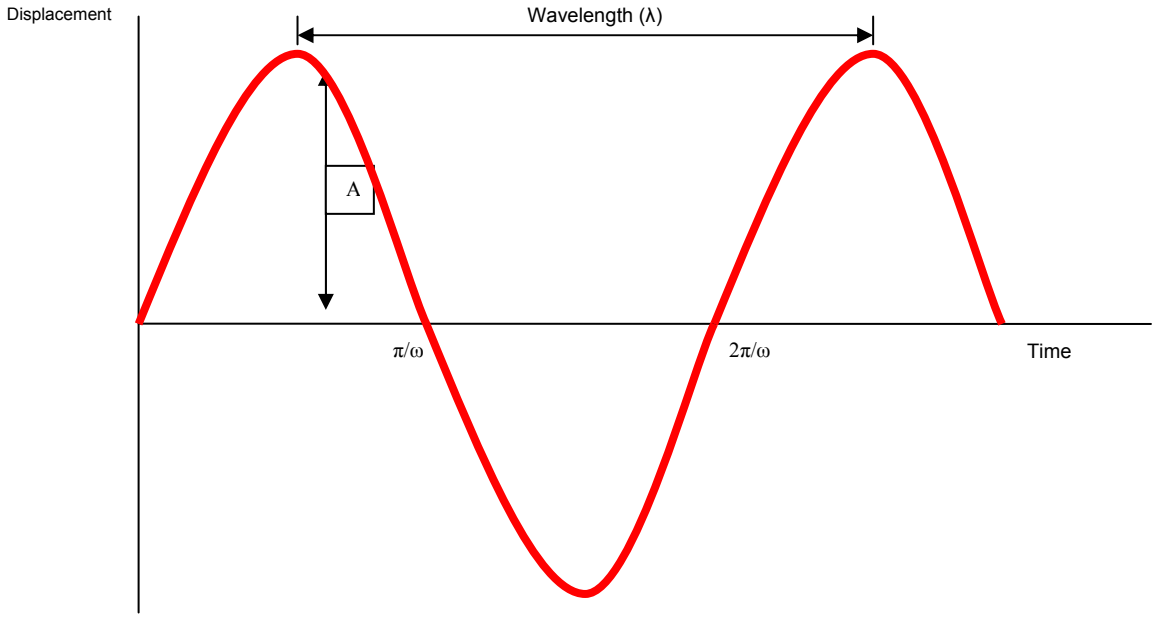

Figure 1.14 The Sinusoidal path of light through space

The above figure illustrates a harmonic wave: this has the same properties of a sine wave:

$$y=A \sin \theta \qquad (1)$$

For any point travelling along the wave: y is the displacement, A is the maximum value of the displacement and θ is an angle varying between 0 and 360° (or 0 and 2π radians) dependent upon its position on the curve.

If it is considered that a point travels with uniform velocity ω rad s^{-1} then the time taken to complete an angle is equivalent to:

$$\theta= \omega t \qquad (2)$$

From this it can be inferred that the displacement described in equation (1) can also be described as below:

$$y= A \sin \theta = A \sin \omega t \qquad (3)$$

The time through a complete cycle is therefore:

$$2\pi/\omega \qquad (4)$$

The number of times the cycle repeats itself in 1 second (s) is referred to as the frequency, v, the SI unit is Hertz (Hz) with the dimensions s^{-1}:

$$v=\omega/2\pi \qquad (5)$$

From this, the following equation of wave motion can be written:

$$y= A \sin \omega t = A \sin 2\pi vt \qquad (6)$$

When considering a travelling wave, the distance variation of the displacement is important. The following distance-time relationship is essential for this where x is the distance covered in time t at speed c:

$$x=ct \qquad (7)$$

Combining equations (6) and (7):

$$y= A \sin 2\pi vt = A \sin (2\pi vx/c) \qquad (8)$$

The distance travelled by the wave in a complete cycle is referred to as its wavelength, λ. If velocity equals c metres per second and there are v cycles per second, there will be v waves in c metres or:

$$v\lambda = c \text{ from which we can say } \lambda = c/v \text{ metres} \qquad (9)$$

Combining equations (8) and (9):

$$y= A \sin (2\pi x/\lambda) \qquad (10)$$

In infrared spectroscopy the wavelength is usually given in micrometers (μm) also sometimes described as microns ($1\mu m = 10^{-6}m$). Electromagnetic radiation can also be characterised in terms of wavenumber ύ. This is the reciprocal of the wavelength and expressed in centimetres:

$$ύ = 1 / \lambda \ cm^{-1} \qquad (11)$$

and hence:

$$y = A \sin 2\pi\acute{u}x \qquad (12)$$

Wavenumber is the number of complete waves or cycles in each centimetre length of radiation. Due to the definition being based on centimetres rather than metres, wavenumber is not an official SI unit however it is still used for the discussion of infrared spectra.

The current concept of how light interacts with matter was realised in 1900 by Max Planck. A molecule in space may have many sorts of energy: vibrational energy resulting from the periodic displacement of its atoms from equilibrium, and electronic energy due to the fact that electrons associated with each atom are in constant motion. Electrons in atoms or molecules exist in discrete energy levels: this energy is referred to as quantized. In the same way molecules in different vibrational states are quantized. To move from one level to another requires a sudden jump requiring a finite amount of energy. This is illustrated in figure 1.15 below. Transitions may take place between energy levels E_1 and E_2 (the suffixes 1 and 2 used to describe energy levels in fact represent quantum numbers). In order to move between the levels a specific amount of energy must be emitted or absorbed by the system, ΔE.

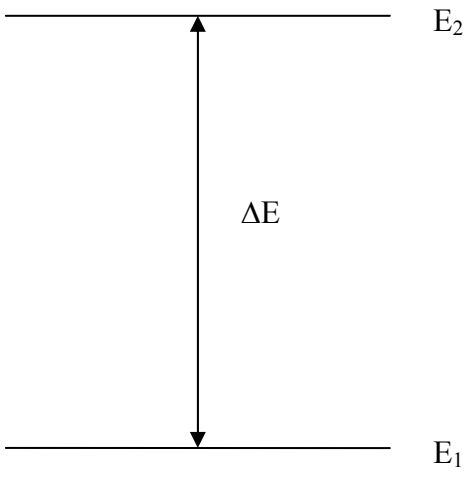

Figure 1.15 Quantized energy states of a molecule

Planck described that electromagnetic radiation could be emitted or absorbed during a transition between levels. The frequency of the radiation:

$$v = \Delta E/h \text{ Hz} \qquad (13)$$

and therefore:

$$\Delta E = hv \qquad (14)$$

where E is expressed as a joule and h is a universal constant – Planck's constant.

This is practically important in molecular spectroscopy because if we take a molecule in state E_1 and direct a beam of electromagnetic radiation of one frequency v (i.e. monochromatic radiation) onto it, where $v = \Delta E/h$, energy will be absorbed from the beam and the molecule will jump to state E_2. If a detector was placed to collect the radiation after its interaction with the molecule the intensity of the beam will have decreased. To expand on this concept, if a beam containing a wide range of frequencies is directed on to a molecule, with a detector to collect the radiation, the detector will show that energy has been absorbed only from that frequency where $v = \Delta E/h$, all the other frequencies will be unchanged in intensity. This is how an absorption spectrum is produced. An emission spectrum would be produced if the molecule reverted from state E_2 to E_1.

The actual energy differences between the levels are very small and are expressed as joules per molecule. Planck's constant has the value:

$$h = 6.63 \times 10^{-34} \text{ joules s molecule}^{-1}$$

Often if interested only in the total energy involved when a gram of a substance changes state, spectroscopists may multiply by the Avogadro number ($N=6.02 \times 10^{23}$).

The electromagnetic spectrum is illustrated in figure 1.15. The molecular processes associated with each region are different. The infrared portion of the spectrum is between the 100μm and 1μm wavelength. Infrared light passes easily through air and is one of the most valuable spectroscopic regions. The infrared region can be subdivided

into near, mid and far infrared. Most Fourier Transform spectrometers and spectroscopists operate in the mid infrared region.

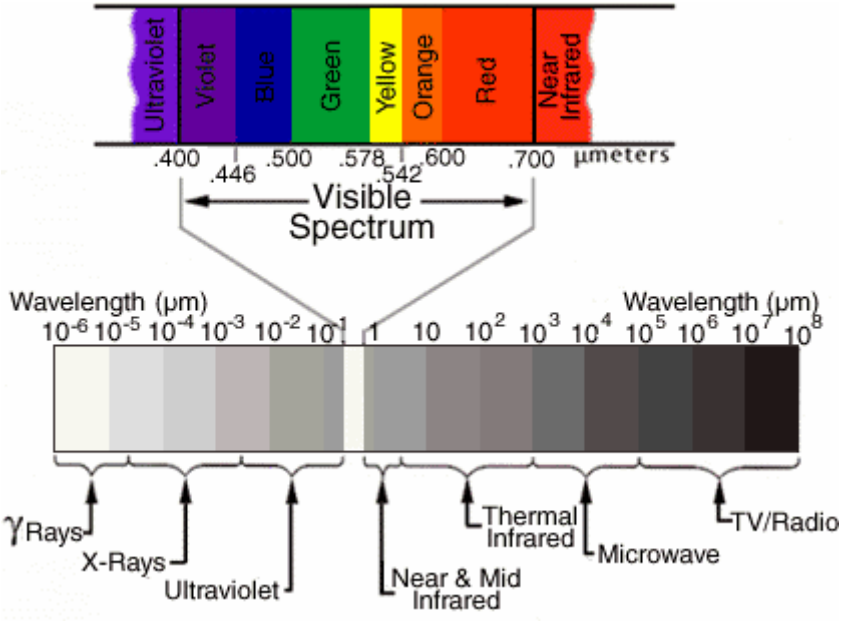

Figure 1.16 The Electromagnetic Spectrum

The concept of how a spectrum is represented can be likened to a conventional X-Ray. If radiation is shone at the plate and nothing is in between the radiation and the plate, the plate will show an even blackening over the frequencies emitted by the radiation source. If a part of the body is placed between the radiation and the plate over the frequencies where radiation is absorbed the blackening will only be present at the frequencies where radiation has not been absorbed. Where absorption has taken place an interaction between radiation and molecules will have occurred and be represented by absorption lines. The intensity of the absorption lines will be dependent on the degree of absorption that has occurred at a specific frequency, different body structures for example bone and soft tissue will absorb to different degrees. This represents the contrast between structures on an X-Ray.

The other important concept is that when radiation is absorbed, to enable a transition a sample (material under investigation) will continue to demonstrate an absorption spectrum for as long as it is irradiated. There is a finite amount of sample, therefore the sample although seemingly capable of absorbing an infinite amount of energy must be

getting rid of the energy absorbed. Some of the energy will be lost as kinetic energy and the sample will become warmer. Another mechanism will be losing the energy as electromagnetic radiation as molecules revert to their ground or resting state. This energy is re-emitted in a random direction, essentially scattered and a negligible proportion reaches the detector in practice which is why it does not affect the absorption spectrum.

1.6.2 Infrared Spectroscopy

Infrared spectroscopy is possible because molecules vibrate when they interact with radiation. If a molecule is considered in its resting stable energy state it will have a number of degrees of freedom: the potential to change position in space and rotation. If N = the number of atoms in the molecule then the number of degrees of freedom if the molecule is non linear is: 3N-6 (3 translational and 3 rotational) and if the molecule linear: 3N-5 (3 translational and 2 rotational). To illustrate if we take oxygen (O_2), shown below in figure 1.17, which is a diatomic linear molecule, only one stretch vibration exists ((3x2)-5 = 1).

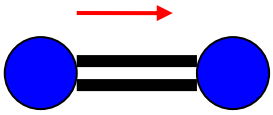

Figure 1.17 Vibrational stretch of oxygen

If we take a non linear molecule such as water (H_2O) it has ((3x3) – 6) = 3 degrees of freedom. This is illustrated in Figure 1.18.

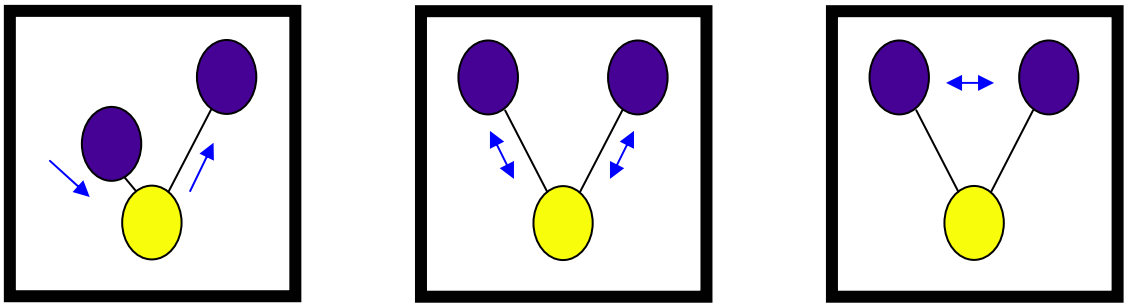

Asymmetrical stretch Symmetrical stretch Deformation

Figure 1.18 Vibrational modes of water

Infrared spectroscopy is an absorption spectroscopy. If incident infrared radiation corresponds to the appropriate ΔE (previously described in section 1.5.1) to cause a molecule to be promoted to a higher energy state it will be absorbed. The change in energy state is represented in infrared spectroscopy by a change in vibrational mode. The key to a substance being infrared active is that there must be a change in dipole moment with the vibrational change. This change in moment is stimulated by the electrical field interaction with the molecules' dipole moment and may be either parallel or perpendicular to the line of symmetry axis.

If we consider carbon dioxide (CO_2) for example as a linear molecule with essentially one degree of freedom in the mode of vibration 'symmetric stretch'; the molecule is symmetrically stretched and compressed with both CO bonds changing simultaneously. The dipole moment or net charge remains unchanged throughout and therefore this vibration is infrared inactive (illustrated in Figure 1.19).

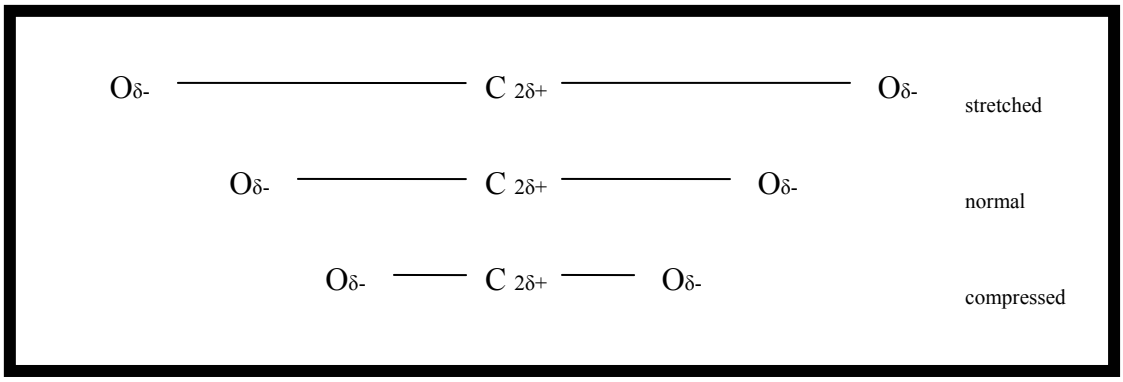

Figure 1.19 Symmetrical stretching of Carbon Dioxide molecule

However if CO_2 is considered in the linear asymmetric stretch mode as shown in Figure 1.20, there is a periodic alteration in dipole moment (illustrated with red arrow) and this vibration is infrared active.

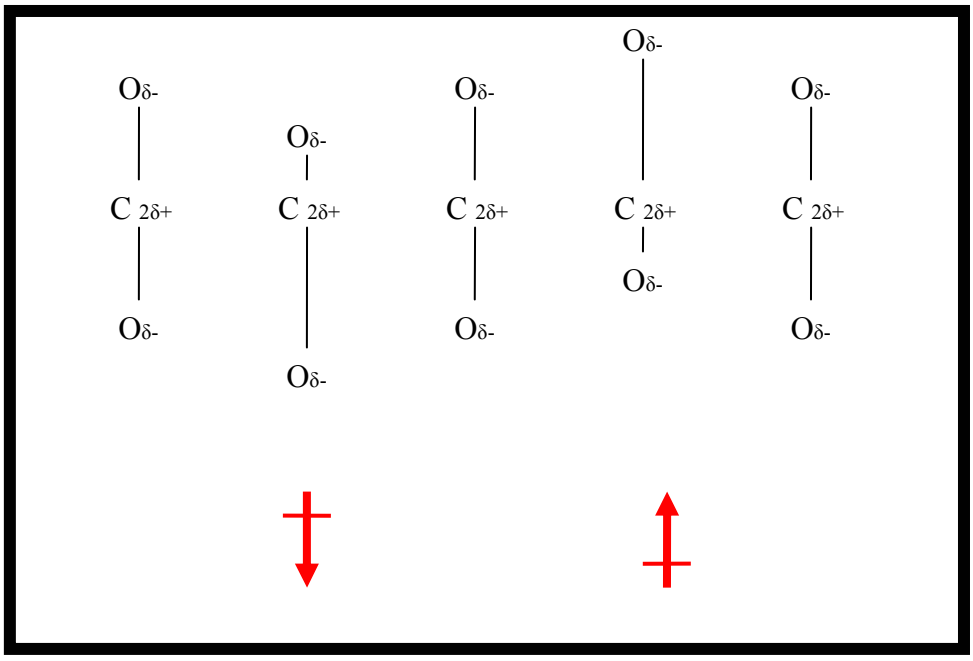

Figure 1.20 Asymmetric stretching of carbon dioxide with change in dipole illustrated

A complex molecule will have a large number of vibrational modes involving the whole molecule. Infrared spectroscopists have defined frequencies at which characteristic bond vibrations will occur when known chemical groups are present within a sample.

Certain bonds will absorb at the same wavelength range regardless of the structure of the molecule. For example the C=O stretch of a carbonyl group occurs at approximately 1700cm^{-1} in ketones, aldehydes and carboxylic acids. This is the principle upon which infrared spectroscopy can be used for chemical identification. Spectroscopists refer to the fingerprint region of a spectrum (<1500cm^{-1}) which is unique for a molecule and the functional group region (1500-4000cm^{-1}) which may be similar for molecules within the same group (illustrated in Figure 1.21). Apart from the qualitative data obtained from an infra-red spectrum, concentration can be estimated using Beer Lambert law:

$$A=\varepsilon \mid c$$

Where: A=absorbance; ε=absorptivity; $\mid$ = pathlength; c = concentration

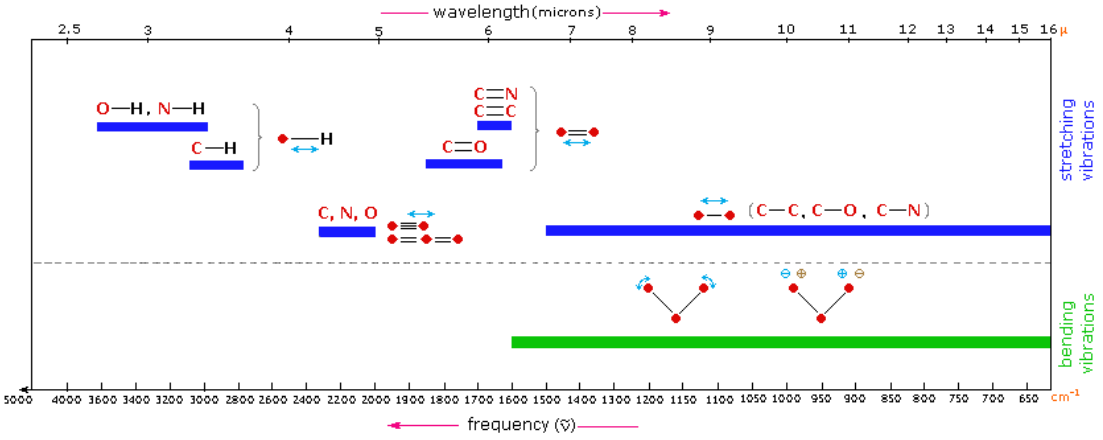

Figure 1.21 The fingerprint region and functional group region with examples of groups that may be involved in the regions[136]

1.6.3 The Infrared Spectrometer

A Fourier Transform Infrared spectrometer contains an infrared light source, an interferometer, a detector, an optical system with a motorised x-y-z stage and a computer to process the data, as shown in Figure 1.22.

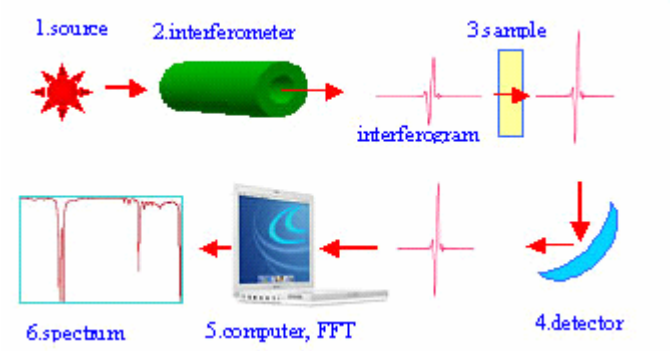

Figure 1.22 The components in order of function of a FTIR Microspectrometer

Traditional infrared spectrometers functioned by recording each part of the spectrum separately. The process started at one end of the frequency and swept to the other, and the detector signal was monitored and recorded. The process was slow and inefficient as apart from the frequencies where a transition occurred the majority of the time was spent recording background noise. A mathematical way of resolving complex waves (sinusoidal waves of different frequencies) into their frequency components was developed by Jean Baptiste Fourier in the early 1800s, however the technology to enable its application to spectroscopy was invented much later. The interferometer is the key component that has facilitated Fourier Transform Infrared Spectroscopy. The *interferometer* was invented by Michelson in 1880 and he was the first American to win a Nobel Prize in 1907 'for his optical precision instruments and the spectroscopic and metrological investigations carried out with their aid'. When a parallel beam of radiation is directed from a source to an interferometer the following happens: A beam splitter (a plate of transparent material coated in a suitable substance to reflect 50% of the radiation falling on it) splits the beam into two separate light paths. Half the radiation goes to a moving mirror and half to a fixed mirror (as illustrated in figure 1.23). The radiation reflected from these mirrors comes back along the same path and is recombined to a single beam at the beam splitter (half the total radiation will be sent back to source).

If monochromatic radiation is emitted by the source, the recombined beam leaving the beamsplitter towards the sample will show constructive or destructive interference depending on the relative pathlengths between the beamsplitter and the two mirrors.

Essentially if the pathlengths are identical or differ by an integral number of wavelengths, constructive interference will give a bright beam. If the difference is a half of an integral number of wavelengths the beams will cancel each other. The moving mirror governs the variation in pathlengths, and as it moves the intensity of the radiation leaving the beamsplitter to the detector will alternate. This is called an interference pattern – a perception of light intensity plotted against optical path difference. If the source emitted two monochromatic frequencies, two different interference patterns would be created and overlay each other. Although the detector would see a more complex pattern, computing the Fourier transform of the resultant signal would obtain the original frequencies and intensities emitted by the source. Taking the process further, the infrared light source in a FTIR spectrometer produces two broad band beams emitting all frequencies within its range, thus producing interference patterns that can be transformed back to the original distribution of frequencies. If the recombined beam is directed through a sample, the sample absorption will show up as a gap in the frequency distribution. Fourier transform analysis will convert this to a normal absorption spectrum. In practice the mirror is moved smoothly over a period of time through about 1 cm and the detector signal may be monitored every thousandth of a second into 1000 storage points. The computer then performs Fourier transform analysis on the stored data.

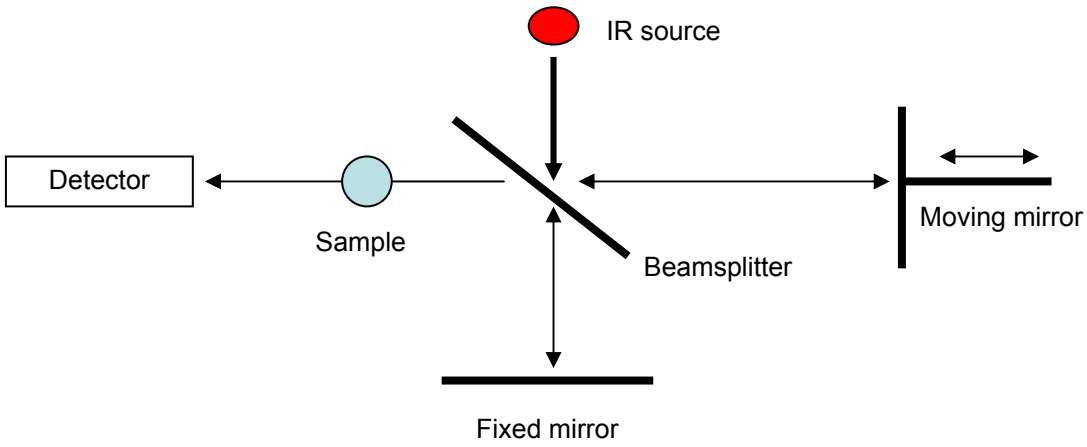

Figure 1.23 A schematic of the interferometer in a Fourier transform spectrometer

FTIR spectroscopy has several advantages over traditional infrared spectroscopy:

- *Speed*: it is not necessary to scan each wavenumber individually because the whole spectrum is contained in the interferogram which is measured in a few seconds
- *Resolution*: Conventional instruments used a slit to focus the radiation but although a fine slit gives good resolving power it only allows a narrow spread of frequencies to fall on the detector at any moment so limited energy could be passed through the instrument and high gain was required resulting in significant noise. In FTIR because parallel beams are used no slit is required and all the energy passes through the instrument. The resolving power remains constant and is limited largely by the moving mirror and the computer capacity
- The digital data obtained by FTIR is easier to analyse

1.6.4 Additional Technical Considerations for Infrared Spectrometry

Infrared microscopes are generally designed with two paths from the sample to the detectors: transmission and reflection. In transmission mode, the light passes through the sample and is collected on the other side. In reflection mode, the infrared light reflects off the sample and passes back through the illuminating objective. In reflection mode, approximately 40-50% of the incident light is blocked by a mirror that collects the reflected light. Thus transmission mode is preferred over reflection because of the increased incident flux on the sample. Reflectance is suitable for thin samples, highly reflective samples, materials which cannot be cut and when an infrared transparent substrate is either not available or prohibited due to budget but all these can cause different spectroscopic issues.

Sample preparation is key to collecting good spectra. Organic samples are generally prepared with thicknesses of 10-15 microns. Specimens are mounted on a 1-2mm thick infrared transparent material; common materials used are listed in table 1.5. Of note potassium bromide is water soluble and diamond is expensive.

Material	Transmission Range (cm-1)
Calcium Fluoride (CaF2)	4000-1100
Barium Fluoride (BaF2)	4000-800
Zinc Sulphide (ZnS)	4000-600
Potassium Bromide (KBr)	4000-400
Diamond	4000-50

Table 1.5 Materials with an infrared transparent window

CO_2 and H_2O although only present in air in small percentages exert a significant absorption effect over much of the infrared spectrum. This obscures valuable spectra at similar frequencies. To remove this effect and study the regions impaired by these absorbances, the CO_2 and H_2O spectra would have to be subtracted from the spectrum of any sample analyzed under comparable conditions. However since the percentage of water vapour in the atmosphere is highly variable a background spectrum would have to be performed for each sample. This affects the quality of the spectra and is time consuming. There are two ways of overcoming this problem:

1. Evacuation of CO_2 and H_2O from the spectrometer - this may be done by flushing a constant current of dry Nitrogen or dry CO_2 free air though the system. This is unlikely to be completely effective as the equipment has many points that are permeable and let the outside atmosphere in.
2. The alternative is to use two beams. The source radiation is divided into two by mirrors. One beam is brought into focus at the sample space, the other follows an equivalent path and is referred to as the reference beam. A moving mirror alternatively reflects the reference beam or allows the sample beam through the spaces into the monochromator. The detector sees the sample beam and the reference beam alternately. Both beams have travelled the same distance through the atmosphere and therefore are both reduced in energy by the same amount due to absorption by CO_2 and H_2O. If a sample capable of absorbing energy from the beam from the monochromator is placed in the sample beam, the detector will receive a signal altering in intensity because the sample beam carries less energy than the reference beam. This can be amplified and a

calibrated attenuator can be driven into the reference beam until the signal is reduced to zero, essentially both beams are balanced again. The distance travelled by the attenuator is a direct measure of the amount of energy absorbed by the sample.

Most spectrometers use some form of amplification to magnify the signal produced by the detector. Every recorded spectrum will have a background of random fluctuations caused by the equipment and additional electronic signals. These fluctuations are referred to as noise. For a spectral peak to distinguish itself from noise its intensity must be approximately three to four times that of the noise. This may be referred to as a signal to noise ratio but highlights that there will be a lower limit on the intensity of observable signals. Computer averaging techniques can improve the effective signal to noise ratio.

1.6.5 Attenuated Total Reflection FTIR

Attenuated total reflection (ATR) is especially useful for samples which do not let light through because either they are highly absorbing or they cannot be cut into thin enough sections. The technique uses an ATR objective containing an ATR crystal made of an infrared transparent material, for example diamond, fitted to the FTIR spectrometer. The ATR crystal is used to probe the sample and must be in contact with the sample to work. Light entering the ATR crystal is totally internally reflected and collected in reflectance mode. When light normally inside the crystal escapes to be absorbed by a sample there is a reflection loss (evanescent waves). A reflection loss spectra can be created and adjusted for the depth of penetration of the sample. Although the ATR technique requires little sample preparation it can be time consuming when used with biological tissues, because the objective must be cleaned between spectral measurements at different points, and the sample must be raised and lowered between sample data points, therefore automated mapping is prohibitive.

1.6.6 Synchrotron FTIR

Synchrotron FTIR (S-FTIR) enables the acquisition of highly resolved images of microscopic areas less than 10 microns in diameter. This has practical application in the

analysis of the contents of small cells. This is achieved because the beam of radiation used by the synchrotron is approximately a few hundred microns in diameter; this is 100 to 1000 times brighter than that emitted from a conventional infrared light source. Conventional spectrometers encounter a signal to noise ratio limitation when apertures confine the beam to 20-30 microns. S-FTIR is able to approach beamlines of 3 microns in diameter with an acceptable signal to noise ratio thus enabling the detailed interrogation of cells.

1.7 Biomedical Applications of Fourier Transform Infrared Spectroscopy

Vibrational spectroscopy techniques including Fourier Transform Infrared Spectroscopy have recently been applied to address biomedical problems. The concept is not new; in 1949 and 1952 Blout, Mellors and Woernley reported that infrared spectra of human and animal tissues could provide information on the molecular structure of tissue[137,138]. Unfortunately, at that time the technology required to practically realise their visions was not available. The development of sensitive and high throughput spectrometers in the last decade has enabled simultaneous global analysis of biological samples and high resolution molecular information to be obtained. Spectroscopic findings are dependent on tissue architecture, the light absorbing or scattering properties of each layer, and the biochemical microenvironment of the tissue. Spectroscopy is non-destructive, requires no extrinsic contrast enhancing agents and allows samples to be analysed directly at room temperature and pressure. This section describes the broad range of FTIR's biomedical applications before a critical review of FTIR experimental studies performed on the prostate. Competing technologies will be discussed in Chapter 1.8.

1.7.1 FTIR Spectrometry for Molecular Structural Analysis

In complex biological cells and tissues the infra red spectrum is an expression of the sum of all the biomolecules present. The most significant components of most biological tissues and cells are proteins, carbohydrates and lipids. Analysis of the structural information obtained about these constituents by FTIR enables the differentiation and determination of clinically relevant factors.

Proteins: proteins are macromolecules, they consist of series' of amino acids known as polypeptides. The way in which these polypeptides are put together is termed the secondary structure. FTIR can be used to determine the secondary structure of proteins[139]. The structure can be determined in terms of percentages of α helix, parallel / anti parallel β sheets, β turn and unordered structure present in a sample[140]. Spectroscopists commonly use amide groups to determine the secondary structure of

proteins. Amide I (-$CONH_2$-) is located at approximately 1700-1600 cm^{-1}, Amide II (-CONH-) is located at approximately 1550cm^{-1}. The position in the frequency range where the amide bands appear is dependent on the hydrogen bonding of the C=O and N-H groups[141,142]. Differentiation of pathologies on the basis of changes in protein concentration alone has been demonstrated to be limited by the fact that significant variations in cellular protein structure may occur, dependent on the position of the cell in its cycle rather than only due to the carcinogenesis process[143,144].

Carbohydrates: carbohydrates are an important source of energy in cells and fuel the majority of processes in the cell. Carbohydrates are most commonly found stored as glycogen in the cell, a polysaccharide chain. Glycogen is broken down into its constituent units of glucose to provide energy for cellular processes. Carbohydrates may also be found bound to lipids, proteins or the ribose moiety of nucleic acids. Key FTIR carbohydrate absorbencies arise at 1170cm^{-1}, 1050cm^{-1}, 1030 cm^{-1} [145]. The significance of changes in concentration of carbohydrates in the cell may give an indication of pathological processes occurring in the cell and this is discussed later in the chapter.

Lipids: Lipids are also present in cells, and comprise fatty acid chains. Their absorbencies are largely due to their long hydrocarbon chain moieties (CH_2 and CH_3). The carboxylic acid moiety of fatty acids has a carbonyl stretch absorbance at approximately 1725 cm^{-1} and the carbonyl group of phospholipids characteristically absorbs at 1740 cm^{-1}. The phosphate component of phospholipids prevalent in cell membranes has absorbance peaks at 1080 cm^{-1} and 1240 cm^{-1} for symmetrical and asymmetrical modes of PO_2 respectively[146]. Changes in lipid concentration may signify changes taking place in the membranes of the cell.

1.7.2 The Cell Cycle

The cell cycle is the process by which normal cells proliferate, essentially mitosis (cell division), and is illustrated in Figure 1.24. The cycle starts with G1, a gap phase, this is the time between previous mitotic division and the next phase beginning. During the S phase DNA synthesis occurs, leading to the cell DNA content to be doubled. Once synthesis is complete there is a second gap phase, G2, before cell division occurs. In the

M phase mitosis occurs in two stages: firstly the DNA separates and then cytokinesis occurs. After this phase cells enter the G0 phase, this is a period of growth arrest until cells are stimulated to resume the cell cycle[147].

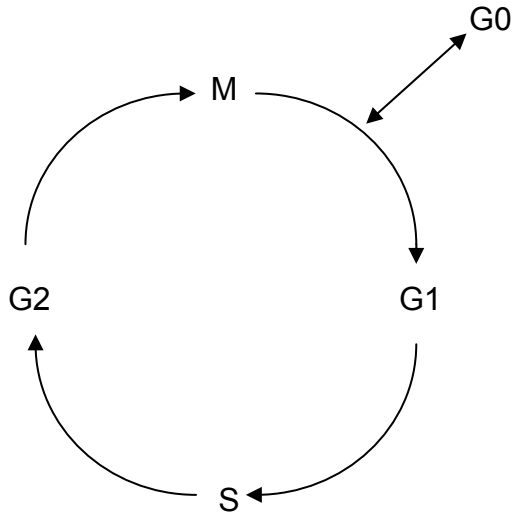

Figure 1.24 The cell cycle

Several mechanisms exist to control the cell cycle. Proteins which regulate the cell cycle include growth factors, cyclin dependent kinases and cyclins. Apoptosis (programmed cell death), is another important mechanism by which abnormal cells or cells which are not needed are eliminated thus regulating proliferation. In malignancy, the normal mechanisms of control of cell proliferation do not operate. One theory for proliferation in malignant prostate cells is that p53 and Bcl-2, proteins which control apoptosis, are over expressed leading to apoptotic resistance[148]. Differences in cell biochemistry resulting from alterations in the normal cell cycle may be identified by FTIR.

1.7.3 Biochemical Changes During Carcinogenesis

The proliferation of an invasive cancer cell capable of local and distant spread is dependent on oxygen delivery and glucose metabolism. Metastatic tumour cells have a high glycolytic metabolic profile and are likely to have low intercellular oxygen tensions (pO_2) as a consequence of high respiration rates (both anaerobic and aerobic)[149]. An increase in glycolytic rate results in decreased cellular concentrations of glycogen, especially in tumour cells. Neoplastic cells must be within a 1-2mm^3

proximity to a blood supply to survive otherwise they will become hypoxic and eventually necrotic[150]. A viable blood supply enables the transport of nutrients to proliferating cells but also enables the waste products of carcinogenesis to be removed. Tumours with the capability to induce formation of new vessels are particularly pathogenic; vascular endothelial growth factor (VEGF) is an example of a potent angiogenic factor[151]. Tumour cells with a poor micro-circulation become hypoxic. Low oxygen tension combined with a poor oxygen supply and removal mechanism leads to increased anaerobic respiration and a several fold lactic acid production[152]. It is acknowledged that even in aerobic respiration tumour cells produce large amounts of lactic acid; this is termed the *Warburg effect*[152]. The removal of lactic acid is also impaired by the poor circulation. Acidic intracellular and extracellular pH is therefore associated with tumour progression and also ischaemia.

In the process of necrosis special enzymes are released by lysosomes, which are capable of digesting cell components or the entire cell. This tissue destruction also results in lactate production.

Carcinogenesis is associated with increased free radical generation. This is acknowledged to induce the formation of lipid, protein and DNA peroxidation products[153]. Phosphocholine and Glycophosphocholine are important metabolites of phospholipid metabolism and are noted to be present in increased quantities in actively dividing or cancerous cells[154].

The critical review which follows describes the way that some of these factors have been used to form a basis of objective discrimination of pathologies.

1.7.4 FTIR and Clinical Chemistry

FTIR has been able to determine molecular concentrations of glucose and cholesterol in blood[155], and protein, creatinine and urea present in urine[156] with good accuracy compared to clinical gold standards. The practical application of this has been limited to date because frequently spectra from different molecules have overlapped in complex

biological molecules especially at protein absorptions. Proteins are major constituents of these fluids, and their spectra may mask the spectral information from other sample contents[157]. These limitations can be overcome by either modifying data processing methods or by using specific transparent windows which are wavelengths where minimal overlapping and known key absorptions occur.

1.7.5 FTIR and Microbiology

Fourier transform infrared spectroscopy is used to classify microorganisms in many non-medically related fields currently, including bioprocess and fermentation monitoring[158]. Organism identification using FTIR analysis is achieved by utilising pattern recognition algorithms such as cluster analysis or linear discriminant analysis (LDA). The principles have been applied to enable classification of common pathogens for example *Enterococcus* species, an organism found in the gut and a leading cause of noscomial infections. A comparative study combined the use of phenotypic, genotypic and vibrational spectroscopy techniques to type a collection of *Enterococcus* strains. Classification by FTIR identified discrepancies in strains classified using the phenotypic systems. The discrepancies were resolved by using elaborate polymerase chain reaction (PCR) and genotypic methods to reclassify the strains in question. The correct strains were consistent with FTIR findings[159]. Thus FTIR has demonstrated promise as a microbiological classification tool.

1.7.6 FTIR and Pathology

The potential of FTIR for rapid, high resolution, unstained biochemical tissue analysis is being investigated. Ultimately it is hoped that the technology will not only reliably distinguish between pathologies but also enable identification of premalignant pathologies and prediction of clinical outcome. FTIR has been applied/studied in the following malignancies: colon[160], cervix[161,162], stomach[163], breast[164], skin[165], oral[166], pancreas[167], lung[168] and cerebral[169]. To date although FTIR has been applied to a number of biological tissues to distinguish pathology, universal patterns for distinguishing between benign and cancerous tissues have proved elusive. Studies have

been limited by small sample numbers and their lack of clinical application; maybe due to the lack of partnership between spectroscopists and clinicians in study design. The next part of the chapter will review the literature specifically regarding FTIR and the prostate to illustrate the applications of FTIR to pathology.

1.7.7 FTIR of the Prostate

Fourier transform infrared spectroscopy has been applied to urological pathologies over the last decade. Exciting work has been reported in prostate tissue, cell and DNA studies.

Tissue studies

Pilot studies evaluating the ability of FTIR to distinguish between benign and malignant prostate pathology to date have used small highly selected numbers of spectra from a small number of prostate tissue samples to test the hypothesis. Gazi *et al*[170], concluded that FTIR could discriminate between benign and malignant prostate pathology using an average of four spectra from each pathology, from five deparaffinated prostate tissue samples, each mounted on KBr and obtained at transurethral resection of the prostate (two BPH, three CaP). The FTIR spectra from single Gleason grades were examined, however no clear relationship was determined. A difference in pathology glycogen/phosphate ratio was proposed to explain the differentiation. Malignant cells have a high metabolic turnover and therefore a lower glycogen content. Thus benign samples had a glycogen/phosphate ratio of greater than or equal to 0.6, and malignant samples a ratio below 0.4. Similar findings have been reported in colorectal studies and pure biochemical studies of the prostate[171,172]. The potential negative effect of diathermy used at TURP on the biochemistry of tissue and thus biochemical analysis obtained at TURP was not addressed. Paluszkiewicz *et al*. used FTIR to analyse fresh frozen prostate tissue mounted on mylar foil[173]. Although the origin and number of samples was not defined, and the mylar foil may have affected the FTIR spectra, it was concluded that cancerous tissue could be distinguished from non cancerous by FTIR using the $v_{as}CH2/v_{as}CH3$ peak ratios at 2930 cm^{-1} and 2960 cm^{-1} respectively, and the/$v_{s}CH3$ peak ratios observed between 2852 - 2874 cm^{-1}. Without knowledge of the origin and number of the tissue samples upon which this study was based in addition to

factoring in the variance of the mylar foil effect and the fact that the ratios proposed are outside the 'fingerprint region', further validatory studies are required to confirm these findings.

More recently the same group has addressed some of the aforementioned issues. Synchrotron FTIR and FTIR Spectroscopy was used to evaluate five prostate samples mounted on mylar foil taken from five samples at prostatectomy[174]. Two prostatectomies were performed for benign disease, two were performed to remove prostate cancer and one prostate was removed during a cysto-prostatectomy for bladder cancer. This study concentrated on examining the spectral characteristics of prostate tissue between 3700 cm^{-1} and 2800 cm^{-1}, particularly where the C-H stretching vibrations are located. They concluded that by using the CH2/CH3 ratio it was possible to differentiate between normal, benign prostatic hyperplasia and cancerous tissue using both FTIR and S-FTIR. Similar findings have been reported in FTIR analysis of breast cancer tissue and prostate cells[175,176].

Attempts have been made to correlate the FTIR spectra taken from cancerous prostate tissue with Gleason score and clinical stage of prostate cancer at the time of biopsy[177]. The heterogeneity of the tissue studied unfortunately may have affected / limited the interesting study findings. Of 40 cancer samples, all were originally paraffinated, and 37/40 were TURP specimens. Fifty-nine percent of the samples came from patients who were undergoing hormone manipulation for their prostate cancer. In addition to this relatively few highly selected spectra from four samples were used to create the test model. A total of 383 spectra were collected. FTIR was able to predict precise Gleason grade with an accuracy of 20 % if two grades were present in the tissue, and 17% if only a single grade was present in the tissue. If the criteria were adapted to those used by Crow et al[178] in Raman spectroscopy to determine the Gleason score of prostate cancer (<7, 7, >7), the sensitivities and specificities rose to greater than 70%. A poor correlation was found when it was attempted to determine disease stage from FTIR spectra. Gleason grade had a sensitivity and specificity of 71% and 67% respectively in determining disease stage. Further work by Baker et al has developed the technique further using supervised principal component discriminant function analysis. The

sensitivities and specificities of discrimination for Gleason <7,7,>7achieved are much improved 92.3% and 98.9% respectively and the potential of FTIR to stage disease have been explored[179]. This early work is promising but uses under 400 spectra from two separate paraffinated tissue sources (TURP and biopsy tissue from - a highly selected group) to build its diagnostic algorithm which may compromise its wider application.

German et al used FTIR with an ATR crystal and synchrotron FTIR to investigate whether FTIR would be able to differentiate structural characteristics between different prostate zones[180]. Paraffinated samples were obtained from six patients who had undergone radical retro-pubic prostatectomy and analysed. In benign prostate tissue five spectra were taken at three individual points at each of three randomly chosen glandular elements. In cancerous tissue three spectra were taken at five randomly chosen glandular elements. Five randomly chosen measurements were taken from the adjacent stroma of both benign and cancerous tissue. In contrast to Gazi's findings, no tissue or region specific characteristics were determined, especially between 1000-1200 cm^{-1} in either epithelial or stromal cell regions. The authors comment on the presence of a prominent paraffin wax peak at 1462 cm^{-1}. When principal component analysis was applied to the dataset, subtle differences between PZ, TZ and CaP regions were determined, especially in the region containing the DNA/RNA bands 1000-1490 cm^{-1} using ATR spectroscopy, and between 1000-1200 cm^{-1} region in synchrotron FTIR analysis. Good separation was demonstrated between CaP free tissues (PZ, TZ) and CaP. The group also performed an interesting study of the PZ and TZ taken from a cancer free prostate gland taken at cysto-prostatectomy which was immediately snap frozen. The spectra were compared with spectra from deparaffinated prostate tissue. Although PZ spectra were tightly grouped there was variation between the TZ spectra. Differences were noted in both the PZ and TZ spectra between the 1700-1750 cm^{-1} region, associated with the C=O stretching vibrations of lipids (1740 cm^{-1}) with a peak not seen in deparaffinated sections. In the spectral region 1490-1000 cm^{-1}, containing the DNA/RNA, median intensity elevations were determined in PZ tissue of glycoproteins (1380 cm^{-1}), amide III (1260 cm^{-1}), and carbohydrates (1155 cm^{-1}) when compared to the TZ. This may point to differences between epithelial cells in this region or it may be a factor of the sample being affected by the processing as the prostate is a

large gland, to snap freeze the inner core will freeze at a different time to the periphery. Biopsy comparison may in the future remove this issue.

Cell studies

Fixatives are used in histopathology to preserve the structural and biochemical constituents of cells as close to *in vivo* conditions as possible. Without fixation, cells would initially alter in size, shape and consistency and eventually decompose by autolysis making morphological analysis impossible. For the same reason, biochemical analysis of a cell would not be representative of *in vivo* conditions if fixation was not used. However, the biochemistry of samples is also disrupted by cross-linking fixatives. FTIR studies to date have addressed this issue by studying fresh frozen tissue, but practically, FTIR analysis of fixed tissue is mandatory if this technology is going to be clinically useful and validated in the near future.

Synchrotron FTIR has been used to evaluate some of the changes which take place within cells during the fixative process. Routinely used histopathological stains were used as a standard against which to compare the changes occurring. The prostate cancer cell line PC-3 was used for these studies. Tryptan blue was used to assess the effect of fixatives on membrane integrity morphologically. Cells with no fixative, formalin fixed, unfixed formalin and gluteraldehyde were assessed. Tryptan blue illustrated that only gluteraldehyde maintains membrane integrity when used in fixation. Synchrotron FTIR analysis was able to determine the cytoplasm and nucleus in formalin and gluteraldehyde fixed cells. S-FTIR was unable to differentiate the cell components clearly in unfixed cells[181]. Harvey *et al* recently determined that growth media and nuclear to cytoplasmic ratio are unlikely to explain FTIR's differentiation of pathology; it is likely to be due to biochemical differences[182].

DNA Studies

Malins *et al* have used FTIR to study DNA sourced from frozen benign and malignant prostate tissue. FTIR achieved sensitivities and specificities of greater than 95% when differentiating DNA extracted from normal tissue, BPH and prostate cancer in 29 samples. No relationship between FTIR analysis and Gleason grade was established[183].

DNA studies have demonstrated that it is also possible to differentiate between non metastatic prostate cancer DNA and metastatic prostate cancer DNA[184]. FTIR analysis of age related changes in prostate DNA, DNA in adjacent tissue areas and markers of susceptibility for prostate cancer have not yielded convincing results[185,186].

Tissue Microarray Studies

FTIR spectroscopy has recently been combined with tissue microarray technology[187]. FTIR analysis of microarrays constructed from formalin fixed archival samples from sixteen patients representing the main prostate pathologies, achieved classification accuracies of greater than 95%. The reported ability of the technique to differentiate between nerves, blood vessels and lymphocytes is both novel and exciting. The origin and Gleason grade of the tissue used to create the microarrays was not discussed in the paper and is a potential weakness of the study, however the potential advantages of microarrays in FTIR laboratory studies are clear:

- Microarray size and purity enable rapid acquisition of high quality FTIR data
- Microarrays could facilitate large scale validation studies of FTIR analysis

FTIR microarray studies may therefore accelerate the development of FTIR diagnostic algorithms which could be investigated in the clinical arena.

1.7.8 Limitations of Prostate FTIR Studies To Date

The studies discussed in this chapter illustrate the potential application of FTIR as a pathological classification tool. To date the majority of FTIR studies of the prostate include a small number of patient samples and varied methodology in tissue processing and analysis. Whilst a technique is being established, power calculations are less important than developing rigorous, repeatable methodology that may be used in large scale trials. It is also important that the application is tested in the target population in which the technology is likely to be used. Complex computer programs are used to determine the spectral differences between pathologies, and cross-validation of the discriminating regions reported is also essential for the FTIR to be accepted in practice. Some of the proposed regions will be evaluated in the studies which follow. The

majority of studies have also failed to present FTIR analysis of control samples from the same patients in their results.

The primary clinical aim for pursuing FTIR technology as a clinical tool is to enable rapid diagnosis of pathology in prepared or unprepared tissue. Whilst important small steps have been taken in understanding the technology and its versatility in prostate tissue analysis, there is still a need to validate the technique for its potential future clinical purpose before large scale studies can be commenced. These issues will be addressed in the experiments in this thesis. Ultimately it is hoped that FTIR may have the potential to identify the presence of cancer even if a morphologically normal sample is being interrogated, and aid early diagnosis of biologically significant prostate cancer.

1.8 Competing Technologies

1.8.1 Raman Spectroscopy

Raman spectroscopy is another form of vibrational spectroscopy which is complementary to infrared spectroscopy. Instead of analysing light passing through a sample, it collects and analyses how samples scatter light. Raman spectroscopy utilises monochromatic light from the ultra violet, visible or near infrared part of the electromagnetic spectrum. The optimum excitation wavelength for analysing human epithelial tissues has been found to be 830nm in the near infra red region of the spectrum[188]. The principle is that when a tissue is illuminated with monochromatic laser light, approximately one in a million of the light photons will inelastically interact with an intramolecular bond in a tissue. The interaction will result in energy being donated or received from the bond. This changes the vibrational state of both the bond and the photon. The resultant photon will have a different energy to the incident photon. This energy change is known as a Raman shift and is specific to each species of intermolecular bond. A Raman spectrometer collects all the photons with shifted wavelengths to produce a spectrum. The Raman spectrum is a plot of light scattering intensity against Raman shift. In the same way as FTIR, a Raman spectrum is a direct function of the molecular composition of the sample in question and therefore an objective measure of the pathology present.

Molecular vibrations may be either infrared or Raman active or both, therefore the techniques may be used together to gain a greater understanding of a samples molecular structure. Key technical differences between the techniques are highlighted in table 1.6.

Raman spectroscopy has demonstrated considerable potential in the identification of epithelial cancers[189]. In the urological field, Crow *et al* have demonstrated that Raman spectroscopy is capable of accurately identifying and grading bladder cancer and prostate cancer *in vitro*[190]. The potential of Raman spectroscopy for *in vivo* application has also been demonstrated by utilising a fibre-optic probe *in vitro* to distinguish between prostate and bladder malignancies[191]. A modification to the Raman

spectrometer called Kerr-gating has also demonstrated significant promise in increasing the sensitivity of Raman signal in the analysis of dark urological tissues[192]. The Kerr gate is a high speed shutter that limits the majority of fluorescence which can significantly affect the Raman signal collected in routine analysis. Kerr gating has allowed early work into depth profiling of prostate and bladder tissue with potential application in targeting prostate biopsies.

Currently in urological tissue analysis, high quality infrared spectra are quicker to obtain than Raman spectra *in vitro*, developments in technology have allowed FTIR spectral imaging of samples to be performed, the benefit of this will be explored in this thesis. Raman has great potential as a probe, *in vivo*, application due to its spectra not being affected significantly by water and will no doubt be complementary as an optical technique *ex vivo* to FTIR.

Raman Spectroscopy	Mid-Infrared spectroscopy
Uses higher energy light photons in the form of a laser and measures the difference between ground state and first vibrational state by subtracting the energy of the inelastically scattered photon from the incident photon	Uses low energy infrared light photons to result in a direct excitation of a molecule to its first vibrational state. The energy of the photon achieving this is identical to the energy difference between ground state and first vibrational state
Results from a change in the polarizability of the electron cloud around the molecule	Results from absorptions caused by change in dipole moment
The Raman spectrometer displays the result of Raman scattering as a spectrum. The shift in energy from that of the laser beam is calculated by subtracting the scattered energy from the incident energy. The scattered light is collected by the spectrometer and the y axis represents scattered light detected versus wavenumber on the x axis. The maximum light detected is at the top of the trace	In Infrared absorption spectra the y axis is the amount of light absorbed and the x axis wavenumber. The peaks represent the light energy absorbed by the molecule. Maximum absorbance is at the highest point of the trace. In transmittance maximum absorbance is at the lowest point of the trace.
Region of interest 3600-200 cm^{-1}	Region of interest 4000-400cm^{-1}
Water does not significantly interfere in near infrared Raman	Water interferes in infrared spectroscopy as it is absorbed in the mid ir wavelengths
Hydroxyl and amine stretch groups in addition to carbonyl groups are weakly determined in Raman. However the C=C bond is strongly determined in Raman.	Hydroxyl and amine stretch groups in addition to carbonyl groups are strong in infrared spectroscopy. The C=C bond does not feature in an infrared spectrum.

Table 1.6 Contrasting features of infrared and Raman spectroscopy

1.8.2 Magnetic Resonance Spectroscopy

Magnetic resonance spectroscopy (MR spectroscopy) is a technique which is able to determine the concentrations of organic compounds *in vivo*. MR spectroscopy is a theoretically complex tool based on the quantum mechanics of magnetic properties of an atom's nucleus. Most of the atoms within samples placed within a magnetic field will spin along the axis of the field. The energy states of these atoms can be altered by changing the magnetic field from low energy spinning to high energy spinning. MR spectroscopy measures the energy difference between these states and produces a spectrum. Each individual atom will have its own characteristic spin.

The technique is acknowledged to have the potential to provide diagnostic and prognostic information. The MR fingerprint from samples of the cervix[193], brain[194], thyroid[195], colon[196], ovary[197], breast[198], oesophagus[199] and liver[200] have detected and differentiated between disease with sensitivities and specificities of greater than 95%. Magnetic resonance spectroscopy has also been piloted to assess prognosis in human cancers[201, 202].

The technique has been applied to the prostate with success in differentiating benign and malignant pathologies. Choline, creatinine, citrate, myo-inositol, lipid, spermine and lysine have all been found to be useful in distinguishing the various patterns of prostatic disease[203,204,205,206,207,208,209,210]. MR spectroscopy has also demonstrated the capacity to be able to profile tumour location. Work is now being pursued to reproducibly characterize prostate cancer.

The technique has demonstrated limitations in classifying central and transitional zone tumours but is likely to be a promising adjunct in the preoperative staging of prostate cancer. It is unlikely to be in direct competition with infrared spectroscopy as a diagnostic pathology tool.

1.8.3 Optical Coherence Tomography

Optical coherence tomography (OCT) obtains high resolution cross-sectional imaging of human tissue. OCT works in a similar way to ultrasound; when light from a pulsed laser or superluminescent diode is directed at a tissue, it is reflected or backscattered by structures within the tissue. OCT uses the estimates from the time taken for light to return from the structures to produce detailed images. OCT has demonstrated promise in differentiating the architectural morphology of urological tissue[211]. This technology is being pursued to enhance surgical precision during prostate surgery. Although early work *in vivo* has demonstrated a reasonable correlation between urological surgical perceptions and OCT images of prostate tissue, further parallel histological studies are required to validate the findings of OCT imaging[212].

1.8.4 Recent Spectroscopic Technologies Applied to the Prostate

Fluorescence spectroscopy evaluates the energy emitted by a molecule as it returns to its ground state after it has been excited by a light energy source. Emission radiation is also known as fluorescence and the emission wavelengths generally mirror the absorption spectrums. The fluorescence of a molecule is dependent on the number of emitted photons compared to the number absorbed and the time taken to return to ground state. Fluorescence may be dependent on natural endogenous properties or rely on exogenous chemicals to induce fluorescence. High frequency impedance spectroscopy uses the dielectric properties of a medium and its interaction with an external electric field to produce a spectrum. The result of a feasibility study of these novel technologies has recently been published, reporting differentiation of benign and malignant pathology with high sensitivity and specificity[213].

1.9 Aims and Objectives

A review has been presented demonstrating the clinical significance of prostate cancer and the urgent need for more sophisticated objective diagnostic and prognostic techniques. The concept of spectroscopic technologies potentially filling this role has been introduced and the limitations of previous FTIR prostate studies discussed. The body of the thesis which follows investigates the potential application of Fourier Transform Infrared spectroscopy (mid-IR) as a tissue diagnostic technique to complement histopathology by giving additional information and its potential for automation. The studies which follow are clinically based in principle encompassing the fundamental requirements of clinicians in any prostate gland investigation.

The hypothesis being tested in the studies was that FTIR has the ability to distinguish objectively between prostate pathologies.

The objectives of this study can be classified into two parts:

Part One

- Observe whether FTIR analysis can be correlated to histopathological analysis of benign, malignant and premalignant tissue in prostate studies.
- Observe whether the ability of FTIR to classify pathologies is affected or changed by type of prostate tissue sample studied. Tissue from radical prostatectomy, trans-urethral resection of the prostate and prostate core biopsies (all possible clinically relevant samples) have been included in this study.
- Observe the effects of fixation on FTIR analysis contrasted with analysis after the fixative has been removed, using the same sample to ensure an appropriate control.
- Observe the contrast between FTIR analysis of tissue which has been fixed against fresh frozen tissue.

Part Two

- If there are significant biochemical differences between prostate pathologies, evaluate whether they are transferable between tissue samples
- To apply parametric non negative least squares analysis to the spectra obtained to attempt to gain further understanding of these differences and the carcinogenesis process

1.10 References

[1] International Agency for Research on Cancer. *GLOBOCAN 2002 database: Cancer Incidence, Mortality and Prevalence Worldwide (2002 estimates).* Cancer Mondial *http://www.dep.iarc.fr* (accessed 15th December 2008)

[2] Sooriakumaran P, Lovell DP, Henderson A, Denham P, Langley SEM, Laing RW. Gleason scoring varies among pathologists and this affects clinical risk in patients with prostate cancer. *Clinical Oncology* 2005, 17(8): 655-658

[3] Melia J, Moseley R, Ball RY, Griffiths DFR, Grigor K, Harnden P, Jarmulowicz M, McWilliam LJ, Montironi R, Waller M, Moss S, Parkinson MC. A UK-based investigation of inter- and intra- observer reproducibility of Gleason grading of prostatic biopsies. *Histopathology* 2006, 48(6): 644-654

[4] Allsbrook WC, Mangold KA, Johnson MH, Lane RB, Lane CG, Epstein JI. Interobserver reproducibility of Gleason grading of prostatic carcinoma: general pathologist. *Human Pathology* 2001, 32(1): 81-88

[5] Allsbrook WC, Mangold KA, Johnson MH, Lane RB, Lane CG, Amin MB, Bostwick DG, Humphrey PA, Jones EC, Reuter VE, Sakr W, Sesterhenn IA, Troncoso P, Wheeler TM, Epstein JI. Interobserver reproducibility of Gleason grading of prostatic carcinoma: urologic pathologists. *Human Pathology* 2001, 32(1): 74-80

[6] Shingleton B. Prostatic hyperplasia. In: *Urology Board Review: Pearls of Wisdom*, 2nd Ed, by Stephen W Leslie. New York: McGraw Hill, 2006: 200

[7] Moore KL, Agur AM. *Essential clinical anatomy,* 1st Ed. Baltimore: Lippincott Williams & Wilkins, 1995

[8] Grey, Henry. *Anatomy of the Human Body*. Philadelphia: Lea & Febiger, 1918. www.bartleby.com/107/illus1135.html (accessed 10th September 2009)

[9] Clegg EJ. The vascular arrangements within the human prostate gland. *British Journal of Urology* 1956, 28:428-435

[10] Vaalasti A, Hervonen A. Autonomic innervation of the human prostate. *Investigative Urology* 1980, 17:293-297

[11] De Marzo AM, Platz EA, Sutcliffe S, Jianfeng X, Gronberg H, Drake CG, Nakai Y, Issacs WB. Inflammation in prostate carcinogenesis. *Nature Reviews Cancer* 2007, 7: 256-269. Adaptation of illustration of sagittal and transverse prostate views illustrating McNeal's zonal anatomy (accessed 10th September 2009)

[12] McNeal JE. Regional morphology and pathology of the prostate. *American Journal of Clinical Pathology* 1968, 49(3): 347-357

[13] McNeal JE. The prostate and the prostatic urethra: a morphological synthesis. *The Journal of Urology* 1972, 107(6): 1008-1016

[14] McNeal JE. Normal histology of the prostate. *American Journal of Surgical Pathology* 1988, 12(8): 619-633

[15] McNeal JE, Price HM, Redwine EA, Freiha FS, Stamey TA. Stage A versus stage B Adenocarcinoma of the prostate: morphological comparison and biologic significance. *The Journal of Urology* 1988, 139(1): 61-65

[16] Support Cells and the Extracellular Matrix. In: *Human Histology*, 2nd Ed, by A Stevens, J Lowe. Edinburgh: Harcourt Publishers, 1997: 49-64

[17] Pontes EJ. Biological markers in prostate cancer. *The Journal of Urology* 1983, 130: 1037-1047

[18] Leung CS, Srigley JR. Distribution of lipochrome pigment in the prostate gland: biological and diagnostic implications. *Human Pathology* 1995, 26(12): 1302-1307

[19] Brandes D, Bourne GH. Histochemistry of the human prostate gland: normal and neoplastic. *The Journal of Pathology and Bacteriology* 1956, 71(1): 33-36
[20] Reese JH, McNeal JE, Redwine EA, Samloff IM, Stamey TA. Differential distribution of pepsinogen II between the zones of the human prostate and the seminal vesicle. *The Journal of Urology* 1986, 136(5): 1148-1152
[21] Reese JH, McNeal JE, Redwine EA, Stamey TA, Freiha FS. Tissue type plasminogen activator as a marker for functional zones, within the human prostate gland. *Prostate* 1988, 12(1): 47-53
[22] McNeal JE, Leav I, Alroy J, Skutelsky E. Differential lectin staining of central and peripheral zones of the prostate and alterations in dysplasia. *American Journal of Clinical Pathology* 1988, 89(1): 41-48
[23] Barry MJ, Fowler FJ Jr, O'Leary MP, Bruskewitz RC, Holtgrewe HL, Mebust WK, Cockett AT. The American Urological Association symptom index for benign prostatic hyperplasia. The Measurement Committee of the American Urological Association. *The Journal of Urology* 1992, 148(5): 1549-1557.
[24] Stevens A, Lowe J. *Pathology*, 2nd ed. London: Mosby, 2000
[25] National High Magnetic Field Laboratory (NHMFL) *Human Pathology Digital Image Library* www.microscopyu.com (accessed 15th November 2009)
[26] Chute CG, Panser LA, Girman CJ, Oesterling JE, Guess HA, Jacobsen SJ, Lieber MM. The prevalence of prostatism: a population-based survey of urinary symptoms. *The Journal of Urology* 1993, 150(1): 85-89
[27] Berry SJ, Coffey DS, Walsh PC, Ewing LL. The development of human benign prostatic hyperplasia with age. *The Journal of Urology* 1984, 132(3):474-479
[28] Donovan JL, Kay HE, Peters TJ, Abrams P, Coast J, Matos-Ferreira A, Rentzhog L, Bosch JL, Nordling J, Gajewski JB, Barbalias G, Schick E, Silva MM, Nissenkorn I, de la Rosette JJ. Using the ICSOoL to measure the impact of lower urinary tract symptoms on quality of life: evidence from the ICS-'BPH' study. International Continence Society – Benign Prostatic Hyperplasia. *British Journal of Urology* 1997, 80(5): 712-721
[29] McConnell JD, Roehrborn CG, Bautista OM, Andriole GL Jr, Dixon CM, Kusek JW, Lepor H, McVary KT, Nyberg LM Jr, Clarke HS, Crawford ED, Diokno A, Foley JP, Foster HE, Jacobs SC, Kaplan SA, Kreder KJ, Lieber MM, Lucia MS, Miller GJ, Menon M, Milam DF, Ramsdell JW, Schenkman NS, Slawin KM, Smith JA. The long-term effect of doxazosin, finasteride, and combination therapy on the clinical progression of benign prostatic hyperplasia. *New England Journal of Medicine* 2003, 349(25): 2387-2398
[30] Emberton M, Neal DE, Black N, Harrison M, Fordham M, McBrien MP, Williams RE, McPherson K, Devlin HB. The National Prostatectomy Audit: the clinical management of patients during hospital admission. *British Journal of Urology* 1995; 75(3): 301-316
[31] Collins MM, Stafford RS, O'Leary MP, Barry MJ. How common is prostatitis? A national survey of physician visits. *The Journal of Urology* 1998, 159(4): 1224-1228
[32] Young RH, Srigley JR, Amin MB, Ulbright TM, Cubilla AL. *Atlas of Tumour Pathology. 3rd series, Fascicle 28: Tumours of the Prostate Gland, Seminal Vesicles, Male Urethra and Penis.* Washington DC: Armed Forces Institute of Pathology, 1998
[33] Bostwick DG. Premalignant lesions of the prostate. *Seminars in Diagnostic Pathology* 1988, 5(3): 240-253
[34] Bostwick DG. Prostatic intraepithelial neoplasia (PIN): current concepts. *Journal of Cellular Biochemistry. Supplement* 1992, 16H: 10-19

[35] Amin MB, Ro JY, Ayala AG. Putative precursor lesions of prostatic adenocarcinoma: fact or fiction? *Modern pathology: an official journal of the United states and Canadian Academy of Pathology, Inc*.1993, 6(4): 476-483
[36] Bostwick DG, Brawer MK. Prostatic intra-epithelial neoplasia and early invasion in prostate cancer. *Cancer* 1987, 59(4):788-794
[37] Drago JR, Mostofi FK, Lee F. Introductory remarks and a workshop summary. *Urology Supplement* 1989, 34:2-3
[38] Sakr WA, Grignon DJ, Crissman JD, Heilbrun LK, Cassin BJ, Pontes JJ, Haas GP. High grade prostatic intraepithelial neoplasia (HGPIN) and prostatic adenocarcinoma between the ages of 20-69: an autopsy study of 249 cases. *In Vivo* 1994, 8(3): 439-443
[39] Kovi J, Mostofi FK, Heshmat MY, Enterline JP. Large acinar atypical hyperplasia and carcinoma of the prostate. *Cancer* 1988, 61(3): 555-561
[40] Srigley J, King S, Van Nostrand AWP, Robinette M. The "preneoplastic" prostate: a giant-section whole-organ study of 72 radical prostatectomies. Laboratory Investigation 1986, 54(1): 30 A
[41] Humphrey, Peter A. *Prostate Pathology*. Chicago: American Society of Clinical Pathology, 2003.
[42] UROlog: The Urology Website. *http://www.urolog.nl* (accessed 10th December 2009)
[43] Bostwick DG. High grade prostatic intraepithelial neoplasia: the most likely precursor of prostate cancer. *Cancer* 1995, 75: 1823-1836
[44] Quinn BD, Cho KR, Epstein JI. Relationship of severe dysplasia to stage B adenocarcinoma of the prostate. *Cancer* 1990, 65(10): 2328-2337.
[45] Tronsco P, Babaian RJ, Ro JY, Grignon DJ, Von Eschenbach AC, Ayala AG. Prostatic intraepithelial Neoplasia and invasive prostatic Adenocarcinoma in cystoprostatectomy specimens. Urology 1989. 34 (Supplement): 52-56
[46] McNeal JE, Reese JH, Redwine EA et al. Cribriform Adenocarcinoma of the prostate. Cancer 1986. 58: 1714
[47] Beckman WC Jr, Camps JL Jr, Weissman RM, Kaufman SL, Sanofsky SJ, Reddick RL, Siegal GP. The epithelial origin of a stromal cell population in adenocarcinoma of the rat prostate. *American Journal of Pathology* 1987, 128(3): 555-565
[48] Bostwick DG, Meiers I. Atypical Small Acinar Proliferation in the Prostate: Clinical Significance in 2006. *Archives of Pathology and Laboratory Medicine* 2006, 130: 952-957
[49] Iczkowski KA, MacLennan GT, Bostwick DG. Atypical small acinar proliferation suspicious for malignancy in prostate needle biopsies: clinical significance in 33 cases. *The American Journal of Surgical Pathology* 1997, 21(12): 1489-1495
[50] Bostwick, DG and Foster CS. Examination of radical prostatectomy specimens: therapeutic and prognostic significance. In: *Pathology of the Prostate,* edited by DG Bostwick, CS Foster. Philadelphia: WB Saunders, 1997, p.172-189
[51] Brennick JB, O'Connell JX, Dickersin GR, Pilch BZ, Young RH. Lipofuscin pigmentation (so-called "melanosis") of the prostate. *American Journal of Surgical Pathology* 1994, 18: 446-454
[52] Ro JY, Ayala AG, Ordonez NG, Cartwright J Jr, Mackay B. Intraluminal crystalloids in prostatic adenocarcinoma immunohistochemical, electron microscopic, and X-ray microanalytic studies. *Cancer* 1986, 57(12): 2397-2407
[53] Epstein JI. Diagnostic criteria of limited adenocarcinoma of the prostate on needle biopsy. *Human Pathology* 1995, 26(2): 223-229

[54] Murphy GP, Busch C, Abrahamsson PA, Epstein JI, McNeal JE, Miller GJ, Mostofi FK, Nagle RB, Nordling S, Parkinson C *et al*. Histopathology of localised prostate cancer. Consensus Conference on Diagnosis and Prognostic Parameters in Localized Prostate Cancer. Stockholm, Sweden, May 12-13, 1993. *Scandinavian Journal of Urology and Nephrology. Supplementum* 1994, 162: 7-42
[55] Gleason DF, Mellinger GT. Prediction of prognosis for prostatic adenocarcinoma by combined histological grading and clinical staging. *The Journal of Urology* 1974, 111(1): 58-64
[56] Mostofi FK, Davis CJ, Sesterhenn IA & Sobin LH. *World Health Organisation International Histological Classification of Tumours: Histological Typing of Prostate Tumours*, 2nd ed. New York: Springer-Verlag, 2002.
[57] Pan CC, Potter SR, Partin AW, Epstein JI. The prognostic significance of tertiary Gleason patterns of higher grade in radical prostatectomy specimens: a proposal to modify the Gleason grading system. *The American Journal of Surgical Pathology* 2000, 24(4): 563-569
[58] Amin M, Boccon-Gibod L, Egevad L, Epstein JI, Humphrey PA, Mikuz G, Newling D, Nilsson S, Sakr W, Srigley JR, Wheeler TM, Montironi R. Prognostic and predictive factors and reporting of prostate carcinoma in prostate needle biopsy specimens. *Scandinavian Journal of Urology and Nephrology. Supplementum* 2005, 216: 20-33
[59] Cote RJ, Taylor CR. Prostate, bladder and kidney. In: *Immunomicroscopy: A Diagnostic Tool for the Surgical Pathologist.* 2nd ed, edited by CR Taylor, RJ Cote. Philadelphia: WB Saunders, 1994, p.256-276
[60] Goel A, Abou-Ellela A, DeRose PB, Cohen C. The prognostic significance of proliferation in prostate cancer: an image cytometric quantitation of MIB-1. *Journal of Urologic Pathology* 1996, 4: 213-225
[61] Wiatrowska BA, Robertson S, Crook JM. Measures of proliferative activity in prostatic adenocarcinoma. *Journal of Urologic Pathology* 1997, 6: 131-138
[62] Ghosh D, Barette TR, Rhodes D, Chinnaiyan AM. Statistical issues and methods for meta-analysis of microarray data: a case study in prostate cancer. *Functional & Integrative Genomics* 2003, 3(4): 180-188
[63] Oyama T, Allsbrook WC Jr, Kurokawa K, Matsuda H, Segawa A, Sano T, Suzuki K, Epstein JI. A comparison of interobserver reproducibility of Gleason grading of prostatic carcinoma in Japan and the United States. *Archives of Pathology and Laboratory Medicine* 2005, 129(8): 1004-1010
[64] Egevad L, Allsbrook WC, Epstein JI. Current practice of Gleason grading among genitourinary pathologists. *Human Pathology* 2005, 36(1): 5-9
[65] Kronz JD, Silberman MA, Allsbrook WC, Epstein JI. A web-based tutorial improves practicing pathologists' Gleason grading of images of prostate carcinoma specimens obtained by needle biopsy: validation of a new medical education paradigm. *Cancer* 2000, 89(8): 1818-1823
[66] Kronz JD, Silberman MA, Allsbrook WC Jr *et al*. Pathology residents' use of a Web-based tutorial to improve Gleason grading of prostate carcinoma on needle biopsies. *Human Pathology* 2000; 31(9): 1044-1050
[67] Jemal A, Siegel R, Ward E *et al*. Cancer statistics, 2006. *CA: A Cancer Journal for Clinicians* 2006, 56(2): 106-130
[68] Cancer Research UK (2008). *CancerStats: Prostate Cancer UK - 2008 Report* (WWW document). *http://www.cancerresearchuk.org* (accessed 10th November 2009)

[69] Northern Ireland Cancer Registry (2008). *Cancer Incidence and Mortality*. (WWW document) *http://www.qub.ac.uk/research-centres/nicr* (accessed 10th November 2009)
[70] Welsh Cancer Intelligence and Surveillance Unit (2009). *Trends in Incidence, 1985-2007* (WWW document) *http://www.wales.nhs.uk/sites3/page.cfm?orgid=242&pid=27758* (accessed 10th November 2009)
[71] NHS Scotland Information Services Division (2009). *Cancer of the prostate: ICD-10 C61: Summary of Incidence* (WWW document) *http://www.isdscotland.org/isd* (accessed 10th November 2009)
[72] Office for National Statistics, Cancer Statistics Registration: *Registrations of cancer diagnosed in 2005*, England Series MB1 no.36. London: National Statistics, 2008.
[73] Selley SD, Donovan J, Faulkner A, Coast J, Gillatt D. Diagnosis, management and screening of early localised prostate cancer. *Health Technology Assessment* 1997, 1(2):(whole volume)
[74] McGregor M, Hanley JA, Boivin JF, McLean RG. Screening for prostate cancer: estimating the magnitude of over detection. *Canadian Medical Association Journal* 1998, 159(11): 1368-1372
[75] Office for National Statistics. *Mortality statistics: Cause 2007-2008*. London: National Statistics, 2009.
[76] Hankey BF, Feuer EJ, Clegg LX *et al*. Cancer surveillance series: interpreting trends in prostate cancer - Part I: Evidence of the effects of screening in recent prostate cancer incidence, mortality and survival rates. *Journal of the National Cancer Institute* 1999, 91(12): 1017-1024
[77] AJ Swedlow, I dos Santos Silva, & R Doll. *Cancer Incidence & Mortality in England & Wales: Trends and Risk Factors*. London: Oxford University Press, 2001.
[78] Coleman M *et al*. *Cancer Survival Trends in England & Wales, 1971-1995: Deprivation & NHS Region*. London: The Stationery Office, 1999
[79] Coleman M, Rachet B, Woods LM *et al*. Trends in socioeconomic inequalities in cancer survival in England and Wales up to 2001. *British Journal of Cancer* 2004, 90(7): 1367-1373
[80] Albertson PC, Hanley JA, Barrows GH, Penson DF, Kowalczyk PD, Sanders MM, Fine J. Prostate Cancer and the Will Rodgers phenomenon. *Journal of the National Cancer Institute* 2005, 97(17): 1248-1253
[81] Cancer Research UK (2009). *Age-specific mortality rates: Prostate Cancer, UK, 1971-2007* figure 2.4 in Prostate Cancer UK Mortality Statistics (WWW document) *http://www.cancerresearchuk.org.uk* (accessed 12th November 2009)
[82] Johns LE, Houlston RS. A systematic review and meta-analysis of familial prostate cancer risk. *BJU International* 2003, 91(9): 789-794
[83] Ben-Shlomo Y, Evans S, Ibrahim F *et al*. The risk of prostate cancer amongst black men in the United Kingdom: the PROCESS cohort study. *European Urology* 2008, 53(1): 99-105
[84] Key TJ, Appleby PN, Travis RC *et al*. Plasma carotenoids, retinol, and tocopherols and the risk of prostate cancer in the European Prospective Investigation into Cancer and Nutrition study. *The American Journal of Clinical Nutrition* 2007, 86(3): 672-681
[85] Rohrmann S, Genkinger JM, Burke A *et al*. Smoking and risk of fatal prostate cancer in a prospective U.S. study. *Urology* 2007, 69(4): 721-725

[86] Renehan AG, Tyson M, Egger M *et al*. Body-mass index and incidence of cancer: a systematic review and meta-analysis of prospective observational studies. *Lancet* 2008, 371(9612): 569-78
[87] Allen NE, Key TJ, Appleby PN *et al*. Serum insulin-like growth factor (IGF)-I and IGF-binding protein-3 concentrations and prostate cancer risk: results from the European Prospective Investigation into Cancer and Nutrition. *Cancer Epidemiology, Biomarkers & Prevention* 2007, 16(6): 1121-1127
[88] Kasper JS, Giovannucci E. A meta-analysis of diabetes mellitus and the risk of prostate cancer. *Cancer Epidemiology, Biomarkers & Prevention* 2006, 15(11): 2056-2062
[89] Dennis LK, Dawson DV, Resnick MI. Vasectomy and the risk of prostate cancer: a meta-analysis examining vasectomy status, age at vasectomy and time since vasectomy. *Prostate Cancer and Prostatic Diseases* 2002, 5(3): 193-203
[90] Browning DR, Martin RM. Statins and risk of cancer: a systematic review and metaanalysis. *International Journal of Cancer* 2007, 120(4): 833-843
[91] Platz EA, De Marzo AM, Giovannucci E. Prostate cancer association studies: pitfalls and solutions to cancer misclassification in the PSA era. *Journal of Cellular Biochemistry* 2004, 91(3): 553-571
[92] Catalona WJ, Ritchie JP, Ahmann FR, Hudson MA, Scardino PT, Flannigan RC, deKernion JB, Ratliff TL, Kavoussi LR, Dalkin BL, Waters WB, MacFarlane MT, Southwick PC. Comparison of digital rectal examination and serum prostate specific antigen in the early detection of prostate cancer: results of a multicenter clinical trial of 6,630 men. *Journal of Urology* 1994, 151(5): 1283-1290
[93] Wang MC, Valenzuela LA, Murphy GP, Chu TM. Purification of a human prostate specific antigen. *Investigative Urology* 1979, 17(2): 159-163
[94] Semjonow A, Brandt B, Oberpenning F, Roth S, Hertle L. Discordance of assay methods creates pitfalls for the interpretation of prostate-specific antigen values. *The Prostate. Supplement* 1996, 7: 3-16
[95] Partin AW, Criley SR, Subong EN, Zincke H, Walsh PC, Oesterling JE. Standard versus age-specific prostate specific antigen reference ranges among men with clinically localized prostate cancer: A pathological analysis. *Journal of Urology* 1996 155(4): 1336-1339
[96] Thompson IM, Pauler DK, Goodman PJ, Tangen CM, Lucia MS, Parnes HL, Minasian LM, Ford LG, Lippman SM, Crawford ED, Crowley JJ, Coltman CA Jr. Prevalence of prostate cancer among men with a prostate-specific antigen level < or =4.0ng per milliliter. *New England Journal of Medicine* 2004; 350(22): 2239-2246
[97] Stamey T, Yang N, Hay AR, McNeal JE, Freiha FS, Redwine EA. Prostate-specific antigen as a serum marker for adenocarcinoma of the prostate. *New England Journal of Medicine* 1987, 317(15): 909-916
[98] Stamey TA, Kabalin JN. Prostate specific antigen in the diagnosis and treatment of adenocarcinoma of the prostate. I. Untreated patients. *Journal of Urology* 1989, 141(5): 1070-1075
[99] Stamey TA, Caldwell, McNeal JE, Nolley R, Hemenez M, Downs J. The prostate specific antigen era in the United States is over for prostate cancer: what happened in the last 20 years? *Journal of Urology* 2004, 172(4): 1297-1301
[100] DeMarzo AM, Nelson WG, Isaacs WB, Epstein JI. Pathological and molecular aspects of prostate cancer. *The Lancet* 2003, 361(9631): 955-964

[101] Thompson IM, Ankerst DP, Chi C, Goodman PJ, Tangen CM, Lucia MS *et al*. Assessing prostate cancer risk: results from the Prostate Cancer Prevention Trial. *Journal of the National Cancer Institute* 2006, 98(8): 529-534
[102] Catalona WJ, Partin AW, Slawin KM, Brawer MK, Flanigan RC, Patel A, Ritchie JP, deKernion JB, Walsh PC, Scardino PT, Lange PH, Subong EN, Parson RE, Gasior GH, Loveland KG, Southwick PC. Use of the percentage of free prostate-specific antigen to enhance differentiation of prostate cancer from benign prostatic disease: a prospective multicenter clinical trial. *The Journal of the Medical Association* 1998, 279(19): 1542-1547
[103] Wilson JMG, Jungner G. Principles and practice of screening for disease. *Public Health Papers No. 34*. Geneva: World Health Organisation, 1968.
[104] Andriole GL, Crawford ED, Grubb RL 3rd, Buys SS, Chia D, Church TR *et al*. Mortality results from a randomized prostate-cancer screening trial. *New England Journal of Medicine* 2009, 360(13): 1310-1319
[105] Ross LE, Berkowitz Z, Ekwueme DU. Use of the prostate-specific antigen test among U.S. men: findings from the 2005 National Health Interview Survey. *Cancer Epidemiology, Biomarkers & Prevention* 2008, 17(3): 636-644
[106] Schroder FH, Hugosson J, Roobol MJ, Tammela TL, Ciatto S, Nelen V *et al.* Screening and prostate-cancer mortality in a randomized European study. *New England Journal of Medicine* 2009, 360(13): 1320-1328
[107] de Kok JB, Verhaegh GW, Roelofs RW, Hessels D, Kiemeney LA, Aalders TW *et al*. DD3(PCA3), a very sensitive and specific marker to detect prostate tumours. *Cancer Research* 2002, 62(9): 2695-2698
[108] Fradet Y, Saad F, Aprikian A, Dessureault J, Elhilali M, Trudel C *et al*. uPM3, a new molecular urine test for the detection of prostate cancer. *Urology* 2004, 64(2): 311-315
[109] Tomlins SA, Rhodes DR, Perner S, Dhanasekaran SM, Mehra R, Sun XW *et al*. Recurrent fusion of TMPRSS2 and ETS transcription factor genes in prostate cancer. *Science* 2005, 310(5748): 644-648
[110] Adam BL, Qu Y, Davis JW, Ward MD, Clements MA, Cazares LH *et al.* Serum protein fingerprinting coupled with a pattern-matching algorithm distinguishes prostate cancer from benign prostate hyperplasia and healthy men. *Cancer Research* 2002, 62(13): 3609-3614
[111] Grizzle WE, Semmes OJ, Basler J, Izbicka E, Feng Z, Kagan J *et al*. The early detection research network surface-enhanced laser desorption and ionization prostate cancer detection study: A study in biomarker validation in genitourinary oncology. *Urologic Oncology* 2004, 22(4): 337-343
[112] Wang X, Yu J, Sreekumar A, Varambally S, Shen R, Giacherio D *et al*. Autoantibody signatures in prostate cancer. *New England Journal of Medicine* 2005, 353(12): 1224-1235
[113] Hara N, Kasahara T, Kawasaki T, Bilim V, Obara K, Takahashi K, Tomita Y. Reverse transcription-polymerase chain reaction detection of prostate-specific antigen, prostate-specific membrane antigen, and prostate stem cell antigen in one milliliter of peripheral blood: value for the staging of prostate cancer. *Clinical Cancer Research* 2002, 8(6): 1794-1799
[114] Reiter RE, Gu Z, Watabe T, Thomas G, Szigeti K, Davis E *et al*. Prostate stem cell antigen: a cell surface marker overexpressed in prostate cancer. *Proceedings of the National Academy of Sciences of the United States of America* 1998, 95(4): 1735-1740

[115] Harden SV, Sanderson H, Goodman SN, Partin AA, Walsh PC, Epstein JI *et al*. Quantitative GSTP1 methylation and the detection of prostate adenocarcinoma in sextant biopsies. *Journal of the National Cancer Institute* 2003, 95(21): 1634-1637
[116] Hoque MO, Topaloglu O, Begum S, Henrique R, Rosenbaum E, Van Criekinge W *et al*. Quantitative methylation-specific polymerase chain reaction gene patterns in urine sediment distinguish prostate cancer patients from control subjects. *Journal of Clinical Oncology* 2005, 23(27): 6569-6575
[117] Paul B, Dhir R, Landsittel D, Hitchens MR, Getzenberg RH. Detection of prostate cancer with a blood-based assay for early prostate cancer antigen. *Cancer Research* 2005, 65(10): 4097-4100
[118] Stephan C, Jung K, Nakamura T, Yousef GM, Kristiansen G, Diamandis EP. Serum human glandular kallikrein 2 (hK2) for distinguishing stage and grade of prostate cancer. *International Journal of Urology* 2006, 13(3): 238-243
[119] Stephan C, Yousef GM, Scorilas A, Jung K, Jung M, Kristiansen G *et al*. Hepsin is highly over expressed in and a new candidate for a prognostic indicator in prostate cancer. *The Journal of Urology* 2004, 171(1): 187-191
[120] Lee F, Torp-Pedersen ST, Siders DB, Littrup PJ, McLeary RD. Transrectal ultrasound in the diagnosis and staging of prostate cancer. *Radiology* 1989, 170 (3): 609-615
[121] Aus G, Ahlgren G, Bergdahl S, Hugosson J. Infection after transrectal core biopsies of the prostate – risk factors and antibiotic prophylaxis. *British Journal of Urology* 1996, 77(6): 851-855
[122] Collins GN, Lloyd SN, Hehir M, McKelvie GB. Multiple transrectal ultrasound-guided prostatic biopsies – true morbidity and patient acceptance. *British Journal of Urology* 1993, 71(4): 460-463
[123] Eichler K, Hempel S, Wilby J, Myers L, Bachmann LM, Kleijnen J. Diagnostic value of systematic biopsy methods in the investigation of prostate cancer: a systematic review. *Journal of Urology* 2006, 175(5): 1605-1612
[124] Donovan J, Hamdy F, Neal D, Peters T, Oliver S, Brindle L, Jewell D, Powell P, Gillatt D, Dedman D, Mills N, Smith M, Noble S, Lane A; ProtecT Study Group. Prostate Testing for Cancer and Treatment (ProtecT) feasibility study. *Health Technology Assessment* 2003, 7(14): 1-88
[125] Epstein JI, Herawi M. Prostate needle biopsies containing prostatic intraepithelial neoplasia or atypical foci suspicious for carcinoma: implications for patient care. *Journal of Urology* 2006, 175(3): 820-834
[126] Javidan J, Wood DP. Clinical interpretation of the prostate biopsy. *Urologic Oncology* 2003, 21(2): 141-144
[127] Heidenreich A, Bellmunt J, Bolla M, Joniau S, Mason M, Matveev V et al. EAU guidelines on prostate cancer. Part 1: screening, diagnosis and treatment of clinically localised disease. *European Urology* 2011, 59: 61-71
[128] National Institute for Health and Clinical Excellence. *Prostate Cancer: Diagnosis and Treatment. Clinical Guideline 58*, Issued February 2008. PDF format available at *http://guidance.nice.org.uk/CG58* (accessed 10th December 2009)
[129] Potosky AL, Miller BA, Albertsen PC, Kramer BS. The role of increasing detection in the rising incidence of prostate cancer. *Journal of the American Medical Association* 1995, 273(7): 548-552
[130] Parker C. Active surveillance: towards a new paradigm in the management of early prostate cancer. *The Lancet Oncology* 2004, 5(2): 101-106

[131] Department of Health. *The NHS Cancer plan: a plan for investment, a plan for reform*. London, Crown Copyright, 2000. PDF format available at *http://www.dh.gov.uk/en/Publicationsandstatistics/Publications/PublicationsPolicyandGuidance/DH_4009609* (accessed 10th December 2009)
[132] National Institute for Health and Clinical Excellence. *Referral guidelines for suspected cancer. Clinical Guideline 27,* Issued June 2005. PDF format available at *http://guidance.nice.org.uk/CG027* (accessed 10th December 2009)
[133] Department of Health. *The NHS Improvement Plan: Putting people at the heart of public services*. London, Crown Copyright, 2004. PDF format available at *http://www.dh.gov.uk/en/Publicationsandstatistics/Publications/PublicationsPolicyandGuidance/DH_DH_4084476* (accessed 10th December 2009)
[134] Hamilton LT. Managing the laboratory technical workforce. *Clinics in Laboratory Medicine* 2007, 27(4): 807-821, vi-vii
[135] Wilson LS, Tesoro R, Elkin EP, Sadetsky N, Broering JM, Latini DM, DuChane J, Mody RR, Carroll PR. Cumulative cost pattern comparison of prostate cancer treatments. *Cancer* 2007, 109(3): 518-527
[136] Reusch W. Infrared Spectroscopy. In: *Virtual Textbook of Organic Chemistry,* edited by W Reusch. Michigan State University, most recent revision 8.10.2007. Image reproduced with permission. ©1999 William Reusch, All rights reserved. *http://www.cem.msu.edu/~reusch/VirtTxtJml/Spectrpy/InfraRed/infrared.htm* (accessed 15th December 2009)
[137] Woernley DL. Infrared absorption curves for normal and neoplastic tissues and related biological substances. *Cancer Research* 1952, 12(7): 516-523
[138] Blout ER, Mellors RC. Infrared Spectra of Tissues. *Science* 1949, 110(2849): 137-138
[139] Fabian H, Naumann D. Methods to study protein folding by stopped-flow FT-IR. *Methods* 2004, 34(1): 28-40
[140] Mantsch HH, Jackson M. The Use and Misuse of FTIR Spectroscopy in the Determination of Protein Structure. *Critical reviews in Biochemistry and Molecular Biology* 1995, 30(2): 95-120
[141] Pelton JT, McLean LR. Spectroscopic methods for analysis of protein secondary structure. *Analytical Biochemistry* 2000, 277(2): 167-176
[142] Krimm S, Bandekar J. Vibrational spectroscopy and conformation of peptides, polypeptides, and proteins. *Advances in Protein Chemistry* 1986, 38: 181-364
[143] Holman HY, Martin MC, Blakely EA, Bjornstad K, McKinney WR. IR spectroscopic characteristics of cell cycle and cell death probed by synchrotron radiation based Fourier Transform IR spectromicroscopy. *Biopolymers* 2000, 57(6): 329-335
[144] Liu KZ, Schultz CP, Mohammad RM, Al Katib AM, Johnson JB, Mantsch HH. Similarities between the sensitivity to 2-chlorodeoxyadenosine of lymphocytes from CLL patients and bryostatin 1-treated WSU-CLL cells: an infrared spectroscopic study. *Cancer Letters* 1998, 127(1-2): 185-193
[145] Chirboga L, Xie P, Yee H, Vigorita V, Zarou D, Zakim D, Diem M. Infrared spectroscopy of human tissue. I. Differentiation and maturation of epithelial cells in the human cervix. *Biospectroscopy* 1998, 4: 43-53
[146] Gomez-Fernandez JC, Villalain J. The use of FT-IR for quantitative studies of the apparent pKa of lipid carboxyl groups and the dehydration degree of the phosphate group of the phospholipids. *Chemistry and Physics of Lipids* 1998, 96(1-2): 41-52

[147] N Woolf. The cell cycle. In: *Pathology: Basic and Systemic*. London: WB Saunders Company Ltd, 1998
[148] Tang DG, Porter AT. Target to apoptosis: a hopeful weapon for prostate cancer. *The Prostate* 1997, 32(4): 284-293
[149] Vaupel P, Kelleher DK, Thews O. Modulation of tumor oxygenation. *International Journal of Radiation Oncology, Biology, Physics* 1998, 42(4): 843-848
[150] Vaupel P, Mayer A. Hypoxia and anemia: effects on tumor biology and treatment resistance. *Transfusion Clinique et Biologique* 2005, 12(1): 5-10
[151] Campbell SC. Advances in angiogenesis research: relevance to urological oncology. *Journal of Urology* 1997, 158: 1633-1674
[152] Stubbs M, Bashford CL, Griffiths JR. Understanding the tumor metabolic phenotype in the genomic era. *Current Molecular Medicine* 2003, 3(1): 49-59
[153] Zieba M, Suwalski S, Kwiatkowska S *et al*. Comparison of hydrogen peroxide generation and the content of lipid peroxidation products in lung cancer tissue and pulmonary parenchyma. *Respiratory Medicine* 2000, 94(8): 800-805
[154] Sharma U, Mehta A, Seenu V, Jagannathan NR. Biochemical characterization of metastatic lymph nodes of breast cancer patients by in vitro 1H magnetic resonance spectroscopy: a pilot study. *Magnetic Resonance Imaging* 2004, 22(5): 697-706
[155] Budinova G, Salva J, Volka K. Application of molecular spectroscopy in the mid-infrared region to the determination of glucose and cholesterol in whole blood and in blood serum. *Applied Spectroscopy* 1997, 51(5): 631-635
[156] Shaw RA, Kotowich S, Mantsch HH, Leroux M. Quantitation of protein, creatinine and urea in urine by near-infrared spectroscopy. *Clinical Biochemistry* 1996, 29(1): 11-19
[157] Davis AMC. Uncertainty testing in PLS regression. *Spectroscopy Europe* 2001, 13(2): 16-19
[158] Schuster KC, Mertens F, Gapes JR. FTIR Spectroscopy applied to bacterial cells as a novel method for monitoring complex biotechnological processes. *Vibrational Spectroscopy* 1999, 19: 467-477
[159] Kirschner C, Maquelin K, Ngo Thi NA, Choo-Smith LP, Sockalingum GD, Sandt C, Ami D, Orsini F, Doglia SM, Allouch P, Mainfait M, Puppels GJ, Naumann D. Classification and Identification of Enterococci: a Comparative Phenotypic, Genotypic and Vibrational Spectroscopic Study. *Journal of Clinical Microbiology* 39(5): 1763-1770
[160] Lasch P, Haensch W, Naumann D, Diem M. Imaging of colorectal adenocarcinoma using FT-IR microspectroscopy and cluster analysis. *Biochimica et Biophysica Acta* 2004, 1688(2): 176-186
[161] Wood BR, Chiriboga L, Yee H, Quinn MA, McNaughton D, Diem M. Fourier transform infrared (FTIR) spectral mapping of the cervical transformation zone, and dysplastic squamous epithelium. *Gynaecologic Oncology* 2004, 93(1): 59-68
[162] Mordechai S, Sahu RK, Hammody Z, Mark S, Kantarovich K, Guterman H, Podshyvalov A, Goldstein J, Argov S. Possible common biomarkers from FTIR microspectroscopy of cervical cancer and melanoma. *Journal of Microscopy* 2004, 215(1): 86-91
[163] Fujioka N, Morimoto Y, Arai T, Kikuchi M. Discrimination between normal and malignant human gastric tissues by Fourier transform infrared spectroscopy. *Cancer Detection and Prevention* 2004, 28(1): 32-36

[164] Fabian H, Lasch P, Boese M, Haensch W. Mid–IR microspectroscopic imaging of breast tumour tissue sections. *Biopolymers* 2002, 67(4-5): 354-357
[165] Tfayli A, Piot O, Durlach A, Bernard P, Manfait M. Discriminating nevus and melanoma on paraffin-embedded skin biopsies using FTIR microspectroscopy. *Biochimica et Biophysica Acta* 2005, 1724(3): 262-269
[166] Lasch P, Boese M, Pacifico A, Diem M. FT-IR Spectroscopic Investigations of Single Cells on the Subcellular Level: An FT-IR spectroscopic study. *Vibrational Spectroscopy* 2002, 28(1): 147-157
[167] Kondepati VR, Keese M, Heise HM, Backhaus J. Detection of structural disorders in pancreatic tumour DNA with Fourier transform infrared spectroscopy. Vibrational Spectroscopy 2006, 40(1): 33-39
[168] Yano K, Ohoshima S, Gotou Y, Kumaido K, Moriguchi T, Katayama H. Direct measurement of human lung cancerous tissues and noncancerous tissues by fourier transform infrared microscopy: can an infrared microscope be used as a clinical tool? *Analytical Biochemistry* 2000, 287(2): 218-225
[169] Krafft C, Sobottka SB, Schackert G, Salzer R. Analysis of human brain tissue, brain tumors and tumor cells by infrared spectroscopic mapping. *The Analyst* 2004, 129(10): 921-925
[170] Gazi E, Dwyer J, Gardner P, Ghanbari-Siahkali A, Wade AP, Miyan J, Lockyer NP, Vickerman JC, Clarke NW, Shanks JH, Scott LJ, Hart CA, Brown M. Applications of Fourier transform infrared microspectroscopy in studies of benign prostate and prostate cancer. A pilot study. *The Journal of Pathology* 2003, 201(1): 99-108
[171] Takahashi S, Satomi A, Yano K *et al*. Estimations of glycogen levels in human colorectal cancer tissue: relationship with cell cycle and tumor outgrowth. *Journal of Gastroenterology* 1999, 34(4): 474-480
[172] Swinnen JV, Verhoeven G. Androgens and the control of lipid metabolism in human prostate cancer cells. *The Journal of Steroid Biochemistry and Molecular Biology* 1998, 65(1-6): 191-198
[173] Paluszkiewicz C, Kwiatek WM. Analysis of human cancer prostate tissue using FTIR microspectroscopy and SRIXE techniques. *Journal of Molecular Structure* 2001, 565-566: 329-334
[174] Paluszkiewicz C, Kwiatek WM, Banas A, Kisiel A, Marcelli A, Piccinini M. SR-FTIR spectroscopic preliminary findings of non-cancerous, cancerous and hyperplastic human prostate tissues. *Vibrational Spectroscopy* 2007, 43(1): 237-242
[175] Gazi E, Dwyer J, Lockyer NP, Miyan J, Gardner P, Hart CA, Brown MD, Clarke NW. A study of cytokinetic and motile prostate cancer cells using synchrotron-based FTIR microspectroscopic imaging. *Vibrational Spectroscopy* 2005, 38(1-2): 193-201
[176] Eckel R, Huo H, Guan HW, Hu X, Che X, Huang WD Characteristic infrared spectroscopic patterns in the protein bands of human breast cancer tissue. *Vibrational Spectroscopy* 2001, 27(2): 165-173
[177] Gazi E, Baker M, Dwyer J, Lockyer NP, Gardner P, Shanks JH, Reeve RS, Hart CA, Clarke NW, Brown MD. A correlation of FTIR spectra derived from prostate cancer biopsies with gleason grade and tumour stage. *European Urology* 2006, 50(4): 750-760
[178] Crow P, Stone N, Kendall CA *et al*. The use of Raman spectroscopy to identify and grade prostatic adenocarcinoma in vitro. *British Journal of Cancer* 2003, 89(1):106-108
[179] Baker MJ, Gazi E, Brown MD, Shanks JH, Gardner P, Clarke NW. FTIR-based spectroscopic analysis in the identification of clinically aggressive prostate cancer. *British Journal of Cancer* 2008, 99: 1859-1866

[180] German MJ, Hammiche A, Ragavan N, Tobin MJ, Cooper LJ, Matanhelia SS, Hindley AC, Nicholson CM, Fullwood NJ, Pollock HM, Martin FL. Infrared spectroscopy with multivariate analysis potentially facilitates the segregation of different types of prostate cell. *Biophysical Journal* 2006, 90(10): 3783-3795
[181] Gazi E, Dwyer J, Lockyer NP, Miyan J, Gardner P, Hart C, Brown M, Clarke NW. Fixation protocols for subcellular imaging by synchrotron-based Fourier transform infrared spectroscopy. *Biopolymers* 2005, 77(1): 18-30
[182] Harvey TJ, Gazi E, Henderson A, Snook RD, Clarke NW, Brown M, Gardner P. Factors influencing the discrimination and classification of prostate cancer cell lines by FTIR microspectroscopy. *The Analyst* 2009, 134(6): 1083-1091
[183] Malins DC, Polissar NL, Gunselman SJ. Models of DNA structure achieve almost perfect discrimination between normal prostate, benign prostatic hyperplasia (BPH), and adenocarcinoma and have a high potential for predicting BPH and prostate cancer. *Proceedings of the National Academy of Sciences of the United States of America* 1997, 94(1): 259-264
[184] Malins DC, Gilman NK, Green VM, Wheeler TM, Barker EA, Vinson MA, Sayeeduddin M, Hellstrom KE, Anderson KM. Metastatic cancer DNA phenotype identified in normal tissues surrounding metastasizing prostate carcinomas. *Proceedings of the National Academy of Sciences of the United States of America* 2004, 101(31): 11428-11431
[185] Malins DC, Gilman NK, Green VM, Wheeler TM, Barker EA, Anderson KM. A cancer DNA phenotype in healthy prostates, conserved in tumors and adjacent normal cells, implies a relationship to carcinogenesis. *Proceedings of the National Academy of Sciences of the United States of America* 2005, 102(52): 19093-19096
[186] Malins DC, Johnson PM, Barker EA, Polissar NL, Wheeler TM, Anderson KM. Cancer-related changes in prostate DNA as men age and early identification of metastasis in primary prostate tumors. *Proceedings of the National Academy of Sciences of the United States of America* 2003, 100(9): 5401-5406
[187] Fernandez DC, Bhargava R, Hewitt SM, Levin IW. Infrared spectroscopic imaging for histopathologic recognition. *Nature Biotechnology* 2005, 23(4): 469-474
[188] Stone N. Raman Spectroscopy of Biological Tissue for Application in Optical Diagnosis of Malignancy. PhD Thesis, Cranfield University: Cranfield Press, 2001
[189] Stone N, Kendall C, Smith J, Crow P, Barr H. Raman spectroscopy for identification of epithelial cancers. *Faraday Discussions* 2004, 126: 141-157
[190] Crow P, Uff JS, Farmer JA, Wright MP, Stone N. The use of Raman spectroscopy to identify and characterize transitional cell carcinoma in vitro. *BJU International* 2004, 93(9): 1232-1236
[191] Crow P, Molckovsky A, Stone N, Uff J, Wilson B, WongKeeSong LM. Assessment of fiberoptic near-infrared Raman spectroscopy for diagnosis of bladder and prostate cancer. *Urology* 2005, 65(6): 1126-1130
[192] Hart Prieto MC, Matousek P, Towrie M, Parker AW, Wright M, Ritchie AW, Stone N. Use of picosecond Kerr-gated Raman spectroscopy to suppress signals from both surface and deep layers in bladder and prostate tissue. *Journal of Biomedical Optics* 2005, 10(4): 44006-44012
[193] Delikatny EJ, Russell P, Hunter JC *et al*. Proton MR and human cervical neoplasia: ex vivo spectroscopy allows distinction of invasive carcinoma of the cervix from carcinoma in situ and other preinvasive lesions. *Radiology* 1993, 188(3): 791-796

[194] Rutter A Hugenholtz H, Saunders JK, Smith IC. Classification of brain tumours by ex vivo 1H NMR spectroscopy. *Journal of Neurochemistry* 1995, 64(4): 1655-1661
[195] Lean CL, Delbridge L, Russell P *et al*. Diagnosis of follicular thyroid lesions by proton magnetic resonance on fine needle biopsy. *Journal of Clinical Endocrinology and Metabolism* 1995, 80(4): 1306-1311
[196] Lean CL, Newland RC, Ende DA, Bokey EL, Smith IC, Mountford CE. Assessment of human colorectal biopsies by 1H MRS: correlation with histopathology. *Magnetic Resonance in Medicine* 1993, 30(5): 525-533
[197] Wallace JC, Raaphorst GP, Somorjai RL, *et al.* Classification of 1H MR spectra of biopsies from untreated and recurrent ovarian cancer using linear discriminant analysis. *Magnetic Resonance in Medicine* 1997, 38(4): 569-576
[198] Mackinnon WB, Barry PA, Malycha PL *et al*. Fine-needle biopsy specimens of benign breast lesions distinguished from invasive cancer ex vivo with proton MR spectroscopy. *Radiology* 1997, 204(3): 661-666
[199] Barry P, Wadstrom C, Falk G *et al*. What is the value of 1H MRS in detecting early malignant changes? In: *The Esophagogastric Junction*, edited by R Guili. Montrouge: John Libbey Eurotext, 1998, p. 1122-1127
[200] Soper R, Himmelreich U, Painter D, *et al*. Pathology of hepatocellular carcinoma and its precursors using proton magnetic resonance spectroscopy and a statistical classification strategies. *Pathology* 2002, 34(5): 417-422
[201] Lean CL, Somorjai RL, Smith ICP, Russell P, Mountford CE. Accurate diagnosis and prognosis of human cancers by proton MRS and a three stage classification strategy. In: *Annual Reports on NMR Spectroscopy,* edited by G Webb. London: Academic press, 2002, p. 71-111
[202] Mountford CE, Somorjai RL, Malycha P, *et al*. Diagnosis and prognosis of breast cancer by magnetic resonance spectroscopy of fine-needle aspirates analyzed using a statistical classification strategy. *The British Journal of Surgery* 2001, 88(9): 1234-1240
[203] Kurhanewicz J, Vigneron DB, Hricak H, Narayan P, Carroll P, Nelson SJ. Three-dimensional H-1 MR spectroscopic imaging of the in situ human prostate with high (0.24-0.7-cm3) spatial resolution. *Radiology* 1996, 198(3): 795-805
[204] Yacoe ME, Sommer G, Peehl D. In vitro proton spectroscopy of normal and abnormal prostate. *Magnetic Resonance in Medicine* 1991, 19(2): 429-438
[205] Cornel EB, Heerschap A, Smits GA, Oosterhof GO, Debruyne FM, Schalken JA. Magnetic resonance spectroscopy detects metabolic differences between seven Dunning rat prostate tumor sublines with different biological behaviour. *The Prostate* 1994, 25(1): 19-28
[206] Kurhanewicz J, Dahiya R, Macdonald JM, Chang LH, James TL, Narayan P. Citrate alterations in primary and metastatic human prostatic adenocarcinomas: 1H magnetic resonance spectroscopy and biochemical study. *Magnetic Resonance in Medicine* 1993, 29(2): 149-157
[207] Kurhanewicz J, Vigneron DB, Nelson SJ *et al*. Citrate as an in vivo marker to discriminate prostate cancer from benign prostatic hyperplasia and normal prostate peripheral zone: detection via localized proton spectroscopy. *Urology* 1995, 45(3): 459-466
[208] Lynch MJ, Nicholson JK. Proton MRS of human prostatic fluid: correlations between citrate, spermine and myo-inositol levels and changes with disease. *The Prostate* 1997, 30(4): 248-255

[209] Swindle P, McCredie S, Russell P, Himmelreich U, Khadra M, Lean C, Mountford C. Pathologic characterization of human prostate tissue with proton MR spectroscopy. *Radiology* 2003, 228(1): 144-151

[210] Cheng LL, Burns MA, Taylor JL, He W, Halpern EF, McDougal WS, Wu CL. Metabolic characterization of human prostate cancer with tissue magnetic resonance spectroscopy. *Cancer Research* 2005, 65(8): 3030-3034.

[211] Tearney GJ, Brezinski ME, Southern JF, Bouma BE, Boppart SA, Fujimoto JG. Optical biopsy in human urologic tissue using optical coherence tomography. *The Journal of Urology* 1997, 157(5): 1915-1919

[212] Aron M, Kaouk JH, Hegarty NJ, Colombo JR, Haber GP, Chung BI, Zhou M, Gill IS. Preliminary experience with the Niris optical coherence tomography system during laparoscopic and robotic prostatectomy. *Journal of Endourology* 2007, 21(8): 814-8

[213] Salomon G, Hess T, Erbersdobler A, Eichelberg C, Greschner S, Sobchuk A, Korolik A, Nemkovich N, Scheiber J, Herms M. The Feasibility of Prostate Cancer Detection by Triple Spectroscopy. *European Urology* 2009, 55(2) 376-384

" I think your solution is just; but why think? Why not try the experiment? "

John Hunter 1728-1793

2. Materials and Methods

Gloucestershire Local Research Ethics Committee granted ethical approval to collect prostate tissue from appropriately consented patients for FTIR spectroscopic studies (Gloucestershire Local Research Ethics Committee no. 00/159G). This section describes how samples were collected and prepared for analysis. The samples were analysed using a laboratory based bench-top Fourier Transform Infrared Microspectrometer at Gloucestershire Royal Hospital; the spectrometer and analysis methods will also be described.

2.1 Prostate Tissue Collection and Preparation

2.1.1 Transurethral Resection of the Prostate Specimens: Collection

Transurethral resection of the prostate (TURP) samples were collected at routine operating lists at Gloucestershire Royal Hospital. All patients were undergoing surgery for bladder outflow obstruction and had consented to have one of their TURP chips used for research purposes. The samples were taken using a resectoscope (Stortz 27040 DH). Figure 2.1 illustrates transurethral resection of a prostate chip. Figure 2.2 shows how multiple chips are obtained during this procedure. None of the patients were known to have prostate cancer prior to their procedure. Each prostate chip was positioned on a section of acetate paper which had been marked on one corner to enable orientation of

the sample. The acetate together with the sample was then placed in a 2ml cryogenic vial (Corning Incorporated). The vial was immediately placed into liquid nitrogen to snap freeze the sample. The sample was stored in a -80°C freezer between collection and sectioning. Each frozen sample was sectioned using a cold cryotome at approximately -28°C. Sections were 8-10μm in thickness. Consecutive sections were mounted onto a histology slide (Snowcoat X-tra, Surgipath) for standard haematoxylin and eosin staining and a calcium fluoride slide (Cystran Limited) for later FTIR analysis. The remainder of the sample was replaced in the cryogenic vial and returned to the -80°C freezer together with the mounted calcium fluoride slide pending FTIR examination. In total fifty TURP chips were collected, of which 27 TURP samples were used for the FTIR mapping studies. A relatively small number of prostate specimens were included in the final analysis due to difficulties obtaining suitable samples for FTIR analysis using the cryotome. Table 2.1 illustrates how the samples were broken down.

	Benign	**Malignant**
Pathology	BPH and stroma	Adenocarcinoma prostate
Number of Samples	23	4

Table 2.1 The pathology of the TURP samples included in study

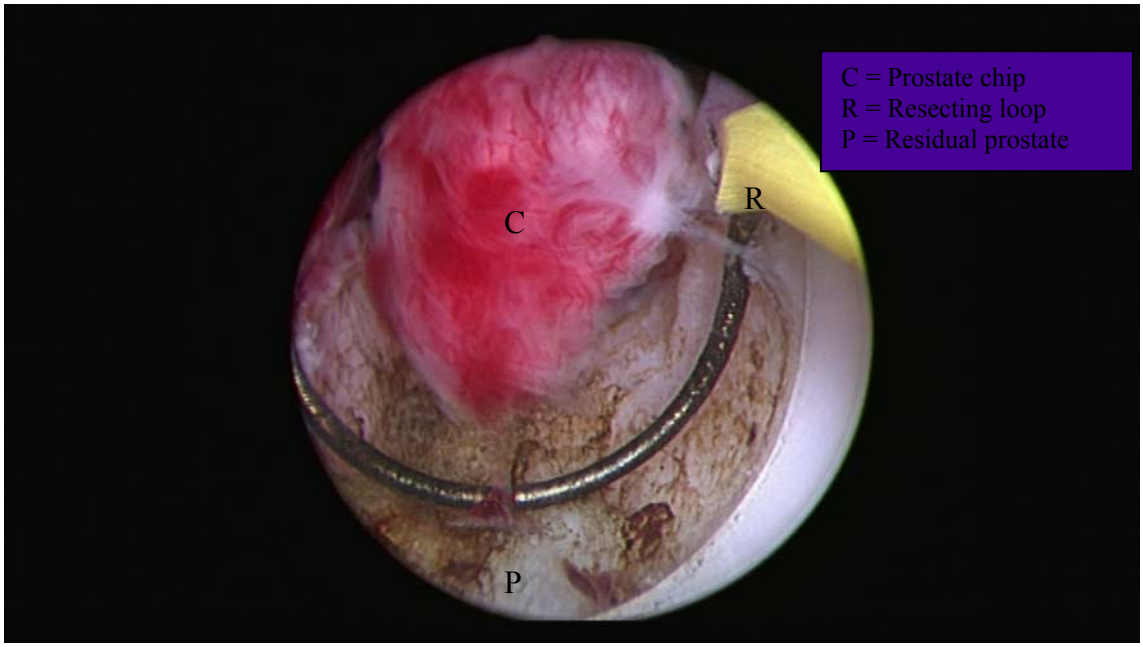

Figure 2.1 Resection of a prostate chip using electrode

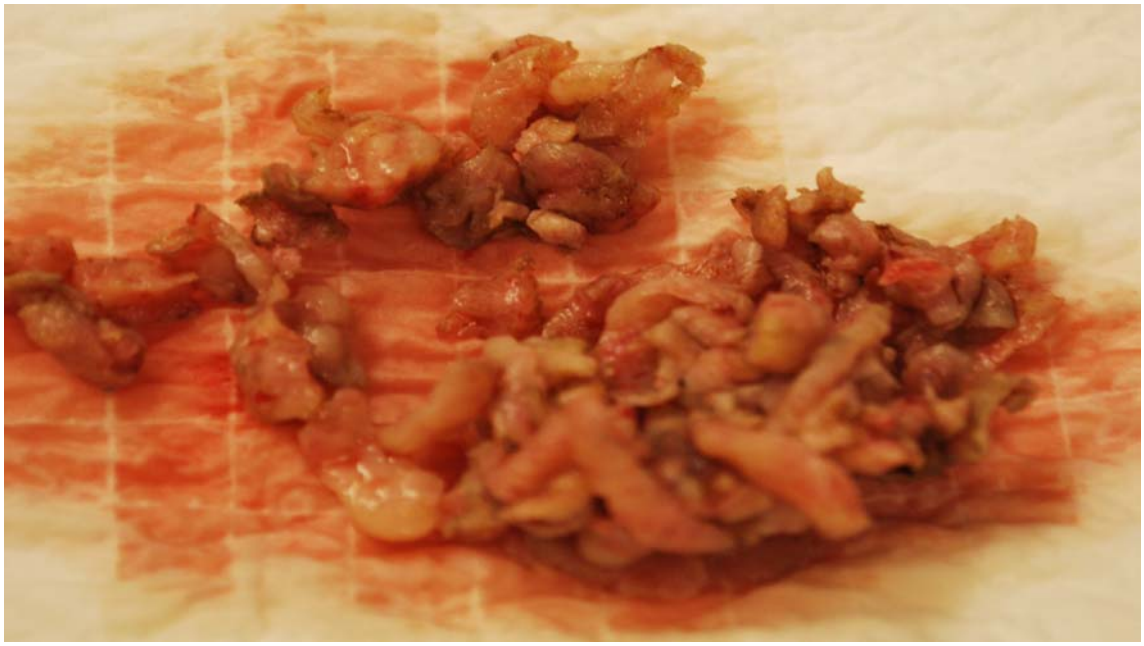

Figure 2.2 Example of total prostate tissue removed as multiple chips during TURP

2.1.2 Transrectal Ultrasound Guided Prostate Biopsy specimens: Collection

Prostate biopsy samples were collected from patients at Gloucestershire Royal Hospital and Cheltenham General Hospital. Patients attending for biopsy had been previously reviewed by a urologist and were suspected to have prostate cancer on the basis of either an elevated PSA blood test or abnormal digital rectal examination or both. All patients gave consent for an extra biopsy to be taken and used for purely research purposes. The biopsy was positioned onto a section of acetate paper, which had been marked on one corner, placed in a cryogenic vial and snap frozen in liquid nitrogen. The sample was stored in a -80°C freezer between collection and sectioning. The specimen was sectioned as described above in section (2.1.1). Of fifty biopsy samples obtained, 33 were suitable for final FTIR analysis after sectioning. Figure 2.3 illustrates a biopsy section prior to FTIR analysis. Table 2.2 details the breakdown of pathology in the 33 biopsies included in FTIR studies. Table 2.3 details the most recent PSA reported prior to TRUS biopsy (where recorded), the final formal TRUS biopsy histology and the research biopsy histology in each sample.

Pathology	No evidence of malignancy	Adenocarcinoma of the prostate	Prostatic Intraepithelial Neoplasia
Number of samples	28	4	1

Table 2.2 The pathology of prostate biopsy sections included in study

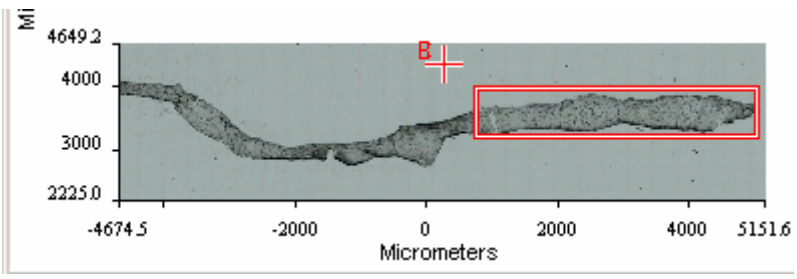

Figure 2.3 White light image of a prostate biopsy section prior to FTIR analysis

Sample No	PSA	TRUS pathology	Research biopsy
1	4.2	3+3=6, single left core	NM
2	8.5	3+3=6, multiple cores left and right	NM
4	8.5	NM	NM
5	9.0	3+4=7, multiple left cores	NM
6	288	5+3=8, multiple cores left and right	Malignancy
7	3.6	NM	NM
8		NM (2^{nd} set Bx)	NM
10	7.8	4+5=9, multiple right cores	NM
11	170	5+4=9, multiple cores left and right	Malignancy
12	8.1	PIN	NM
13	13	3+2=5, multiple cores left and right	NM
14	6.8	NM	NM
15	30	4+3=7, multiple cores left and right	NM
18	5.4	NM	NM
19	15	NM	NM
20	7.9	NM	NM
21		NM	NM
22		NM	NM
23		NM	NM
25	17	NM	NM
26	14	3+3=6, multiple right cores	NM
27	12	NM	NM
28		NM	NM
29	139	4+4=8, multiple cores left and right	Malignancy
30		3+3=6, multiple cores left and right	NM
31	8	NM	NM
32	11	3+4=7, multiple cores left and right	Malignancy
33	6.7	NM	NM
34	93	3+4=7, multiple cores left and right	NM
36		4+4=8, multiple cores left and right	NM
38	4.1	NM	NM
39	27	3+4=7, multiple left cores	PIN
42	6.2	NM	NM

Table 2.3 The characteristics of the TRUS Biopsy specimens included in study

2.1.3 Radical Prostatectomy Specimens: Collection

Patients undergoing radical prostatectomy for treatment of their prostate cancer at Gloucestershire Royal Hospital were consented for FTIR analysis of sections of their prostate after histological analysis of their prostates for formal post operative pathological staging had been completed. These samples differed from the tissue samples taken above because instead of snap freezing the prostate tissue, the prostate tissue was formalin fixed and paraffin embedded post operatively prior to histological and FTIR analysis. The analysis of this tissue forms a key part of this thesis because this represents how prostate tissue is routinely fixed and analysed in current clinical practice and the heterogeneity within each sample provides an intrinsic control for each specimen. A description of how the radical prostatectomy specimen was fixed follows below in section 2.2.3. Consecutive ten micron transverse prostate sections were taken from selected paraffin embedded blocks using a microtome, and mounted on glass and calcium fluoride slides for histological and FTIR analysis respectively. Sections were analysed by FTIR in both paraffinated and deparaffinated states. Table 2.4 details the pathology groups within each sample.

Radical prostatectomy specimen	Pathologies within specimen
1	BPH, Prostatitis, Prostatic Calculi, PIN, Gleason 4+3=7
2	BPH, Gleason 3+4=7
3	No BPH, Gleason 3+3=6
4	PIN, Gleason 4+3=7
5	BPH, Gleason 3+4=7
6	No BPH, Gleason 3+4=7
7	No BPH, PIN, Gleason 3+3=6
8	No BPH, PIN, Gleason 3+3=6
9	BPH, PIN, Gleason 3+4=7

Table 2.4 Pathology of the radical prostatectomy specimens included in the study

2.1.4 TURP, Prostate biopsy and Radical Prostatectomy Specimens: Histological Examination

The stained haematoxylin and eosin (H & E) sections were examined by a consultant uropathologist at Gloucestershire Royal Hospital, Dr Jeremy Uff. The mark placed on the specimen prior to initial snap freezing allowed sample orientation and relative mapping of locations of prostate pathology present. The pathologist defined and recorded the prostate pathologies present within the sample with the principal researcher present. If prostate cancer was identified within a specimen, a Gleason grade was assigned and the sample was re-examined by a second consultant pathologist with a special urological interest and concordance in Gleason grade agreed. The areas of

interest were marked on the H & E slides in indelible ink, relative positions of the pathologies were measured and allocated (x, y) co-ordinates relative to an orientation mark in the bottom left hand corner of the sample. The FTIR spectrometer had an inbuilt (x, y) measurement facility enabling FTIR targeting of specific areas for spectral measurements.

2.1.5 TURP, Prostate biopsy and Radical Prostatectomy Specimens: Exclusion criteria for FTIR analysis

1) H & E sections had to be of sufficient quality to allow precise histological classification which could be compared with FTIR sample analysis – where classification could not be performed the sample was excluded
2) Following cold cryotome sectioning, consecutive sections needed to be comparable to allow histological mapping – where this was not the case the sample was excluded
3) Specimens which were damaged or uneven and therefore would not allow good quality FTIR spectra to be collected were excluded from the study. Where possible adjacent consecutive specimens were analysed.

2.2 Prostate Tissue Fixation

The aim of fixation is to maintain the form and structure of tissue elements in a condition as close to *in vivo* as possible. Prostate specimens obtained by TURP, TRUS biopsy and radical prostatectomy are routinely fixed in formalin prior to histological analysis in clinical practice today. Without fixation, once the prostate tissue is removed from its blood supply autolysis (the enzymatic digestion of cells by the enzymes contained within them) and movements in intracellular water molecules will occur. Both of these factors may cause destruction of normal intracellular structures and biochemistry and thus may limit the value of FTIR analysis. In the studies which follow two methods of cell fixation have been used; flash freezing (for the biopsy and TURP specimens) and formalin fixation followed by paraffin embedding (for the radical prostatectomy specimens).

2.2.1 Flash Freezing of Prostate Tissue

Prostate tissue is hydrated when *in vivo*; when chemical reagents are used to preserve tissue their interactions to achieve dehydration invariably affect tissue biochemistry. Liquid nitrogen emersion of a sample within a cryo-vial enables a small specimen to be completely frozen in less than a second. The speed of freezing reduces the likelihood of intracellular ice crystal damage and preserves tissue biochemistry. Although studies have demonstrated in other tissues that freezing followed by drying may cause artefacts such as chemical migration and reduction in frozen cell size. Specifically in the prostate however, FTIR studies have demonstrated that valid spectra can be obtained from prostate cells or tissue which has been flash frozen[1,2]. The unstained frozen sections

used in this work were removed from the freezer and allowed to defrost and air dry for at least one hour prior to FTIR analysis.

2.2.2 Formalin Fixation of Prostate Tissue

Although many chemical fixatives exist, formalin is used universally in clinical practice for prostate and the radical prostatectomy specimens detailed in this thesis. Formalin fixation in radical prostatectomy specimens is necessary to determine the margin status, tumour volume and grade in routine histological practice[3]. The standard buffered formalin fixative is an aqueous solution containing formaldehyde 37% and methyl alcohol 10-15%. Formalin is a highly reactive dipolar compound that forms protein - nucleic acid and protein – protein crosslinks *in vitro*. Glycogen and lipids are also preserved by this process. Formalin fixation is followed by paraffin embedding in routine histological practice prior to haematoxylin and eosin staining and examination using white light microscopy[4]. Depending on the size of the gland, formalin fixation at Gloucestershire Royal Hospital takes at least 48 hours, followed by a further 24 hours for further processing and paraffin embedding. Although formalin fixation is a relatively simple process which provides superior morphological detail and consistency, it is time consuming and its limitations with respect to the potential effects of fixative cross linkage on molecular studies are acknowledged.

2.2.3 Preparation of Radical Prostatectomy Specimens for FTIR Analysis

Radical prostatectomy specimens were removed at operation, placed in buffered formalin and transferred to the pathology department at Gloucester Royal Hospital. All prostate specimens were prepared in a similar fashion. Formalin fixation of the specimen for a minimum of 48 hours was allowed. The specimen then underwent '*cut*

up' by a pathologist. At '*cut up'* the prostate was weighed, orientated and its dimensions measured. Macroscopic examination of the prostate specimen was performed. The external surface of the prostate was then marked with different colours (for example red for right, blue for left and green for base) to ensure orientation after further processing. The gland was sliced in 5mm intervals from apex up and laid in clearly labelled, consecutive individual cassettes, called blocks. The prostate sections in the blocks were then dehydrated in graded alcohols, cleared in xylene and embedded as flat as possible in paraffin wax using a processor and left to set. The Royal College of Pathologists prostate minimum dataset guidelines were adhered to in all processing steps. 10 μm sections were then harvested from selected blocks using a microtome. Consecutive sections were taken for histological and FTIR analysis respectively to enable mapping of pathology (Figures 2.4 and 2.5 respectively). To achieve deparaffination, sections were placed in a xylene bath followed by a warm water bath. Specimens were mounted on calcium fluoride slides and air dried prior to FTIR analysis. Sections for histological analysis were H & E stained.

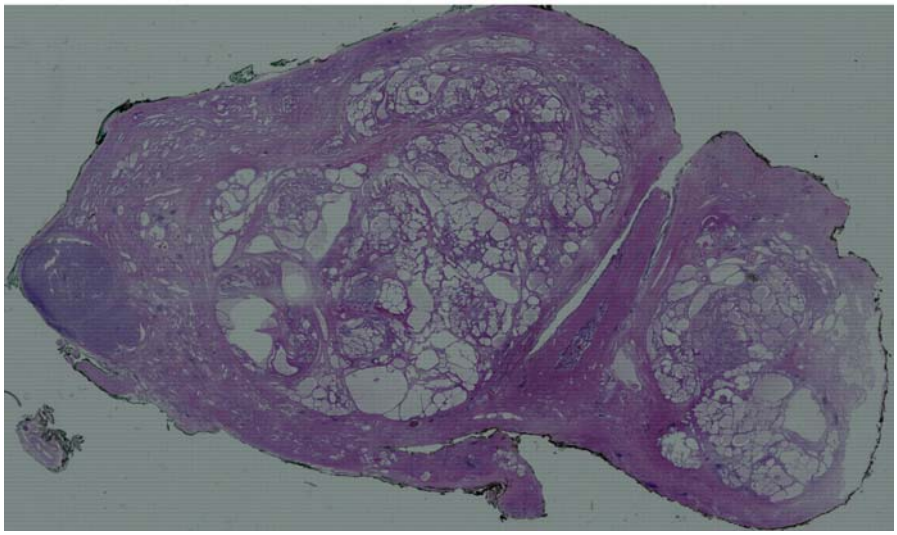

Figure 2.4 Haematoxylin & eosin stained radical prostatectomy section

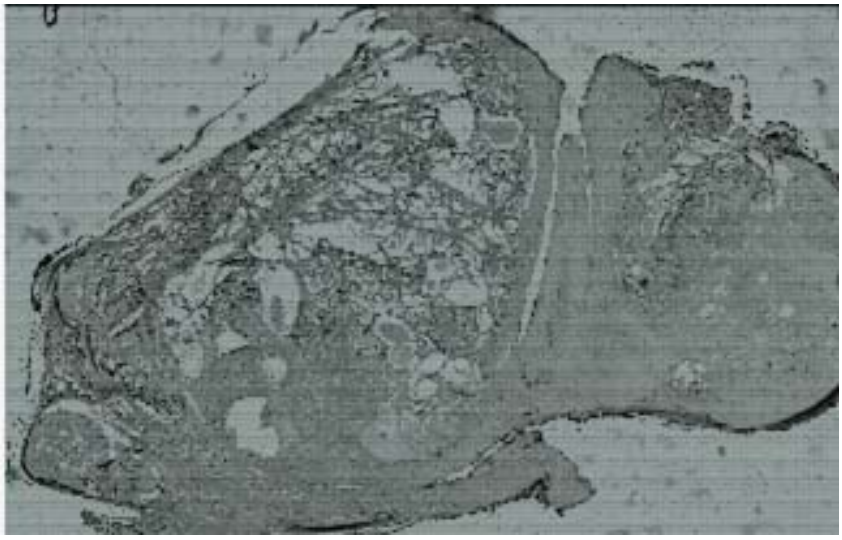

Figure 2.5 White light image of unstained prostate section corresponding to above H&E section for FTIR analysis

2.3 Fourier Transform Infrared Spectroscopy

2.3.1 Instrumentation

Prostate specimens were analysed using a Perkin Elmer® Spotlight 300 Fourier Transform Infrared Spectroscopy system in a temperature and humidity controlled laboratory (see Figure 2.6). The system consists of a liquid nitrogen cooled single point 100 x 100μm^2 mercury-cadmium-telluride (MCT) detector and 16 x 1 element (400 x 25 μm^2) MCT array detector for image and single point measurements. Resolutions achieved by the single point MCT by the MCT array detectors are 25 and 6.25 μm respectively. The spectral range covered by the array and single point detector are 7800 to 720cm^{-1} and 7800 to 580 cm^{-1} respectively. The spectrometer is attached to a microscope equipped with a CCD camera and white light LED illumination in order to view optical images of the sample. The x-y-z stage with sample holder was programmable. White light images could be collected together to construct map images. The aperture of the instrument to focus infrared light onto the sample and the cassigrain to collect the infrared light transmitted through the sample are adjustable. Settings for the FTIR studies are described below. On start-up of the FTIR spotlight spectrometer, calibration, stage and motor checks are performed automatically. Prior to measurements the liquid nitrogen cooled detector was filled with liquid nitrogen, the spectrometer ensured that sufficient energy was available to perform the studies and an alert warning informed the user if refilling of the detector was required to continue recording data. Background scans from a blank area of calcium fluoride were performed prior to all data acquisition and ratioed against the sample spectrum.

Figure 2.6 Perkin Elmer® Spotlight 300 FTIR Spectroscopy System

2.3.2 Settings for Mapping Measurements of Prostate Specimens

The term *mapping* describes the process of obtaining the spectral / biochemical equivalent of the visual representation obtained at microscopic analysis of tissue. Air dried or preserved prostate tissue specimens, mounted on calcium fluoride were placed on the silver sample holder and positioned on the stage. The software settings were set to image mode, FTIR spectra were measured in transmission mode, 8cm^{-1} wavelength resolution, 25 μm pixel resolution (interval steps), 16 co-scans per pixel and wavelength range of 4000-720cm^{-1}. The mapping studies analysed areas of specific interest guided by histological analysis of the adjacent haematoxylin and eosin stained consecutive section. The white light mode and video capture from the microscope enabled the appropriate positioning of the sample for interrogation. Map measurements were guided and recorded as number of steps in both the x and y direction across a specimen. The size of the map measured was limited by time constraints firstly to perform a map

using the above settings and secondly the duration of cooling conferred by the liquid nitrogen in the detector. A complete fill allowed for typically 8 hours of measurements. It was not possible to examine an entire large radical prostatectomy specimen without running out of liquid nitrogen in the detector. Therefore the primary method used was to split the analysis of large specimens into size-compatible portions. The possible method of refilling the detector with liquid nitrogen during measurements was examined in the larger radical prostatectomy specimens' analysis. On completion the intensity *.imp file, white light image *.vw and spectral map *.fsm data were saved on to the computer attached to the spectrometer. Hyperview® software enabled the map parameters to be viewed. The *.fsm map file was converted into an ASCII *.dat map file containing the transmittance and wavenumbers for each map. Matlab® programs designed in house by Dr Nick Stone were used to perform data processing: as described in section 2.3.4.

2.3.3 Settings for Point Measurements

Air dried or preserved prostate tissue samples, mounted on calcium fluoride, were analysed using the spectrometer in point mode, in transmission. The radical prostatectomy specimens were mapped in their entirety. Due to the constraints of the liquid nitrogen cooled detector the specimen was divided into smaller sections for manageable point maps (Illustrated in figure 2.7). The specimens were not removed from the stage until complete analysis had been performed. The effect of altering the spectral resolution, aperture and number of co-scans per pixel were explored in point map radical prostatectomy studies. Wavelength range was 4000-720cm^{-1}. When targeted point spectra were taken from specific pathologies, ten selected spectra were

taken from each pathology present within a sample (Figure 2.8). Spectral files were saved to the computer attached to the spectrometer. The point maps of the radical prostate sections were converted from *.fsm files to ASCII *.dat map file in a similar fashion as in section 2.2.2 above. The mean spectra from point spectra taken from selected pathology areas was analysed, compared and contrasted and will be discussed in the following results chapters. Matlab® programs designed in house by Dr Nick Stone were used to process the data: described in section 2.3.4.

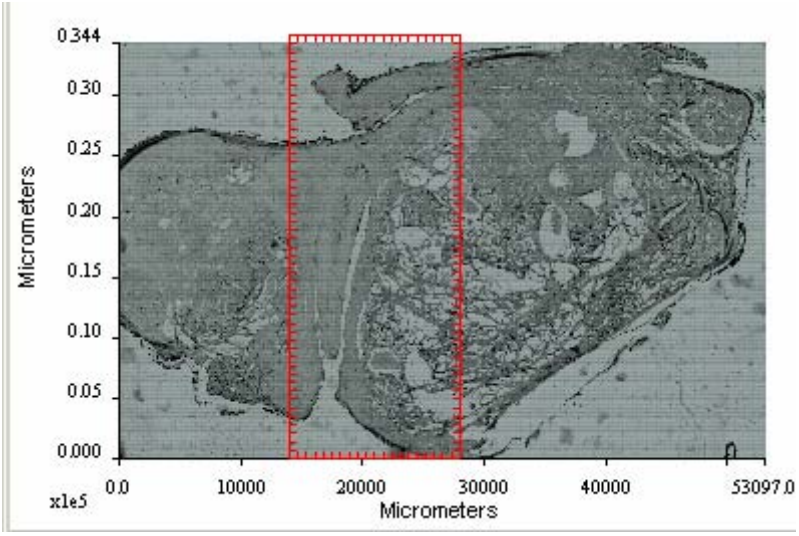

Figure 2.7 White light image illustrating methodology in point mapping of radical prostatectomy sections

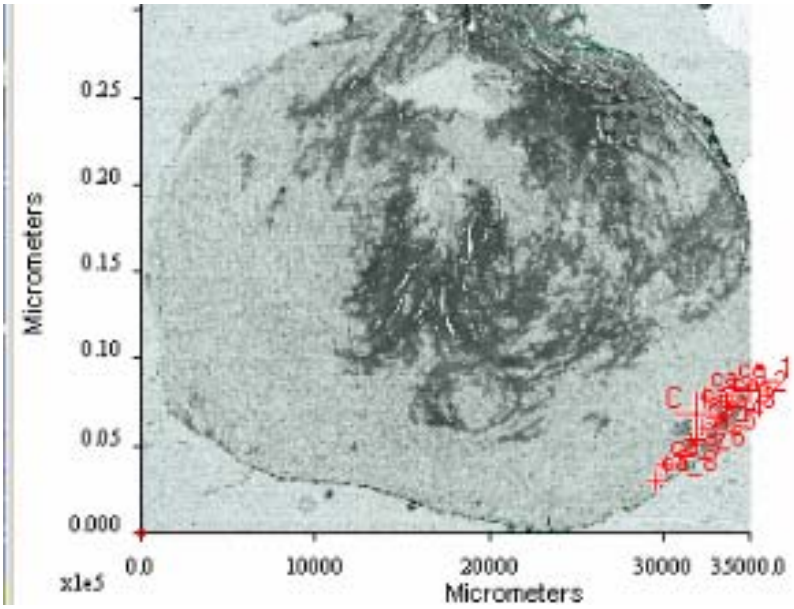

Figure 2.8 White light image demonstrating targeting of point spectra (marked with a cross) enabling measurement of specific areas of interest

2.3.4 Data Processing

Matlab® was used to load the spectral data from the ASCII map file and generate Principle Component Analysis (PCA) pseudo-colour maps (Illustrated below in figures 2.9 and 2.10). During the map loading process the spectra were interpolated to 4cm^{-1} wavenumber spacing, converted to absorbance using (log(max(transmittance))-log(transmittance)), where transmittance = I_{out}/I_{in} and smoothed using Savitzky-Golay (polynomial) to remove noise. The data was represented within Matlab® as a 3D matrix. The PCA score maps were compared to the white light image and H & E slide. A Matlab® script allowed regions to be selected from the pseudo-colour maps and labelled as to their appropriate pathology. Mean spectra from these pathologies could then be plotted and interrogated as described below.

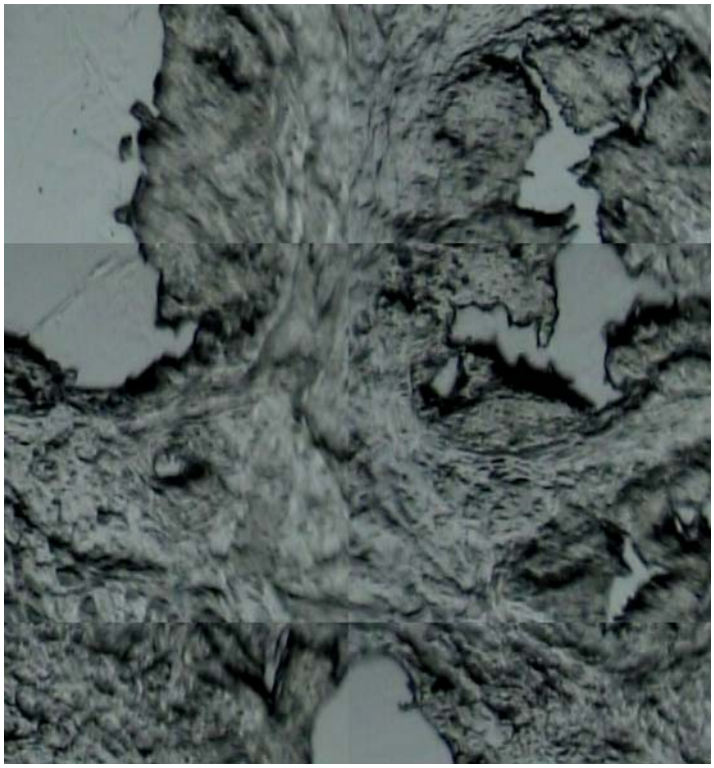

Figure 2.9 White light image of selected area of interest in prostate TURP section

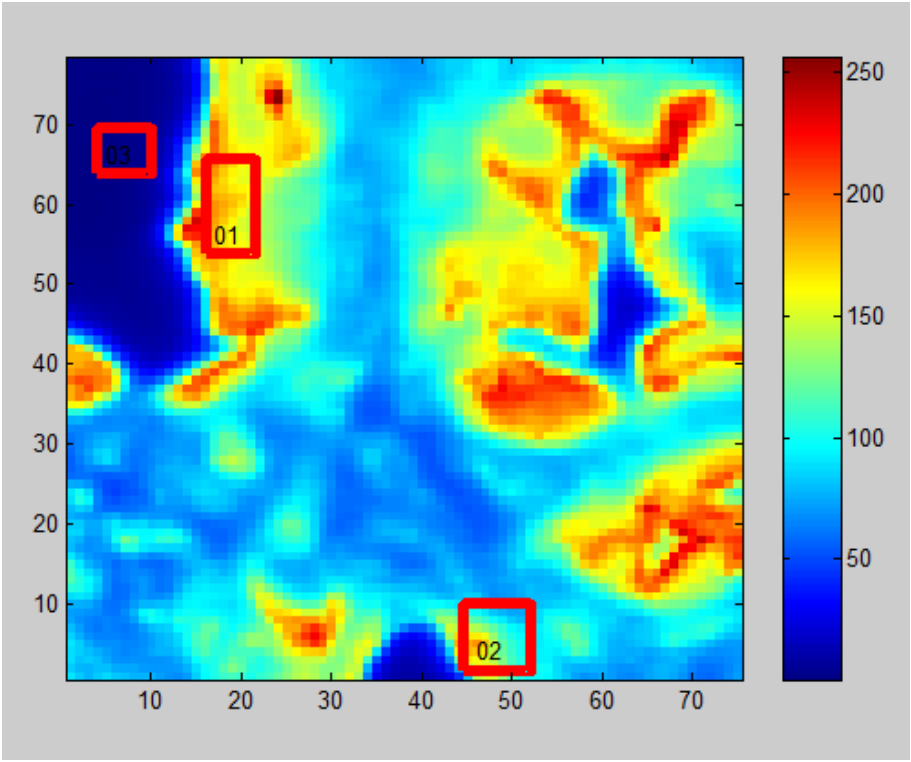

Figure 2.10 PC score pseudocolour map corresponding with above white light image, the red squares illustrate how specific regions may be selected

2.4 Data Analysis

Visual spectral interpretation has formed the backbone of spectroscopic analysis since the establishment of spectrometers but may be highly subjective, particularly in modern spectroscopy, where a huge amount of spectral data is collected by FTIR focal plane array detectors. Pattern recognition techniques are applied to infrared data, which attempt to remove subjectivity and allow realistic processing of large datasets. The choice of analysis technique is dependent on the samples' spectral characteristics and individual group preference for data analysis software.

2.4.1 Peak Position / Peak Height / Peak Area

Peak position can be correlated with known verified tables of key functional group absorbance peak positions. Differences in key functional group may be observed between pathologies. Peak height and area correspond to relative concentration of constituents. Analysis of peak intensity ratios can be the most straightforward way of identifying concentrations and locations of different substances as long as the component groups can be easily distinguished. Peak intensity ratios may enable differentiation between pathologies either from directly comparing single peak intensities between samples or establishing the ratio between key peaks within one sample and then comparing this ratio with other pathologies in separate samples.

2.4.2 Multivariate Analysis

Multivariate analysis enables the majority of the data within an infrared spectrum to be utilised and is especially useful in determining and separating subtle differences in pathology groups under examination. Multivariate analysis is necessary in tissue

diagnostics because it permits simultaneous analysis of multiple independent and dependent variables present in the spectral dataset. This analysis may be supervised or unsupervised. In this thesis because histological analysis allows us to know the pathologies within a sample and their location when we attempt to associate the pathology groups with the inputted spectral dataset this is termed supervised analysis. Unsupervised analysis describes when input values are analysed on the basis of the differences between them within the dataset without external interference. The multivariate analysis employed to construct the diagnostic algorithms in this thesis was primarily principal component-fed linear discriminant analysis. Principal component analysis (PCA) is applied to the spectral dataset to compress the data without losing relevant information. PCA is unsupervised. Linear discriminant analysis (LDA) then accentuates the differences between groups in spectral morphology. LDA is supervised. PCA fed LDA can produce a diagnostic algorithm or model which can be tested. The sensitivity and specificity of this algorithm in determining pathologies can be evaluated. The following sections will describe these techniques in detail.

2.4.3 Principal Component Analysis (PCA)

Principal component analysis calculates principal components (PCs) from the spectral dataset. These PCs are also known as loads and describe the greatest variance of spectral data from its mean. The first PC load describes the maximum variance and the second the next highest, progressively decreasing accordingly. As PCs are representations of the original spectra, spectra may be reconstituted by multiplying the loads by a variable termed PC scores. Thus spectra may be represented by either loads or scores. Using PC score data for analysis reduces the number of variables / data

needing to be processed within a dataset whilst retaining the spectral information, allowing each spectrum within the sample to be compared. Depending on the degree of variance of the sample under investigation the number of PC scores used is decided and the loads for the dataset were always retained.

PCA also allows co-linear spectral variations to be considered together. Infrared spectra of tissues have multiple characteristic peaks corresponding to concentration of substances present. Changes in the concentrations of these substances may cause changes in the heights of peaks within the whole spectrum. Loads can therefore reflect significant changes in the concentration of a substance by resembling the substance spectra. This allows valuable insight into the important molecular differences which exist between different pathologies.

PCA can be visualised in multiple ways as will be demonstrated in the Results chapter later. PCA pseudo-colour images of the sample under investigation can also be created by giving each score a colour rating. Each colour then represents the score of that component at each position where that spectrum was measured.

2.4.4 Linear Discriminant Analysis (LDA)

Linear discriminant analysis (LDA) is a technique used to improve the clustering of different pathological groups. In the context of this study, LDA takes into account the different variables (scores) determined by PCA and works out which pathological group the spectrum with that value is most likely to belong to. LDA in combination with PCA acts to maximise the variance in the data between pathological groups and minimize the

variation within a group. PCA ensures the LDA requirement, that the number of input variables (spectral wavenumbers) is less than the number of spectra in the dataset. LDA is supervised because it requires information as to how spectra are classified, specifically the pathological diagnosis which is input by the spectroscopist. PCA fed LDA was used to construct diagnostic algorithms for pathology groupings in this study. The algorithms were tested as to their accuracy.

2.4.5 Testing the Diagnostic Algorithm

The algorithms were tested using a 'leave one sample out' cross validation and using a separate population of test spectra.

'Leave one sample out': A testing protocol is established where a diagnostic algorithm is established leaving the spectra from one sample out of the model and then testing the algorithm using the spectrum not included in constructing the algorithm. The advantage of this technique is that when the number of test spectra / more importantly sample number is low it allows the algorithm to be tested.

Using test spectra population: In this thesis a test spectra group was created from separate samples and the algorithm tested using this separate group. The spectra were obtained from fresh frozen prostate biopsy and TURP samples. The effect of different sampling methods will be discussed in the next section.

2.4.6 Parametric Non-negative Least Squares Fitting

This thesis will explore the application of parametric non negative-least squares fitting to describing and investigating possible biomarkers for prostate cancer. '*Least squares fitting*' describes the technique of applying a best fit curve to a given number of points. This is performed on measured tissue spectra by: identifying the most likely dominant component constituents of the tissue; measuring the pure spectra of these components and then attempting to match the spectra in various combinations to the tissue spectra. The aim is to get a perfect fit with no residual. *Residual* describes the offset of the fitted curve from the actual spectra. This will be discussed later in this thesis.

2.5 References

[1] Wolkers WF, Balasubramanian SK, Ongstad EL, Zec HC, Bischof JC. Effects of freezing on membranes and proteins in LNCaP prostate tumor cells. *Biochimica et Biophysica Acta* 2007, 1768(3): 728-736

[2] Gazi E, Lockyer NP, Vickerman JC, Gardner P, Dwyer J, Hart CA, Brown MD, Clarke NW, Miyan J. Imaging ToF-SIMS and synchrotron based FTIR microspectroscopic studies of prostate cancer cell lines. *Applied Surface Science* 2004, (231-232): 452-456

[3] Aihara M, Wheeler TM, Ohori M, Scardino PC. Heterogeneity of prostate cancer in radical prostatectomy specimens. *Urology* 1994, 43: 60-66

[4] Fox CH, Johnson FB, Whiting J, Roller PP. Formaldehyde fixation. *Journal of Histochemistry and Cytochemistry* 1985, 33: 845-853

“ What we anticipate seldom occurs; what we least expect generally happens. ”

Benjamin Disraeli 1804 - 1881

3 Results

This chapter describes the analysis of the spectra recorded on the FTIR spotlight system. The sub-sections deal with progressive investigation of the different prostate specimens under investigation.

3.1 Preliminary Study of Prostate Tissue from TURP

The purpose of this study was to determine whether FTIR image mapping could differentiate between benign and malignant prostate pathology. Specific areas of known pathology selected in concordance with the pathologists' observations within fresh frozen prostate chippings were analysed by FTIR. Figure 3.1 overleaf illustrates the process of how FTIR images were obtained from each sample.

TURP chips were obtained from fifty patients, of which 27 patient samples were suitable for FTIR analysis. The sections were imaged in transmittance mode with a pixel size of 6.25μm. 203,629 spectra were obtained from the 27 samples. Total scan time 2327 minutes. Selected spectra from histologically classified benign and malignant areas of epithelial and stromal tissue were then taken from PCA score maps.

	Benign prostate tissue	Malignant prostate tissue
Number of patients	23	4
Number of samples	23	4
Number of spectra	7141	5168

Table 3.1 Breakdown of samples measured by FTIR

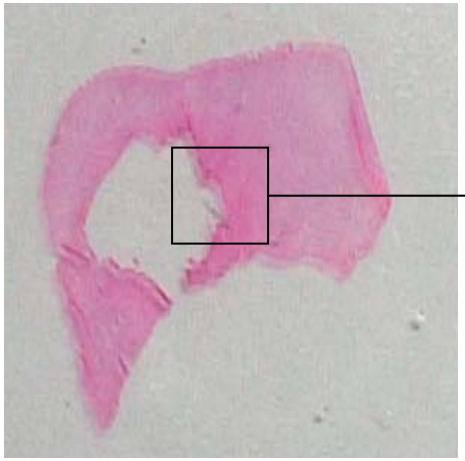

H & E section from TURP chip

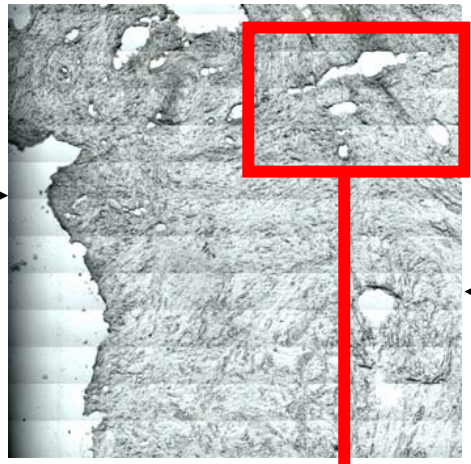

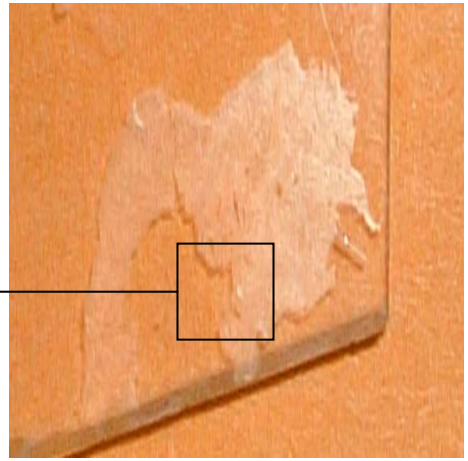

Unstained corresponding section

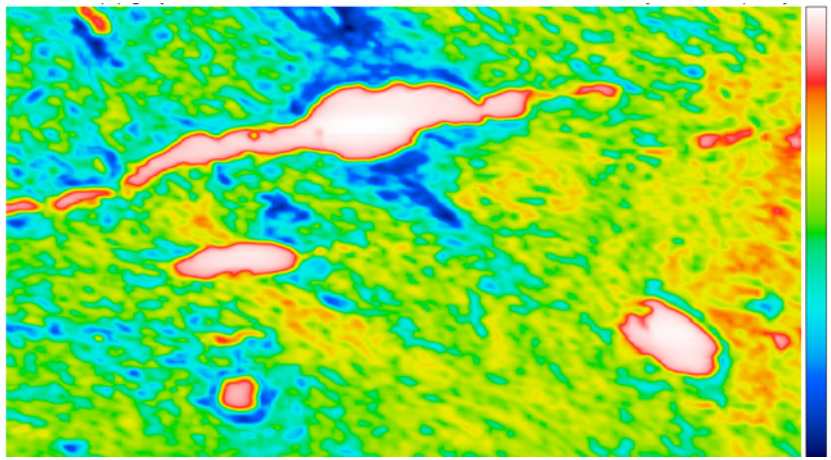

FTIR pseudocolour image map of area of interest

Figure 3.1 The process by which FTIR images of areas of interest are obtained

3.1.1 TURP Spectral Data

Although specific region selection was performed there was variability between the spectra collected, shown in figure 3.2. Part of this variability was expected because of differences between the pathology analysed, however a proportion of the variability results from the mapping process. There will be gaps between cells and the tissue in addition to external potential contaminants. This does not affect the majority of the spectra or the ability of the spectra to be used to discriminate between pathologies. It is possible to remove the spectra of concern when composing the model by a process of *normalisation* to exclude the spectra at extremes.

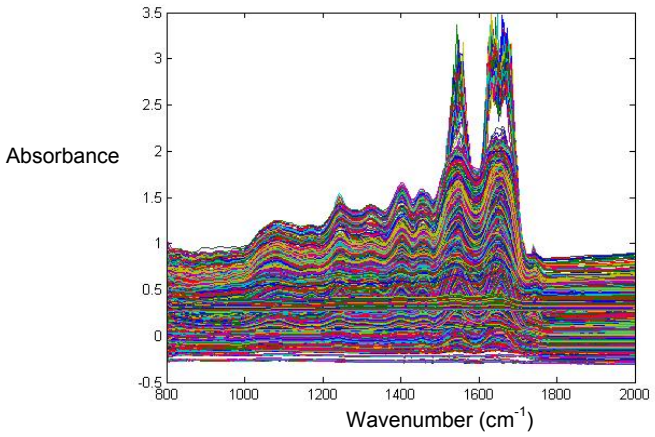

Figure 3.2 Total selected spectra from benign and malignant pathologies

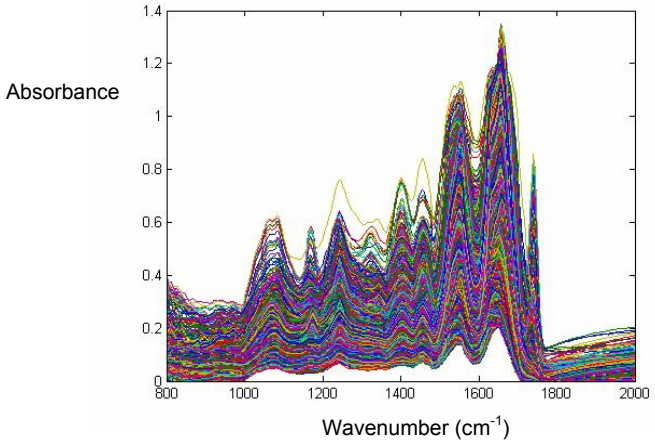

Figure 3.3 Normalised spectra from benign and malignant pathologies

Figure 3.3 illustrates the normalised spectral data. The data has been processed by removing the minimum value from all the spectra, thus making all spectra positive and using the amide region to ensure all the relevant spectra have been kept. The mean spectra from each pathology group was also calculated, and is shown in Figure 3.4.

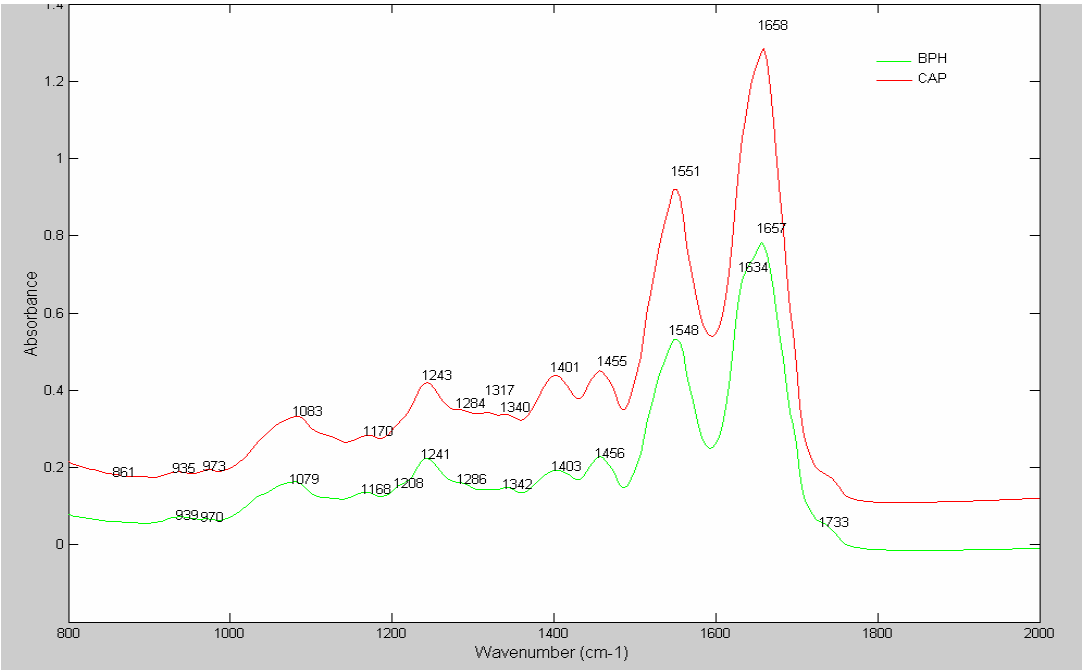

Figure 3.4 Mean spectra from benign (BPH) and malignant (CaP) pathologies

3.1.2 Analysis of Peak Absorbance Ratios

Although at first glance benign and malignant mean spectra appear identical in shape, for example similar peaks at 1456cm^{-1}, 1550cm^{-1} and 1660cm^{-1}, closer inspection reveals subtle differences. An extra peak in benign tissue at 1634cm^{-1}, a less prominent peak at 1403 in benign tissue and an extra peak in malignant tissue at 1317cm^{-1}is observed. Table 3.2 illustrates the potential biochemical differences between the pathologies on the basis of known peak assignments.

Biomolecule	Bond Vibration	Wavenumber (cm-1)	References
Amide I (random coil ~)	H bonded amide / peptide groups	1652-1695 (α-helix ~1655) (β-sheet ~1637)	Neviliappan *et al* 2002[1] Beleites *et al* 2005[2] Erukhimovitch *et al* 2005[3] Jackson *et al* 1995[4] Diem *et al* 2000[5]
Proteins	CH3 (methyl) CH2 (methylene)	1400 1450	Neviliappan *et al* 2002[1] Sule-Suso *et al* 2005[6] Schultz *et al* 1996[7]
Carbohydrates (e.g. glycogen)	C-O stretch C-OH bend C-OH stretch	1200-900 1025 1047 1085 1155 (1000-1190)	Neviliappan *et al* 2002[1] Erukhimovitch *et al* 2005[3] Lasch *et al* 2002[8,9]

Table 3.2 Referenced known infrared peak assignments corresponding to mean spectra differences between pathology groups

3.1.3 Multivariate Analysis

Multivariate analysis in the form of PCA fed linear discriminant analysis was applied to the spectral dataset as discussed in section 2.4. For each FTIR map analysed, ten principal components were calculated. The loads and scores were observed; see example in figure 3.5. The loads, which describe the variance from the mean of the dataset, reflect changes in molecular concentration of the substance. If significant differences in concentration are present, the loads may actually represent the spectrum of the substance which has changed. The score maps, which reduce the data needed to be processed, are a good representation of the tissue under analysis.

Figure 3.5 – PC scores and loads for a single prostate section analysis

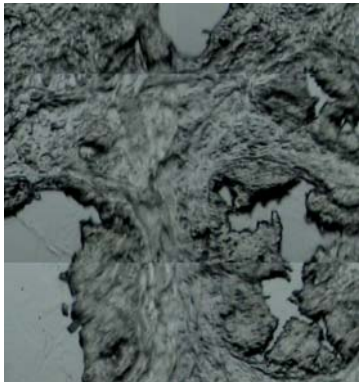

White light image

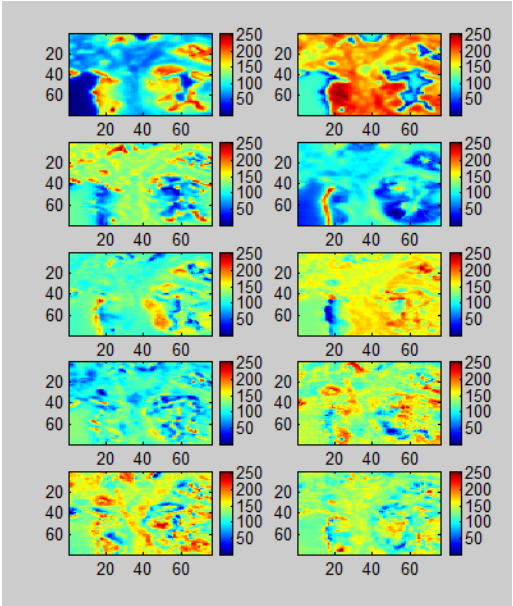

PC Score maps

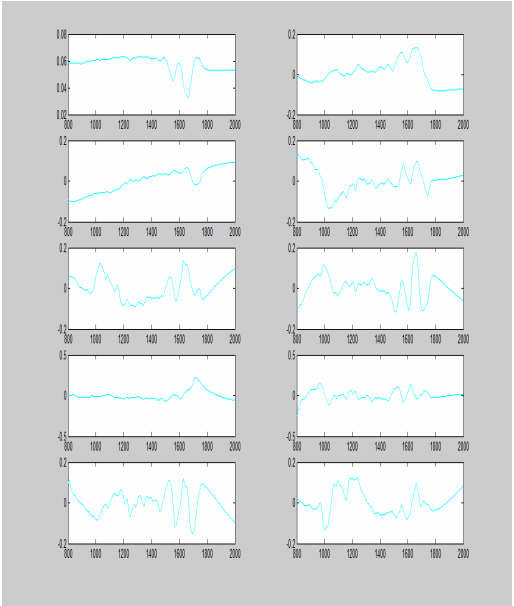

PC Loads

Linear discriminant analysis uses a linear discriminant function to maximise the distance between groups but minimise the distance between group members. The histogram in figure 3.6 below illustrates the degree of separation between benign and malignant pathologies achieved by PCA linear discriminant analysis.

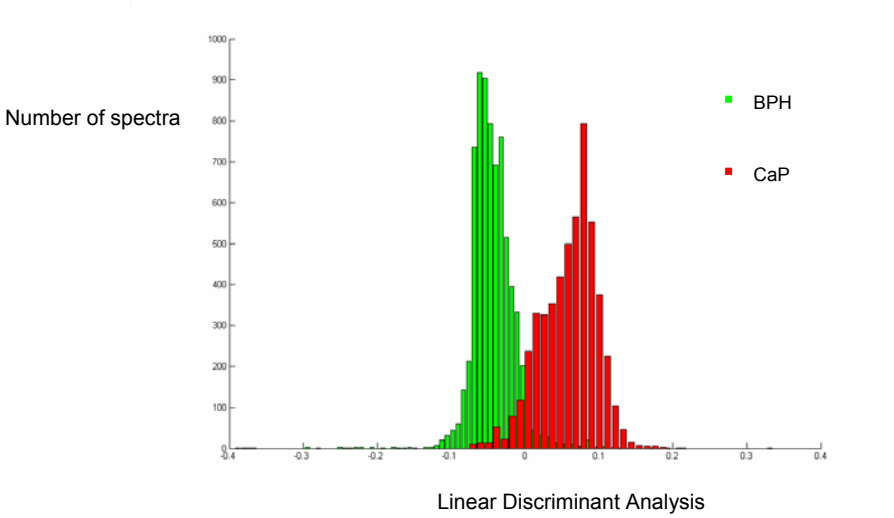

Figure 3.6 Histogram illustrating separation achieved between benign and malignant tissue with PCA fed Linear Discriminate Analysis

The predicted performance of the two group model created by the included spectra can also be demonstrated in tabular form (table 3.3). The sensitivity and specificity of the algorithm may be determined from this. The sensitivity is the number of spectra from the pathological group correctly predicted to be in the right group (true positives). The specificity of the group is the number of spectra correctly identified as not belonging to the group (true negatives). The two group model sensitivity was 97% and the specificity was 90%.

	FTIR Algorithm-predicted diagnosis (number of spectra)		
Histological Diagnosis (number of spectra)		Benign	Malignant
	Benign	6909	232
	Malignant	499	4669

Table 3.3 Results achieved by two group algorithm: benign versus malignant tissue

3.1.4 Expansion of the Diagnostic Algorithm Groups

The pathology groupings for the primary analysis were benign and malignant tissue only, based on the rationale that the pathologies were clear and that the individual patient sample number was relatively low. Once the results discussed above were realised, the concept of more in depth analysis of tissues was explored. Sub-classification of benign prostate tissue into epithelial tissue, ductal tissue and stroma in benign tissue was investigated. Sub-classification of malignant prostate tissue into *adenocarcinoma* (glandular and ductal areas) and *cancerous stroma* (surrounding cancer cells) was investigated. The tables which follow summarise the models performance. The key finding from a pathology perspective was the stromal analysis (tables 3.4 and 3.5); usually pathologists are unable to gain a significant amount of information from prostate stromal tissue, however PCA fed linear discriminant analysis elicits a clear distinction between stromal tissue related to benign tissue and stromal tissue related to malignant tissue.

	Algorithm-predicted diagnosis (number of spectra)			
Histological Diagnosis (number of spectra)		Benign Stroma	Malignant Stroma	Total No Spectra
	Benign Stroma	1500	1	1501
	Malignant Stroma	4	679	683

Sensitivity = 99.93; Specificity = 99.41

Table 3.4 Results achieved by two group algorithm: benign versus malignant stroma

	FTIR Algorithm-predicted diagnosis (number of spectra)				
Histological Diagnosis (number of spectra)		BPH	Benign stroma	CAP	Malignant stroma
	BPH	**3072**	770	32	119
	Benign stroma	194	**1239**	0	68
	CaP	133	3	**787**	139
	Malignant stroma	22	54	10	**597**

Table 3.5 Results achieved by four group algorithm

In the four group model, percentages of spectra allocated correctly for BPH, benign stroma, CaP and malignant stroma were 76.93%, 82.55%, 74.11% and 87.41% respectively (see table 3.5).

	FTIR Algorithm-predicted diagnosis (number of spectra)						
Histological Diagnosis (number of spectra)		Benign Ductal	BPH	Benign Stroma	CAP	Malignant Ductal	Malignant Stroma
	Benign Ductal	**1385**	142	2	16	0	1
	BPH	465	**2726**	617	10	75	100
	Benign Stroma	79	202	**1166**	0	1	53
	CaP	18	94	0	**765**	55	130
	Malignant Ductal	12	22	6	5	**254**	67
	Malignant Stroma	0	38	29	9	0	**607**

Table 3.6 Results achieved by six group algorithm

In the six group model, percentages of spectra allocated correctly for Benign ductal tissue, BPH, benign stroma, CaP, malignant ductal tissue and malignant stroma were 89.59%, 68.27%, 77.68%, 72.03%, 69.40% and 88.87% respectively (see table 3.6).

3.1.5 Cross Validation of Diagnostic Algorithms

'*Leave one sample out*' cross validation was used to evaluate the diagnostic algorithm. The testing protocol removed all the spectra of one sample from the diagnostic algorithm and used the removed spectra to test the algorithm. The process was repeated for all samples. This method is rigorous because the test spectra are not included in the constructed diagnostic algorithm. It is slightly less scientifically robust than evaluating the diagnostic algorithm with a large test cohort of new samples, however this method of analysis enables algorithm testing when the sample numbers are relatively low. The result of cross validation for benign versus malignant tissue spectra is illustrated in the table 3.7 below:

	FTIR algorithm-predicted diagnosis (number of spectra)			
Histological Diagnosis (number of spectra)		Benign	Malignant	Total No Spectra
	Benign	3822	198	4020
	Malignant	292	2362	2654
	Total no. of Spectra	4114	2560	6674

Sensitivity = 95%; Specificity = 89%

Table 3.7 Cross validated results for two group algorithm benign versus malignant tissue spectra

3.1.6 Commentary on Results from Preliminary TURP Study

This preliminary study demonstrated that FTIR was able to interrogate prostate tissue and by analysis of FTIR spectra it was possible to discriminate between benign and malignant prostate pathology. The potential of FTIR to obtain useful biochemical information from all tissue under investigation including areas not normally utilised by the pathologist was also realised.

The limitations of the technique and the study were also recognised:-

- Small sample number
- The potential confounding effect of diathermy on TURP tissue biochemistry
- The lack of a study control to account for differences between samples
- How to determine true biochemical changes within samples
- FTIR analysis had been performed only on fresh frozen tissue
- The considerable time required to FTIR map even small samples

These thoughts stimulated the progression of the study to use FTIR to analyse radical prostatectomy sections in their entirety to address the aforementioned issues.

3.2 Study of Prostate Tissue from Radical Prostatectomy

The purpose of the studies which follow in this section of the thesis were to evaluate the clinical potential of FTIR as a pathology classification tool by performing detailed analysis of radical prostatectomy specimens. The concept of point mapping was explored and related to formal FTIR mapping; the ability of FTIR to discriminate between pathologies within prostate specimens and between different prostate specimens was examined. The sections were able to act as their own controls in pathology studies as each contained multiple pathologies. Prostate sections were analysed in paraffinated and deparaffinated forms to examine whether spectral information was lost in the deparaffination process and inform the potential clinical application of the technique. The reproducibility of measurements was also assessed. Prostatic Intraepithelial Neoplasia was also interrogated by FTIR and its spectra analysed for the first time in such tissue studies.

3.2.1 Point Map Analysis of Radical Prostatectomy Sections

Initially, five radical prostatectomy sections were analysed in their entirety using the point map technique in both their paraffinated and deparaffinated forms. Table 3.8 describes the data collected from each sample. Figure 3.7 illustrates the point mapping process. The *step size interval* (the distance between each point measurement) was calculated to allow measurement of equal sections of the prostate, each within the eight hour time constraint of effective detector function after filling with liquid nitrogen. Areas were measured using the microscope ruler. Spectra were obtained in point mode, transmission, spectral resolution $4cm^{-1}$, 16 co-scans, aperture size 100μm

x 100μm and wavelength range 4000-720cm^{-1}. Background scans were taken prior to each measurement.

Radical prostatectomy specimen	Step size interval (microns)	Number of composite sections	Total section dimensions x:y (mm)	Total number of spectra collected	Pathologies present
1	500	3	42:25.5	4350	BPH, Prostatitis, PIN, Gleason 3+4=7 CAP
2	700	4	45.5:32.2	3243	BPH, Gleason 4+4=8 CAP
3	700	4	56:35	4074	Benign tissue, Gleason 3+3=6 CAP
4	500	5	42:40	7209	PIN, Gleason 4+3=7 CAP
5	600	4	47.4:42	5893	BPH, Gleason 3+4=7 CAP

Table 3.8 Breakdown of data collected from prostate sections

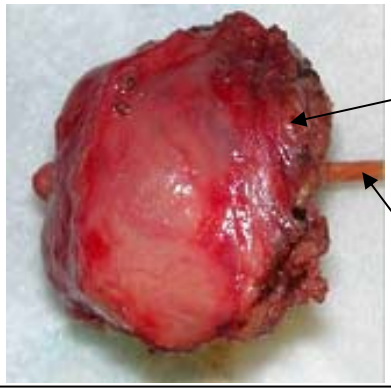

Radical prostatectomy specimen

Urethral catheter, left in situ post operation to orientate specimen

Radical Prostatectomy Specimen 1

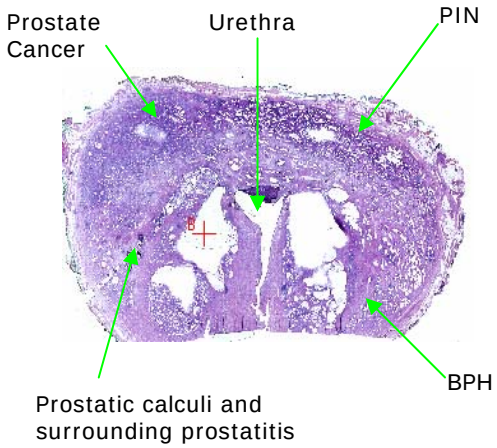

Transverse H&E stained 10 micron section, after pathological analysis

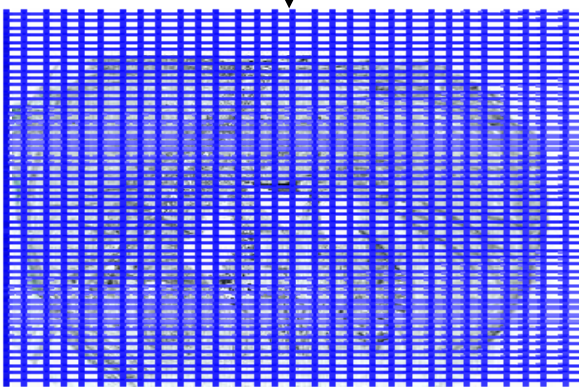

Corresponding unstained 10 micron section for FTIR analysis, crosses on grid illustrate where spectra were taken from

Figure 3.7 The point mapping process

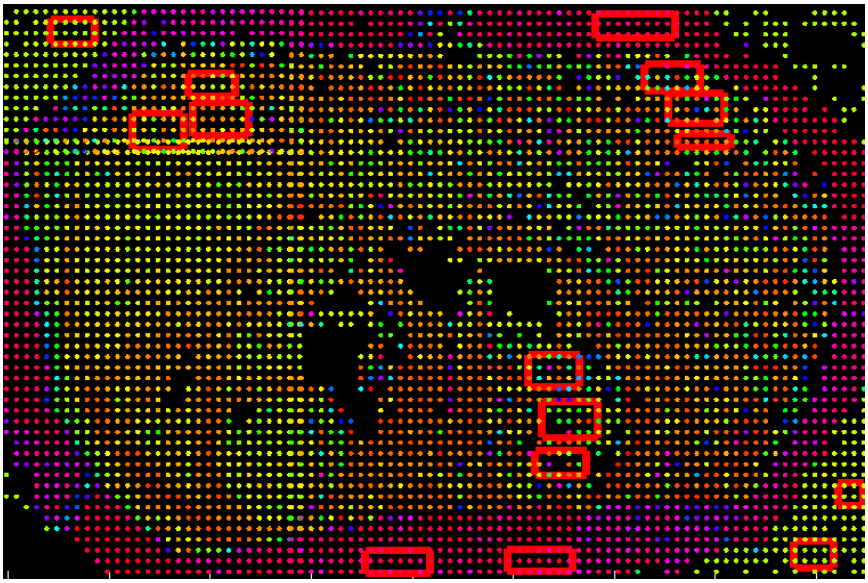

Figure 3.8 Region selection in prostatectomy section one from pseudocolour PCA score map

3.2.2 Radical Prostatectomy Five Section Specimen Spectral Analysis

The point maps were zipped together using Matlab® software and converted into pseudocolour PCA score maps representative of the sections under analysis in a similar manner to that described in section 3.1. Region selection of specific spectra from identified pathologies was then performed. Figure 3.8 illustrates the region selection process in the large prostate sections. The spectra then underwent normalisation and mean spectra for the pathologies under analysis were produced for the individual sections alone and the cohort of five sections in both paraffinated and deparaffinated form.

Using prostate section four as an example, this section contained benign and malignant prostate tissue in addition to PIN, in clearly demarcated areas. The mean spectra of the pathologies from section four in paraffinated and deparaffinated forms are shown in figures 3.10 and 3.11 respectively.

The first important observation is that excellent spectra may be obtained from both paraffinated and deparaffinated prostate sections. The paraffin peak is evident at approximately 1460cm^{-1} in the paraffinated sections and not when the same section has been deparaffinated. Although the paraffin peak obscures the tissue peak at 1460 it does not seem to interfere with or prevent interpretation of absorbance at other wavenumbers. The second finding was that the spectral morphology seemed more distinctive when prostate tissue was analysed in its paraffinated form. Similar changes in spectral morphology are evident between benign and malignant prostate tissue as determined in the analysis of fresh frozen TURP chippings (section 3.1). There are peak ratio differences between different prostate pathologies in the Amide I region. Benign tissue has an additional peak at 1440cm^{-1}. At approximately 1440cm^{-1} CaP has a prominent distinctive peak which is less prominent in benign tissue. The mean spectra of PIN has similar morphology to CaP. These findings were mirrored in all sections.

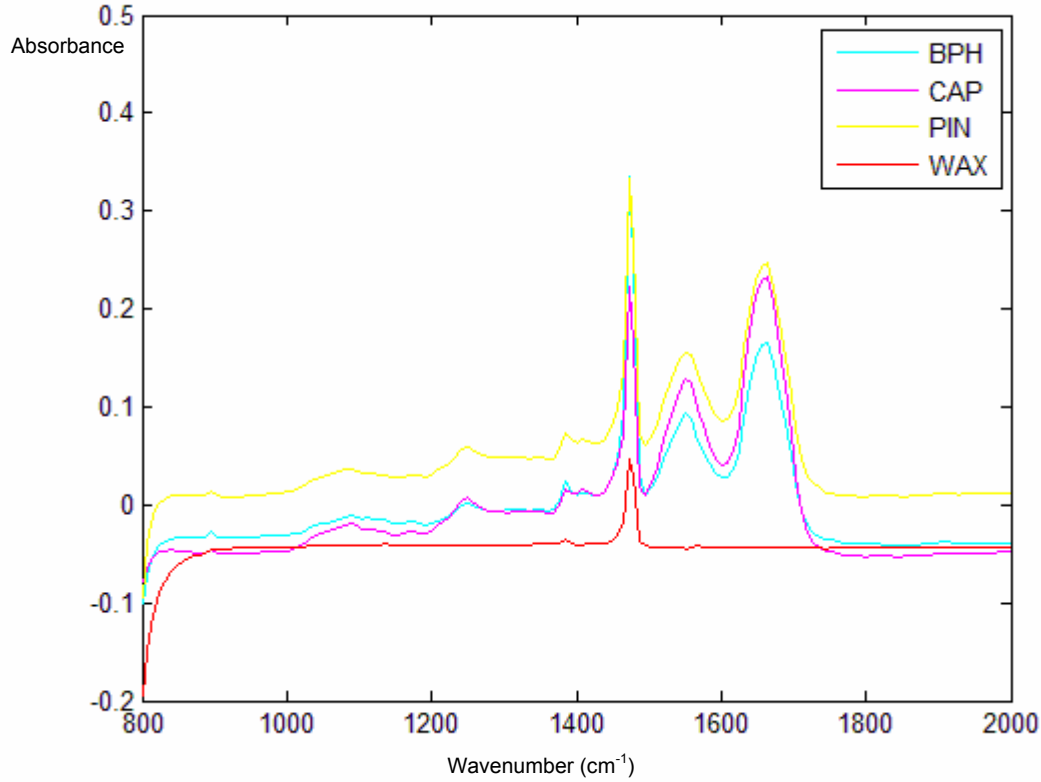

Figure 3.10 Mean spectra from pathologies in paraffinated section four

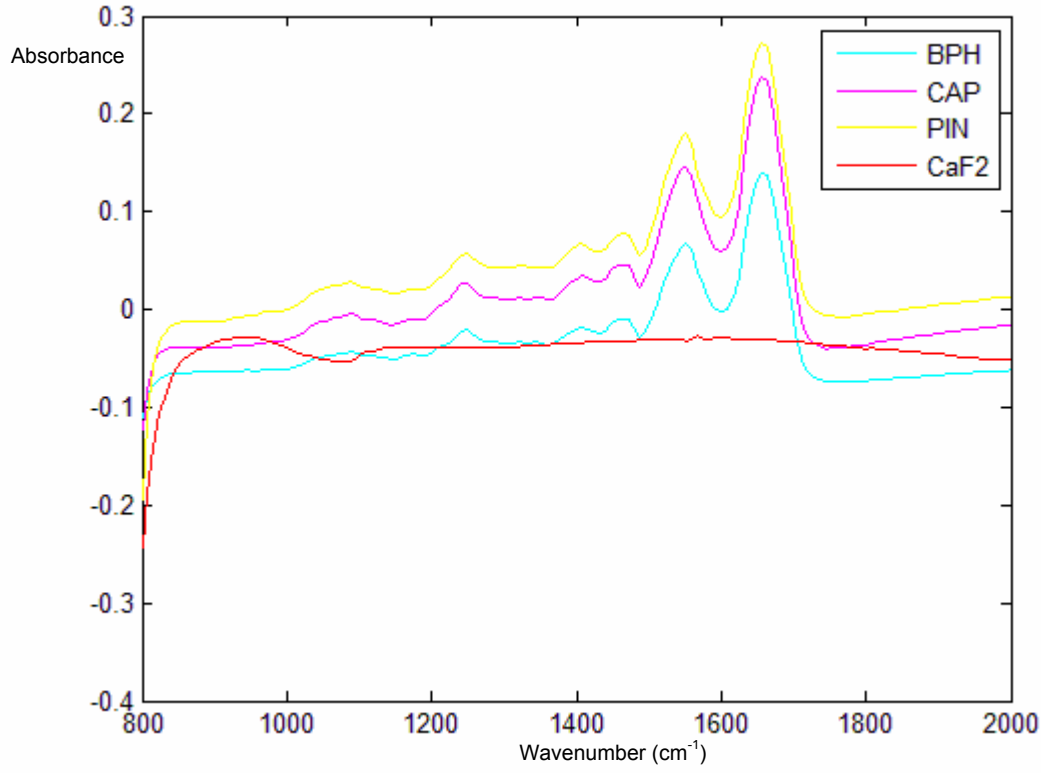

Figure 3.11 Mean spectra from pathologies in deparaffinated section four

Having determined clear distinction between the spectra of pathologies in heterogeneous individual prostate sections, the pooled mean spectra for all samples were then examined. The deparaffinated dataset is used to illustrate this in figure 3.12, the paraffin and CaF_2 spectra have not been included. The findings were almost identical to the individual section findings.

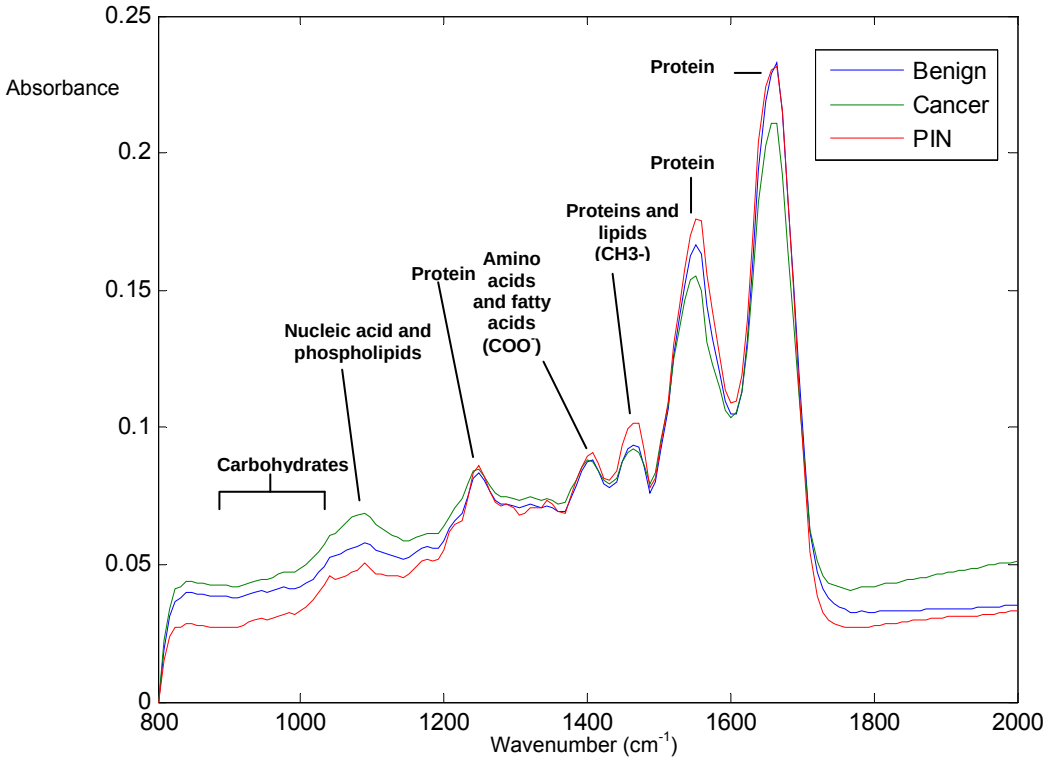

Figure 3.12 Analysis of mean spectra from all pathology groups from five sections

3.2.3 Multivariate Analysis of the Five Section Spectral Dataset

Principle component fed linear discriminant analysis was performed on the selected spectra. The degree of separation achieved for benign, malignant prostate tissue and PIN is illustrated in figure 3.13. The sensitivities and specificities achieved by the three pathology group model are described in table 3.9.

Pathology	Benign	Prostate Cancer	PIN
FTIR Sensitivity (%)	82	85	80
FTIR Specificity (%)	87	84	96

Table 3.9 Sensitivities and specificities of the three pathology group algorithm

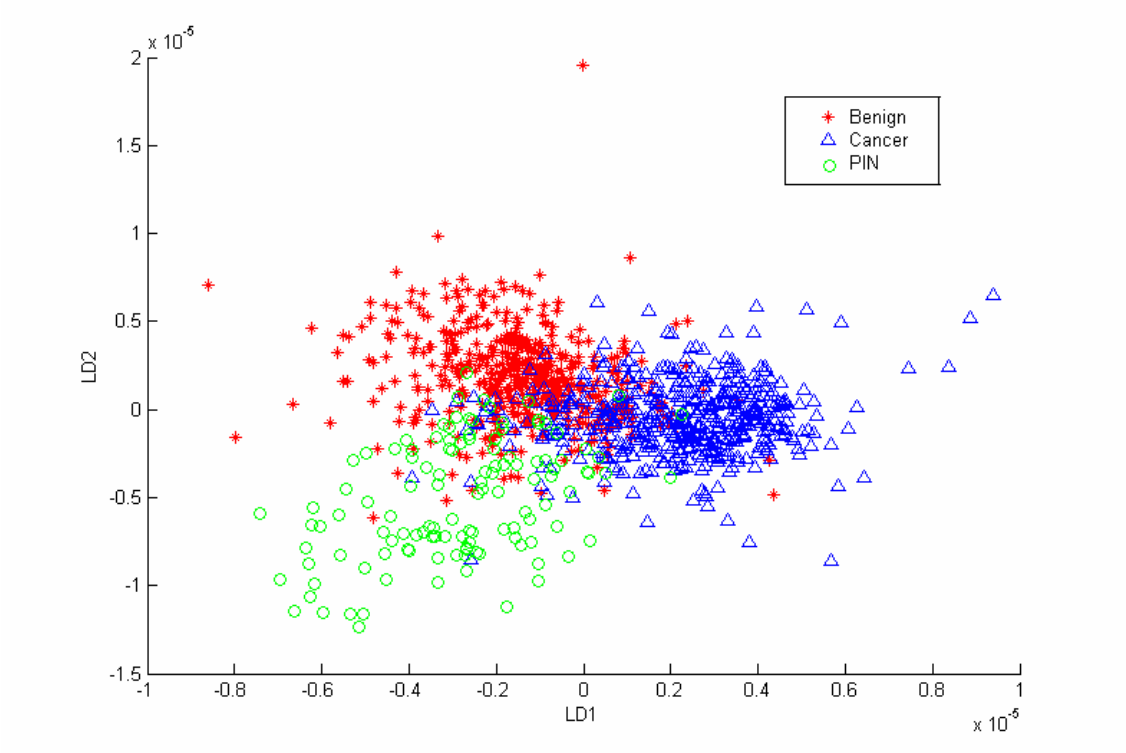

Figure 3.13 Scatter plot illustrating linear discriminant analysis of pathologies

3.2.4 Evaluating Why Discrimination of Pathologies May Not Be Perfect

Although the above model achieved reasonably good classification of the main pathologies, an obvious critique is why is the classification not perfect? One hypothesis may be that individuals' prostate cancer might differ biochemically. This might be accounted for by differences in Gleason grade between individuals, however before this theory may be explored further it was necessary to ascertain whether differences between cancers exist within a specimen. Three of the nine radical

prostatectomy sections used in this thesis contained multifocal tumours, allocated with the same Gleason grade within the specimen. The mean spectra from each area were compared. Radical prostatectomy specimen six and seven are used to illustrate these results.

Figure 3.14 Prostatectomy section six: H & E stained section with two areas of Gleason 3+4=7 prostate cancer

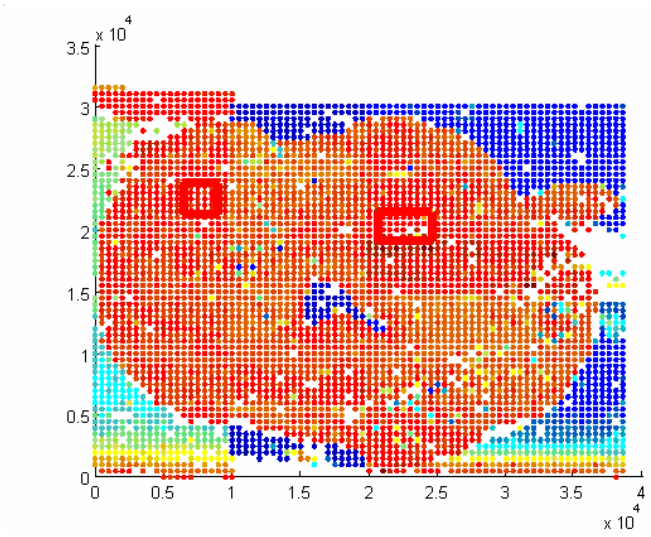

Figure 3.15 PC score map of prostatectomy section six: Region selection of two areas of Gleason 3+4=7 prostate cancer (mapped from H & E stained section in Figure 3.14 above)

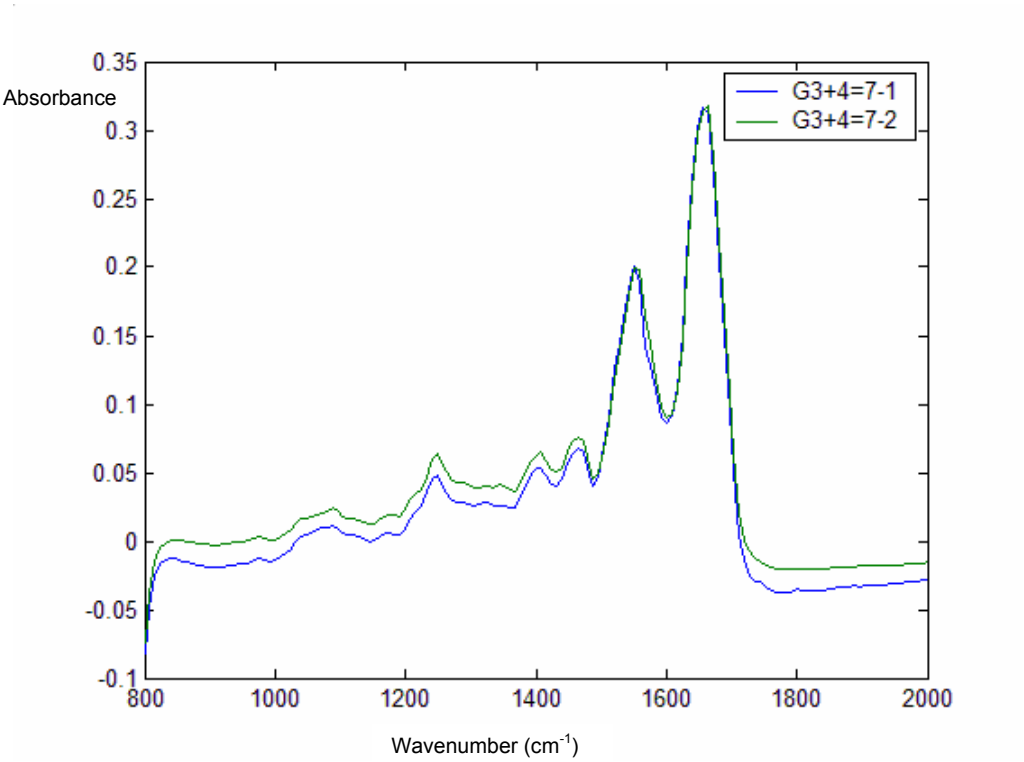

Figure 3.16 Mean spectra from two separate Gleason 3+4 areas in prostatectomy section six

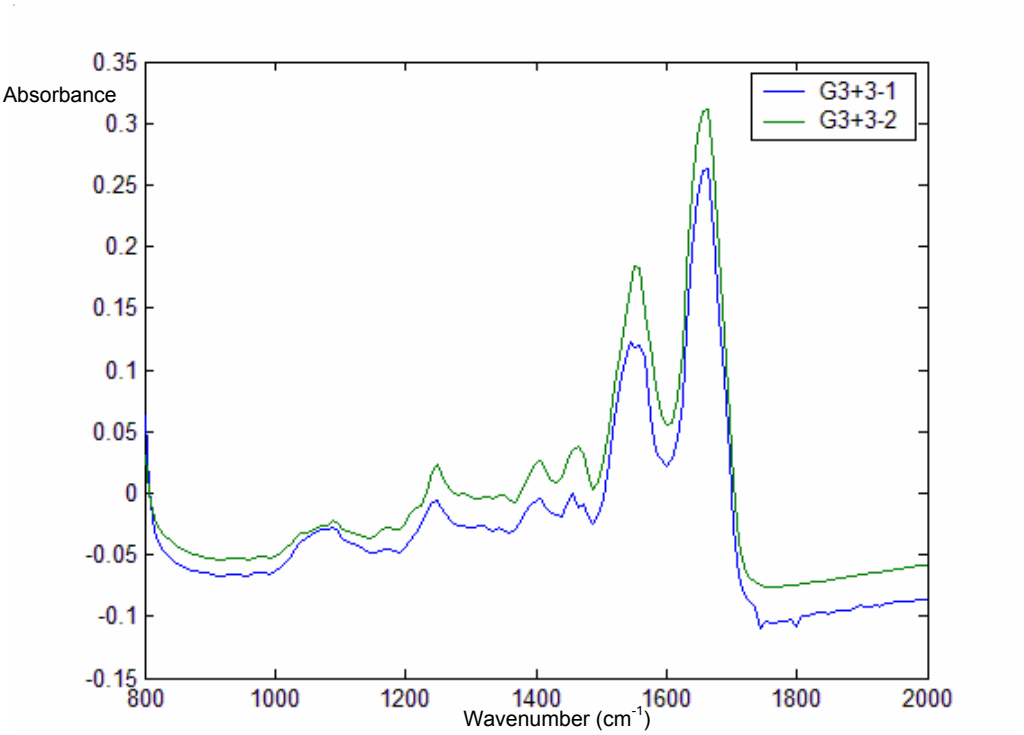

Figure 3.17 Mean spectra from two separate Gleason 3+3=6 areas in prostatectomy section seven

Figures 3.16 and 3.17 show the mean spectra of two areas of prostate cancer, of the same Gleason grade, exhibiting different mean spectra, in prostatectomy sections six and seven.

3.2.5 Cross Validation of Three Group Model

***'Leave One Sample Out'* Cross Validation** of the three group model was performed for deparaffinated radical prostatectomy sections one to five. The performance of the algorithm is shown below in table 3.10. The percentages predicted correct for Benign, Cancer and PIN pathologies were 77%, 88% and 91% respectively. The overall training performance of the model was 83.16%; the prediction performance was 24.62%.

	FTIR algorithm-predicted diagnosis (number of spectra)				
Histological diagnosis (Number of spectra)		Benign	Cancer	PIN	Total number of spectra
	Benign	**366**	76	36	478
	Cancer	27	**396**	27	450
	PIN	7	3	**107**	117
	Total number of spectra	400	475	170	**1045**

Table 3.10 *Leave one sample out* cross validation results for three group model in prostatectomy sections one to five

Blind Test Group Validation of the three group model was then performed by projecting the data from radical prostatectomy specimens six to nine onto the above prostatectomy sections' three group model, as a test group. Findings are shown in table 3.11. The percentages predicted correct for Benign, Cancer and PIN pathologies were 28%, 13% and 91% respectively.

	FTIR algorithm-predicted diagnosis (number of spectra)				
Histological diagnosis (number of spectra)		Benign	Cancer	PIN	Total number of spectra
	Benign	**101**	46	208	355
	Cancer	40	**44**	245	329
	PIN	2	1	**32**	35
	Total number of spectra	143	91	485	**719**

Table 3.11 Blind test group validation of the three group model

3.2.6 Commentary on Results from Point Map Analysis of Radical Prostatectomy Sections

The results from point mapping of the specimens so far reinforce the hypothesis that FTIR may have a role as a potential histological classification tool. FTIR has differentiated between pathologies within the same specimen and in multiple specimens. It has been demonstrated that stain free biochemical imaging is possible of both paraffinated and deparaffinated specimens. Therefore practically this may have application as in practice it could remove the need for and time taken for processing steps. The spectra of PIN has been classified as an entity, and is similar in morphology to CaP, but more importantly is identifiable as a distinct pathology from benign and malignant tissue. Point mapping, as a concept, allows a greater proportion of the tissue to be imaged and enables adequate spectral data collection of pathologies. The point mapping of entire sections has enabled the evaluation of heterogeneous tumours and their differences. The effect of TURP diathermy does not

appear to have a significant effect on prostate tissue biochemistry as the same spectral differences have been elicited in both TURP and Radical Prostatectomy tissue.

3.3 FTIR System Validation Experiments

In clinical practice, point mapping of specimens would appear to be the ideal method to allow high throughput of samples with in depth image mapping reserved for specific areas of interest. The immediate concern regarding the point map technique is whether pathology would be missed by critical *step size interval*. In addition to this, knowledge with respect to the reproducibility of the technique is also important if FTIR is to have a clinical application. These issues were addressed in technique validation studies which are described in this section.

3.3.1 Point Map Validation Studies

The purpose of the studies in this section are to investigate the reproducibility of biochemical analysis achievable by the FTIR system; the effect of number of co-scans on the biochemical data obtained by FTIR; and finally evaluate the effect of step size on the detail of the biochemical data obtained by FTIR from prostate pathologies. Radical prostatectomy sections six and eight were used for this analysis.

3.3.2 Reproducibility of the System

These studies were performed on section eight which contained three pathologies: Cancer, Benign tissue and PIN. The aim was to establish whether the FTIR system analysis of pathologies were reproducible over a three day period. Each pathology was examined three times within a 24 hour period and subsequently at 24 hour intervals over a three day period. The specimen under analysis was not removed or repositioned between measurements. For each pathology, twenty targeted point spectra (see figure 2.8) were taken at each measurement and measurements were repeated three times each time the pathology was examined. If t = time of first

measurement, the time of measurements in hours were: (t), (t+1), (t+12), (t+24), (t+48), (t+72). The software settings were set to: point collection mode, transmission mode, aperture 30µm x 30µm, 1cm^{-1} spectral resolution, 75 number of co-scans / 128 number of co-scans. The mean spectra obtained at (t) and (t+12) for PIN is illustrated in figure 3.18, the mean spectra obtained at (t+24), (t+48) and (t+72) for benign tissue are illustrated in figure 3.19.

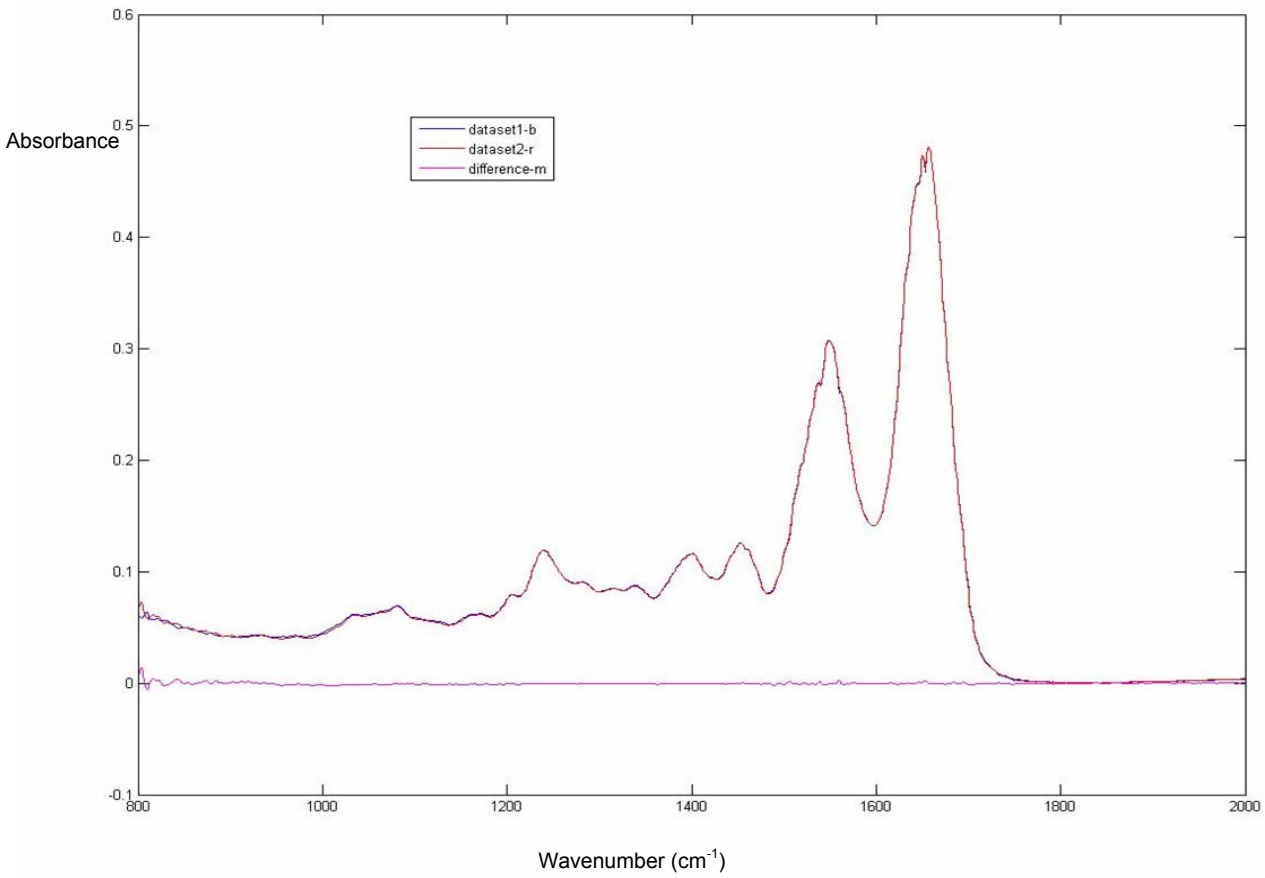

Figure 3.18 Mean point spectra obtained from PIN at t (dataset 1) and t+12 (dataset 2) with the difference between the curves illustrated

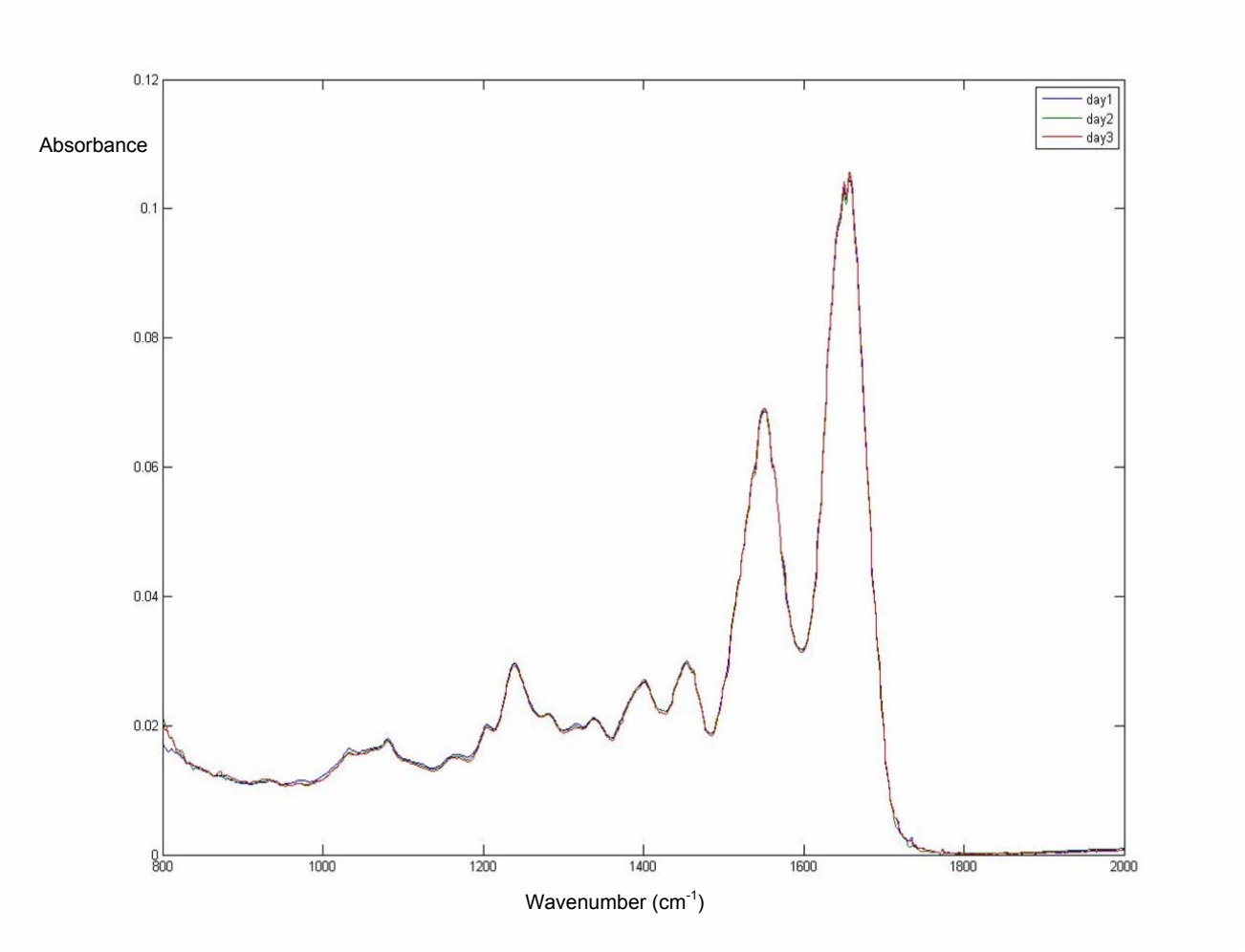

Figure 3.19 Mean point spectra obtained from benign tissue at t+24, t+48, t+72

In keeping with the findings shown in figures 3.18 and 3.19, there was no significant variation in the spectra obtained from all pathologies in section eight by FTIR over a three day period. This is reassuring as it implies that not only is FTIR analysis reproducible but also that the biochemical information contained in preserved sections does not degrade over time.

3.3.3 The Effect of Co-scan Number on Prostate Tissue Analysis

Each time point spectra are taken, the spectra recorded is a mean of the number of *co-scans* performed. Co-scans in infra-red spectroscopy refer to the co-adding of scans, this improves the signal to noise ratio. This is important because increasing

co-scan number achieves a higher signal to noise ratio but correlates with an increase in time taken for sample analysis. Therefore in these studies the co-scan number was varied but the aperture maintained at 30µm x 30µm and the spectral resolution set at 1cm^{-1}. Targeted point spectra were taken from pathologies in section six which contained two pathologies; benign and malignant prostate tissue. Each measurement consisted of 20 spectra; measurements were repeated three times at each co-scan number setting. Both pathologies were evaluated at co-scan numbers 128, 75, 50, 25, 10, 5, 2 and 1. Figures 3.20 and 3.21 demonstrate the mean spectra obtained from each pathology at each co-scan setting.

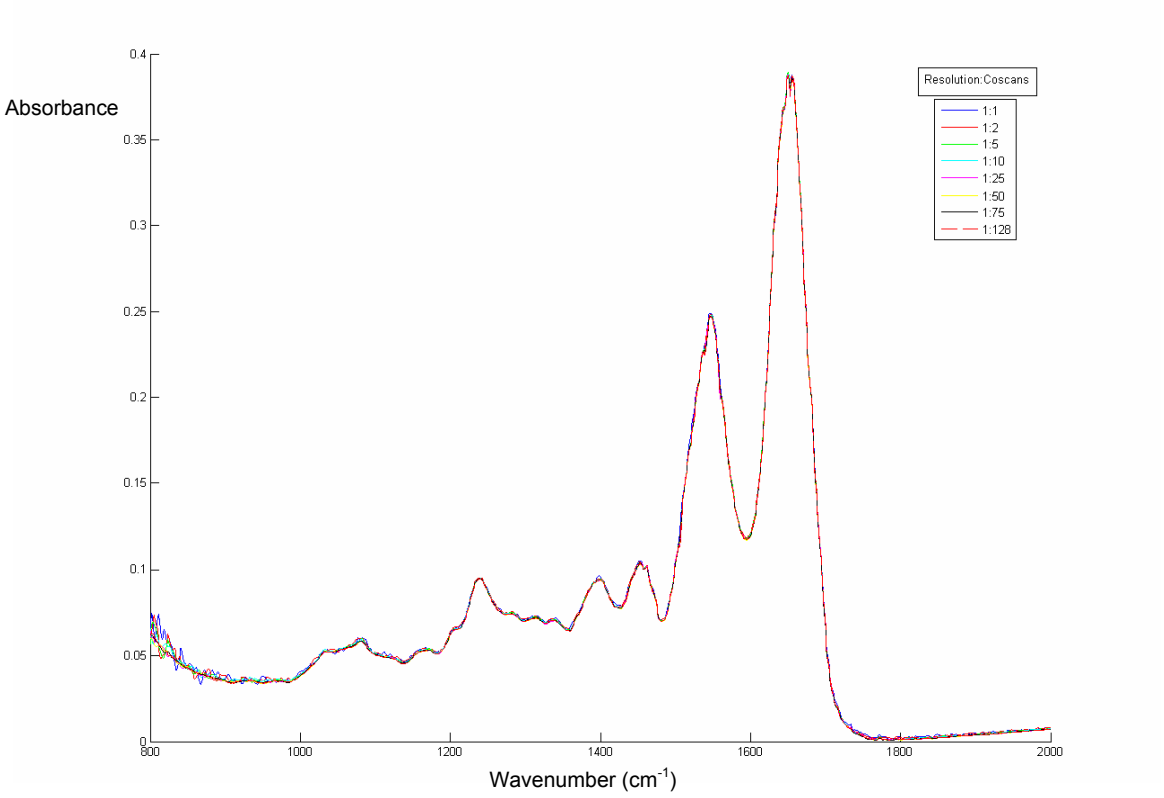

Figure 3.20 Mean spectra obtained for benign tissue at labelled co-scan number

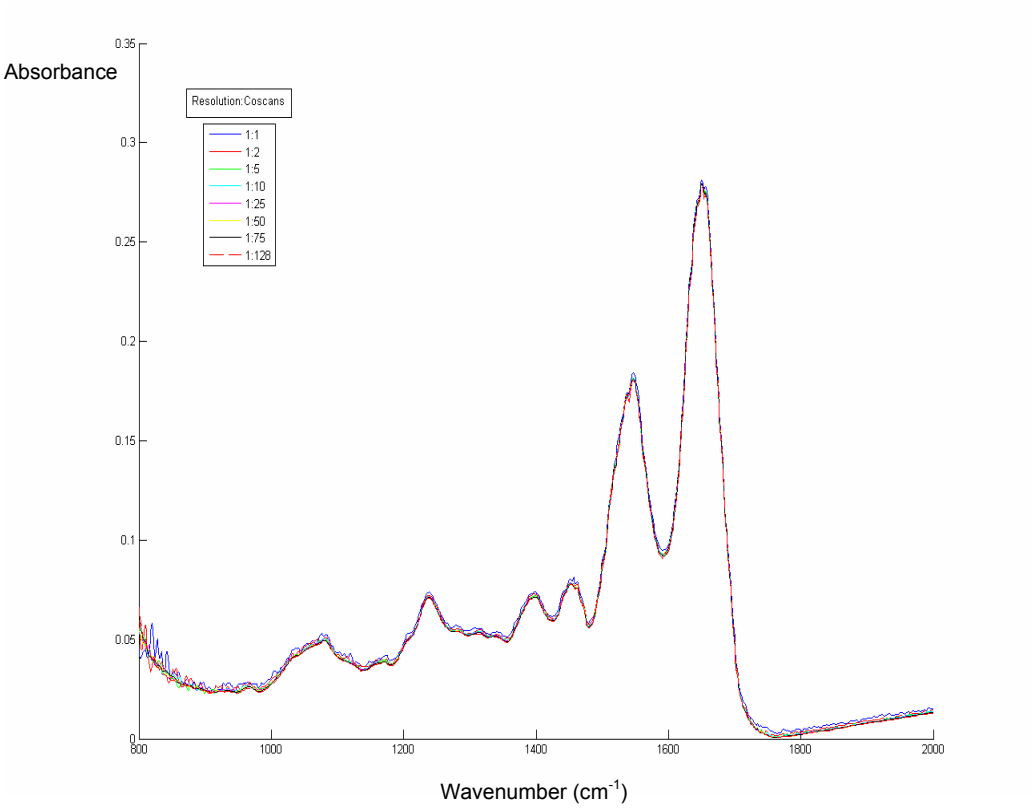

Figure 3.21 Mean spectra obtained for prostate cancer tissue at labelled co-scan number

Although all co-scan numbers yielded good spectra between wavenumbers 2000-1000 cm^{-1}, the lowest co-scan number to achieve good quality spectra without noise between 2000 and 720 cm^{-1} was 25. There was uniformity in this finding in both pathologies.

3.3.4 The Effect of Step Size in the Evaluation of Prostate Pathologies

The studies prior to this section (section 3.3.3) describe the evaluation of the optimum FTIR software settings for analysis of prostate pathology. This section of the thesis addresses the potential limitation of point mapping in FTIR tissue analysis – step size. The concern regarding step size for evaluating prostate pathologies is chiefly the risk of missing valuable biochemical information between the steps during tissue analysis. This concept is illustrated in figures 3.22 and 3.23.

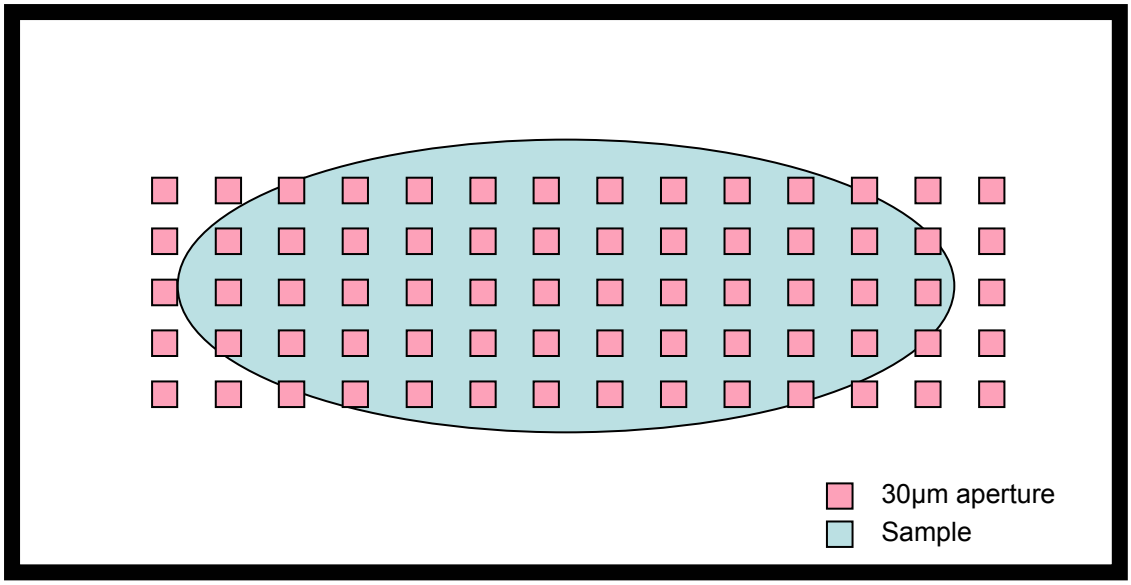

Figure 3.22 Point mapping of fictitious sample with narrow steps

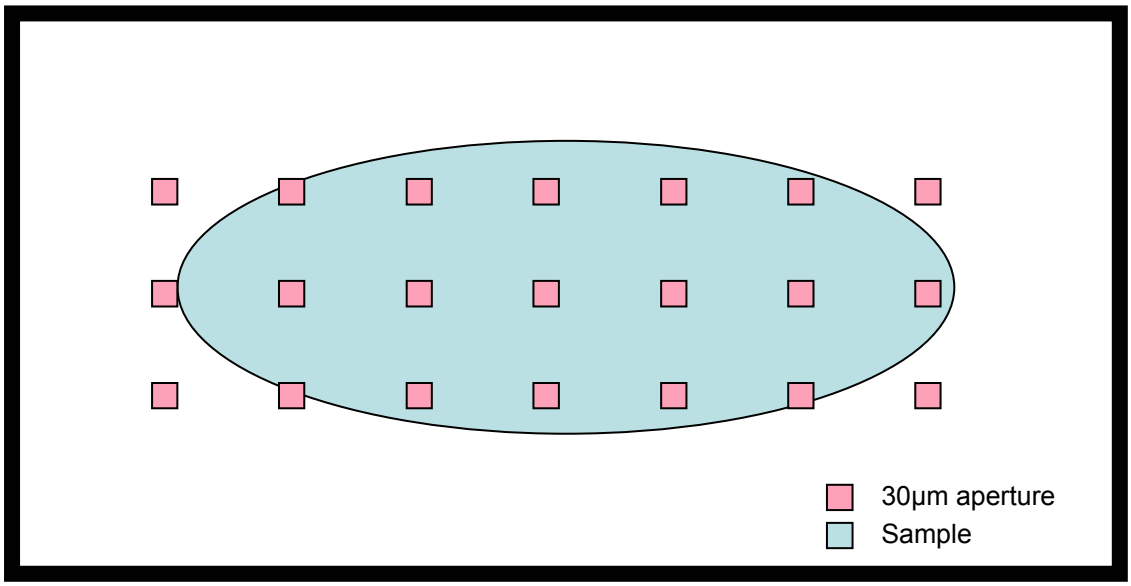

Figure 3.23 Point mapping of a fictitious sample with wide steps

The aim of this step size study was to investigate the effect of increasing step size on the quality of spectral information obtained from individual pathologies. Radical prostatectomy specimen Nine, which contained three pathologies, was evaluated in this analysis using the optimum FTIR software settings determined in the previous studies: spectral resolution 1cm^{-1}, number of co-scans 25, aperture 30µm x 30µm.

Step sizes ranging from 25µm to 500µm were examined. Benign prostatic hyperplasia was the pathology interrogated. Figure 3.24 shows the sample under analysis and figures 3.25, 3.26 and 3.27 illustrate the results.

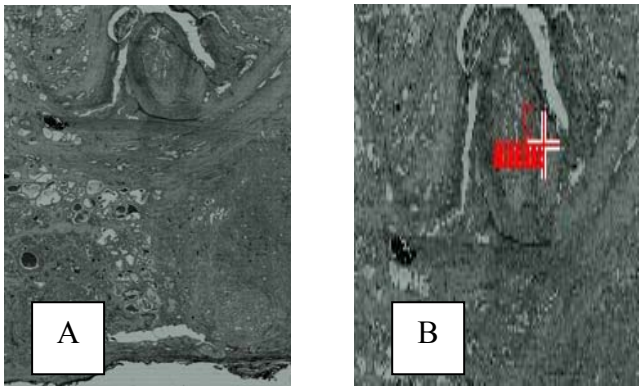

Figure 3.24 White light image of central part of prostate section nine (A) and close up image of BPH and selected area for point mapping (B)

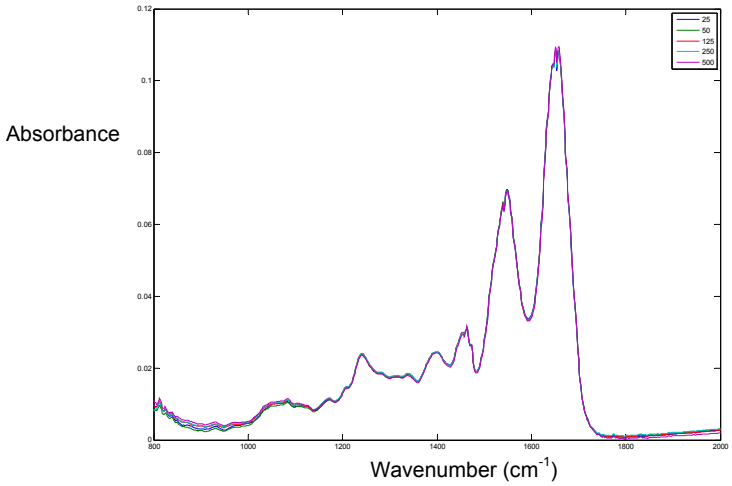

Figure 3.25 Plot of mean spectra from all point maps of BPH at different spatial resolutions

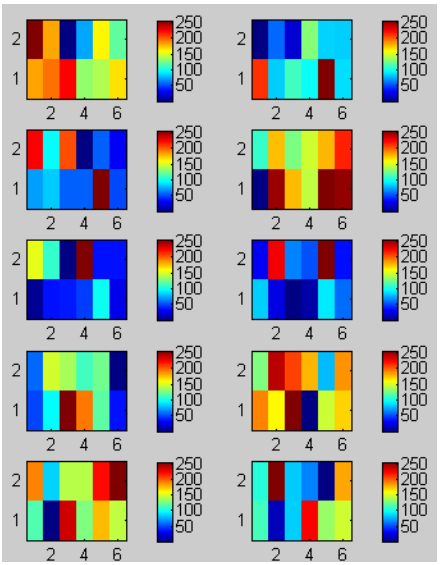

500µm

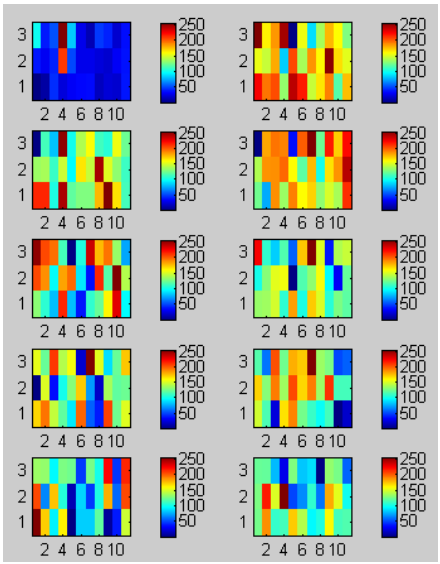

250µm

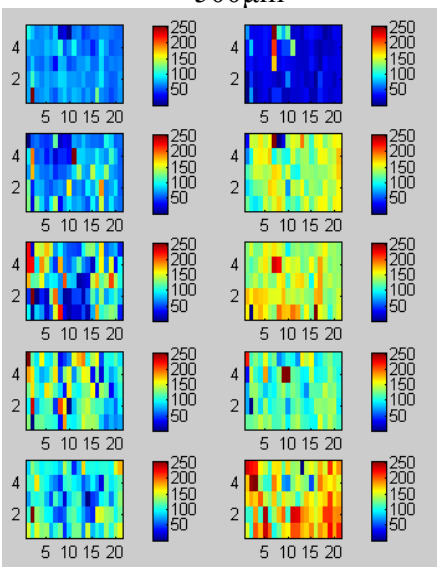

125µm

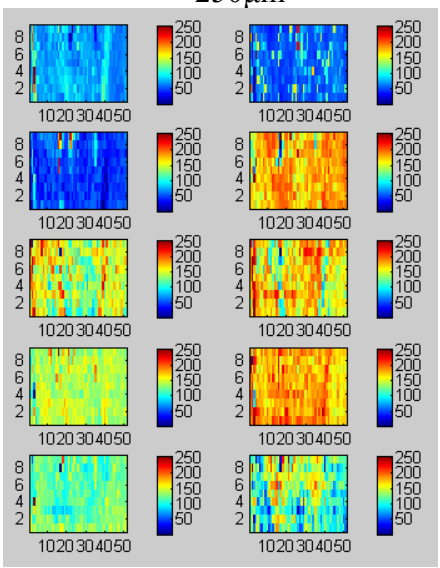

50µm

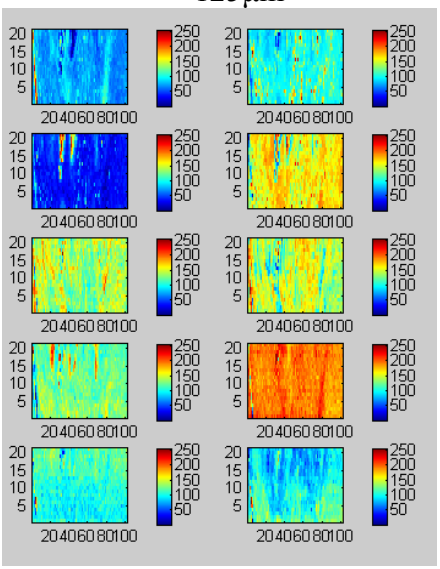

25µm

Figure 3.26 PCA score maps of BPH measured in step size study

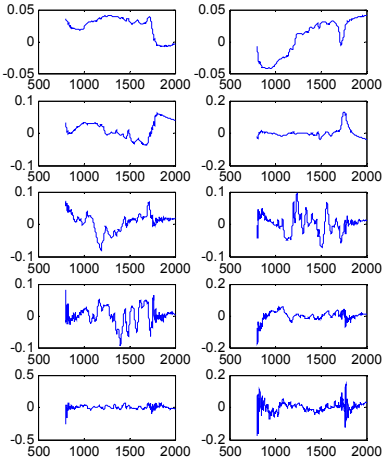

500µm

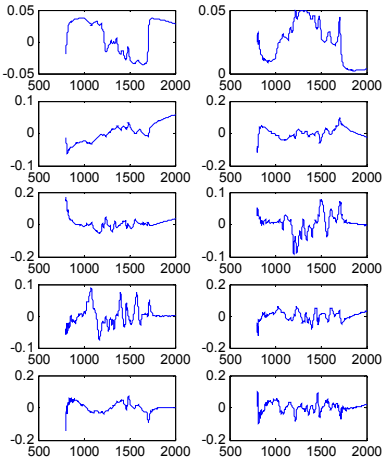

250µm

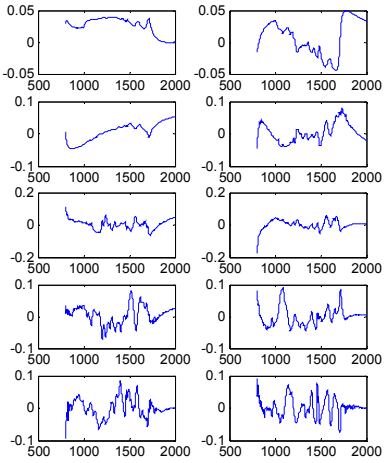

125µm

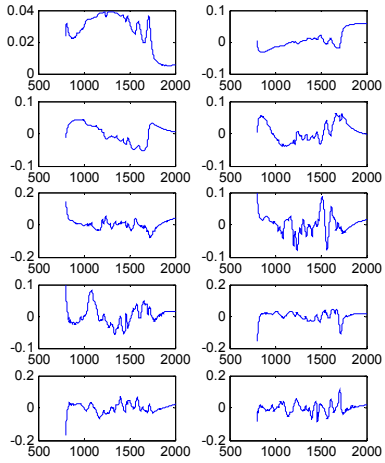

50µm

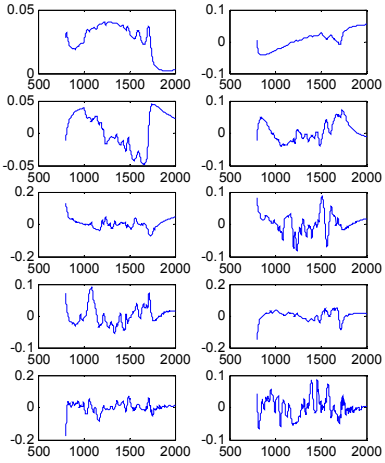

25µm

Figure 3.27 PCA loads for BPH measured in step size study

The mean spectra obtained for individual pathologies during this analysis demonstrate that increasing step size does not have a significant detrimental effect on the mean spectra required to differentiate prostate pathologies. However close examination of the principal component loads and scores clearly illustrate that important biochemical information and detail is lost with increasing step size. This detail may yield important information regarding borders of pathology. Thus for the in depth analysis of pathologies or differentiation / region selection of subtleties, a smaller step size is mandatory.

3.3.5 Commentary on point map technique validation studies

Knowledge of the optimum FTIR parameters for tissue analysis is crucial for the development of the technique as a relevant clinical tool. This is particularly important because the goal of gold standard tissue analysis is to collect the necessary amount of information to diagnose and assess severity of pathology and thus guide patient management. FTIR clearly reproducibly interrogates more information than visual morphological analysis alone. The biochemical information attained by FTIR may at the minimum complement histological analysis but the potential to both automate and yield greater objective information regarding tissue under analysis is attractive. As a research tool it may facilitate a rapid way to understand more about prostate cancer biopotential as archival prostate tissue may be analysed with high sensitivity and specificity. Practically, for clinical applications a compromise regarding resolution and time efficiency may be sought. A thorough understanding of the biochemical information obtained by FTIR from prostate tissue would also be necessary before clinicians would consider adoption of the technique. The best way of obtaining detailed biochemical information may be by using FTIR in image mapping mode, to obtain fine detail about areas of interest. This is shown in Figures 3.28 and 3.29,

which illustrate specific targeting of image mapping at pathologies within the radical prostatectomy specimens.

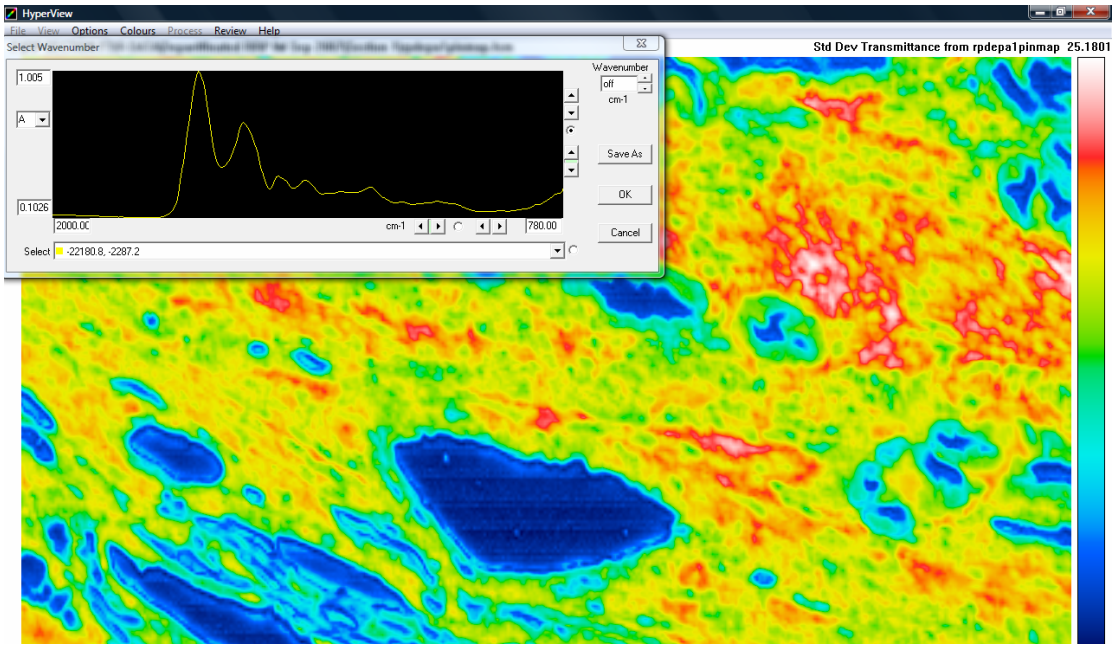

Figure 3.28 Image map of area of PIN from prostatectomy section one; with mean spectra overlaid

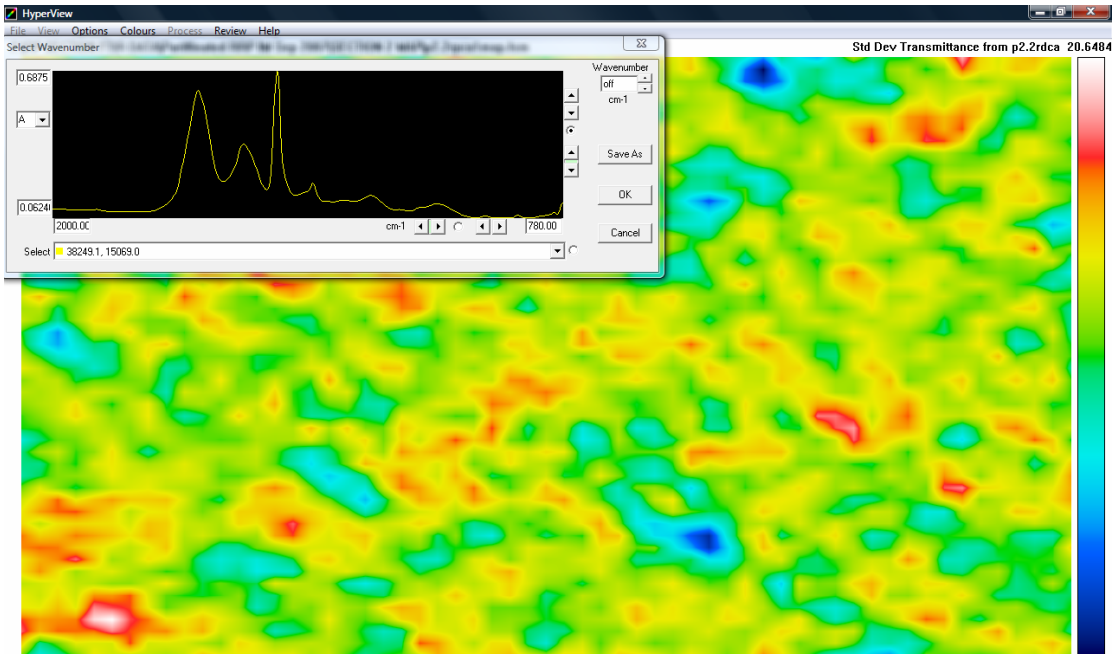

Figure 3.29 Image map of an area of prostate cancer from paraffinated prostatectomy section two; with mean spectra overlaid

3.4 Biochemical Analysis of Radical Prostatectomy Spectra

This section describes the biochemical interpretations of spectra obtained from the radical prostatectomy studies, and attempts to apply a novel method of biochemical fitting of pure biochemical standards, using non-negative least squares analysis to describe the differences between pathologies.

3.4.1 Parametric Non-Negative Least Squares Biochemical Fitting

Discrimination between prostate pathologies has predominantly been on the basis of spectral characteristics and hypothesised underlying structural differences between pathologies to date. This section describes the experience of experimenting with a novel approach to achieving biochemical characterisation of prostate pathologies. The technique, in simple terms, involves combining the spectra from referenced pure biochemical standards to form a best fit curve, which best represents the spectra of the tissue pathology under analysis. The standards were measured locally and included constituents which were thought to best represent dominant components of prostate tissue. These constituents were deduced from the known biochemical reference peak assignments and accepted knowledge about cell constituents (i.e. proteins, amino acids, carbohydrates, lipids and nucleic acids). The component constituents were then fitted in various combinations against the mean spectra of each prostate pathology. The term *residual* is used in this study to define the difference between the constructed biochemical model spectra and the tissue pathology spectra. The concentrations of constituents (c) within the sample were estimated using parametric

non-negative least squares using the equation (1), where E is the matrix of the reference spectra and A is the measured composite spectra[10]:

$$c = (E^T E)^{-1} E^T A \qquad (1)$$

The residuals visually demonstrate the quality of the biochemical model. In addition a process called *orthogonality* was performed to ensure that component spectra were not too similar. This was to avoid misjudging the component estimates. Orthogonality was calculated using the equation (2):

$$a \bullet b = |a| \, |b| \cos\theta \qquad (2)$$

A resulting dot product of 1 means no orthogonality and so perfect correlation, while a dot product of 0 represents no correlation and perfect orthogonality. In these experiments a threshold dot product of 0.95 was used to exclude components which were too similar to each other. Non-negative least squares fitting was applied to the radical prostatectomy spectral dataset described in section 3.2.1.2 from radical prostatectomy specimens one to five. In total, 1078 selected spectra were included from Benign, Malignant and PIN pathologies. The biochemical fitting was performed in Matlab® using programs written by Dr Martin Isabelle and Dr Nick Stone. Table 3.12 illustrates the FTIR prediction of prostate pathology against histopathology; the sensitivity and specificity achieved by the three group algorithm was previously described in table 3.9.

	FTIR algorithm-predicted diagnosis (number of spectra)				
		Benign	**Prostate cancer**	**PIN**	**Total**
Histological Diagnosis (number of spectra)	**Benign**	400	64	26	490
	Prostate cancer	60	396	10	466
	PIN	18	7	97	122
	Total	478	467	133	1078

Table 3.12 FTIR prostate pathology prediction against histopathology

Radical prostatectomy section one is used to illustrate the technique in practice below. Figure 3.24 illustrates the composite spectra of the pure biochemical composite spectra, and figure 3.25 the mean spectra of the pathologies.

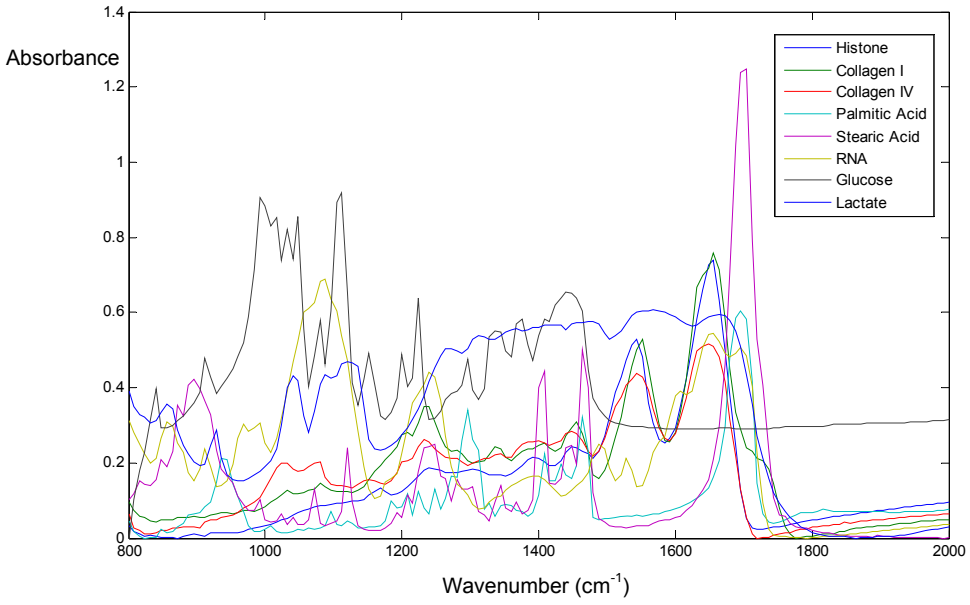

Figure 3.30 The composite spectra of dominant biochemical constituents

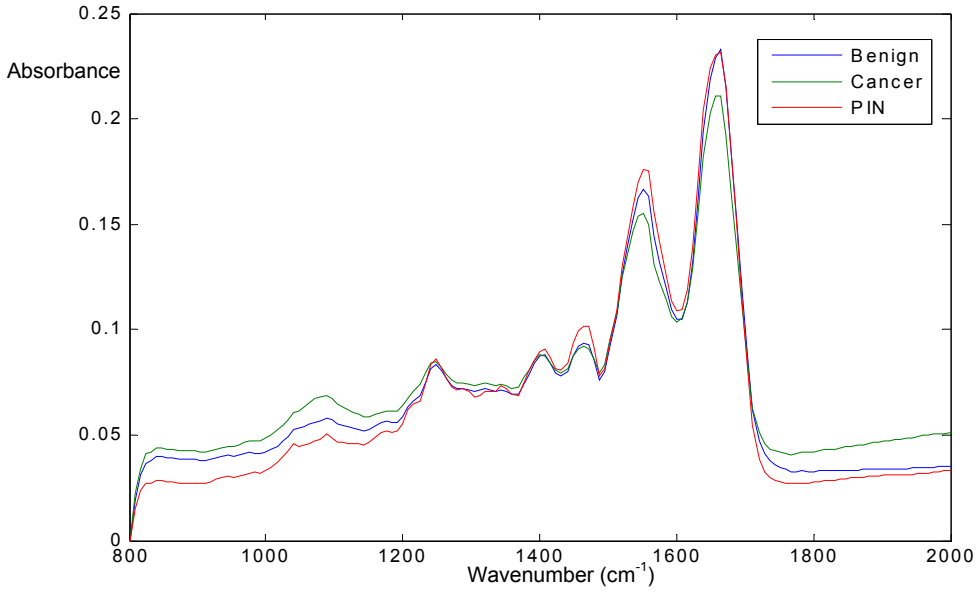

Figure 3.31 Plot of normalised mean spectra for each pathology type

Biochemical fitting was then applied to the individual pathologies' mean spectra and the results are illustrated in figures 3.32, 3.33 and 3.34.

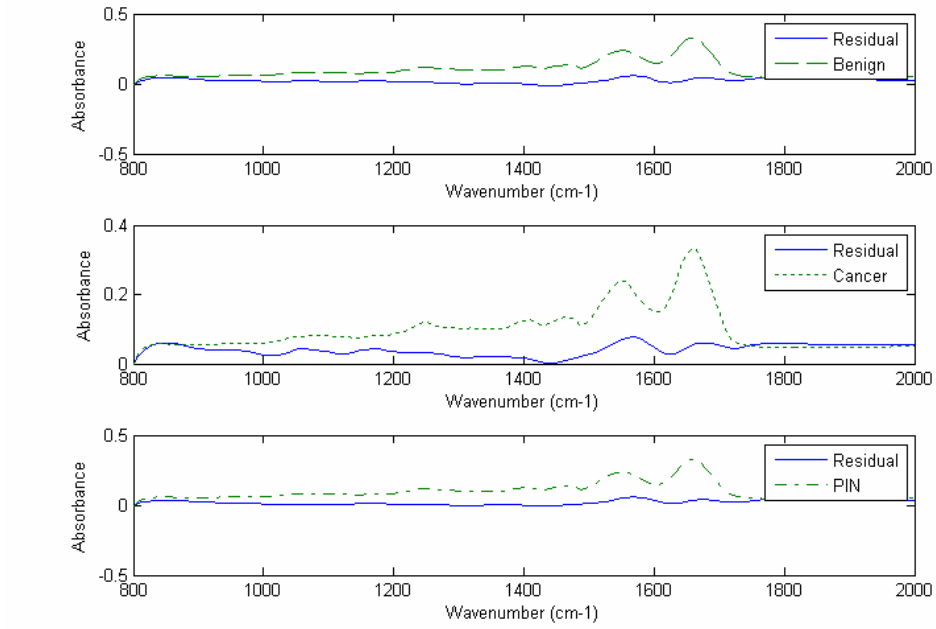

Figure 3.32 Sub-plot of residual versus mean spectra for each pathology after non-negative least squares fitting

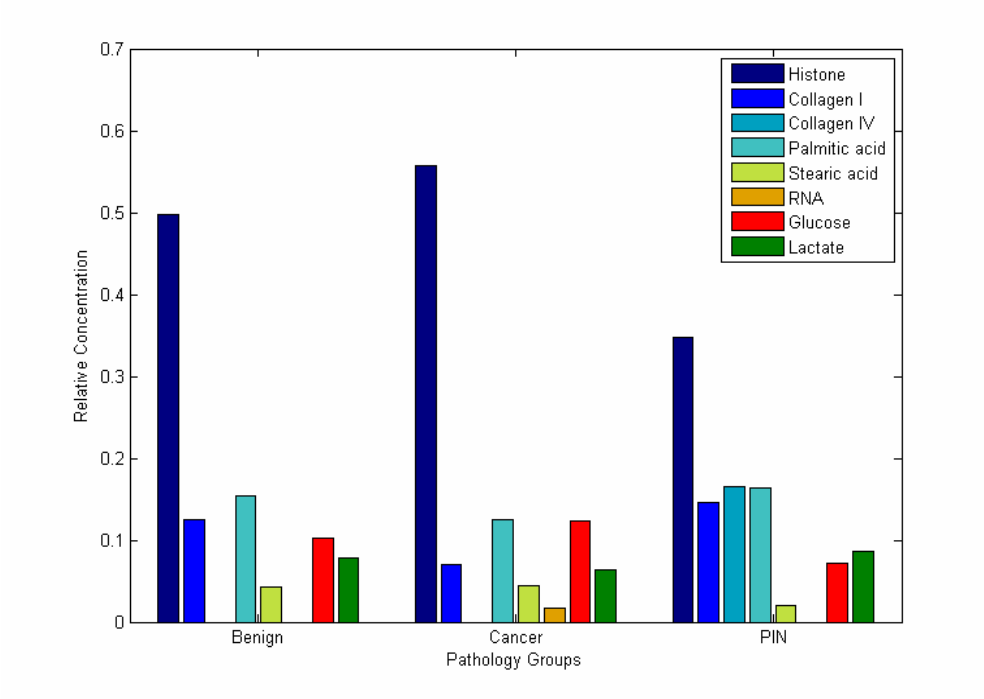

Figure 3.33 Bar chart illustrating estimated relative concentration between pathologies as determined by non-negative least squares fitting

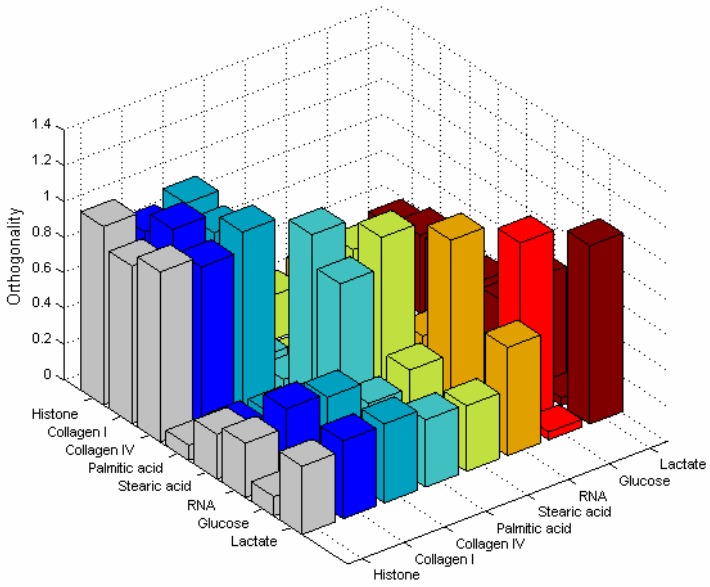

Figure 3.34 3D-Barchart illustrating orthogonality between individual reference constituents

The reference spectral dataset was obtained by measuring *proteins* (histone, collagen I and collagen IV), *lipids* (palmitic acid and stearic acid), *carbohydrates* (glucose), *carboxylic acid* (lactate) and *nucleic acid* (RNA). The orthogonality illustrated in figure 3.34 was used to ensure that the component spectra were not too similar. Monitoring the residuals enabled the best possible biochemical fit to be achieved which is illustrated in figure 3.32. An 80 % fit was achieved using the component constituent spectra.. The differences in biochemical concentrations between the pathologies are summarised in table 3.13. The relationships are described, using arrows, as the latter against the former.

Biochemical constituent concentration	**Benign vs. PIN**	**PIN vs. Cancer**	**Benign vs. Cancer**
Histone	▼	▲	▲
Collagen I	▲	▼	▼
Collagen IV	▲	▼	
Palmitic acid		▼	▼
Stearic acid	▼		
Glucose	▼	▲	▲
Lactate	▲	▼	▼
RNA		▲	▲

Table 3.13 Relative differences in biochemical concentration between pathologies

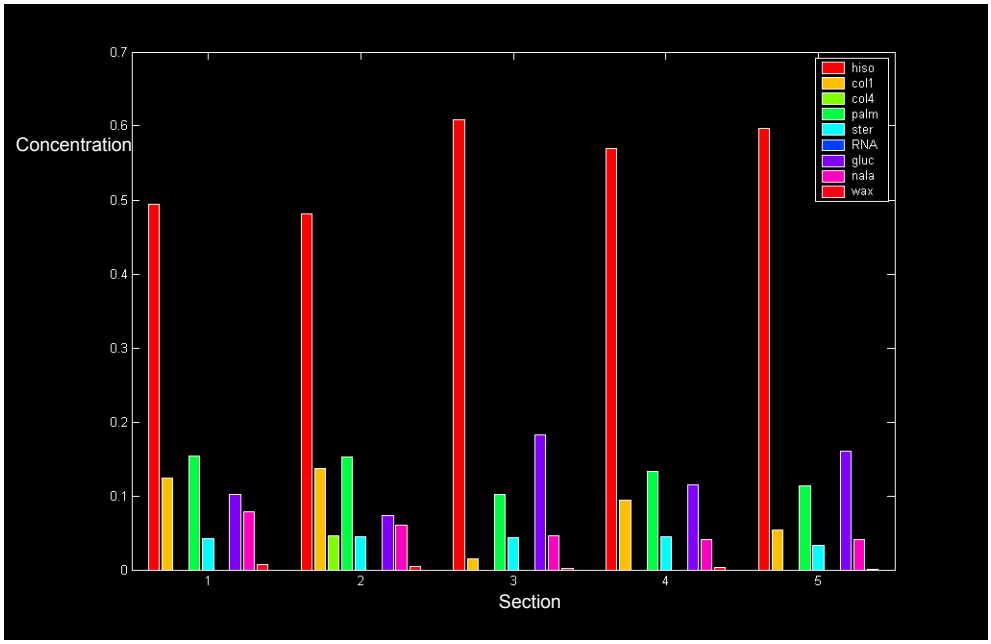

Figure 3.35 Bar chart illustrating estimated benign relative biochemical concentrations in prostatectomy sections one to five

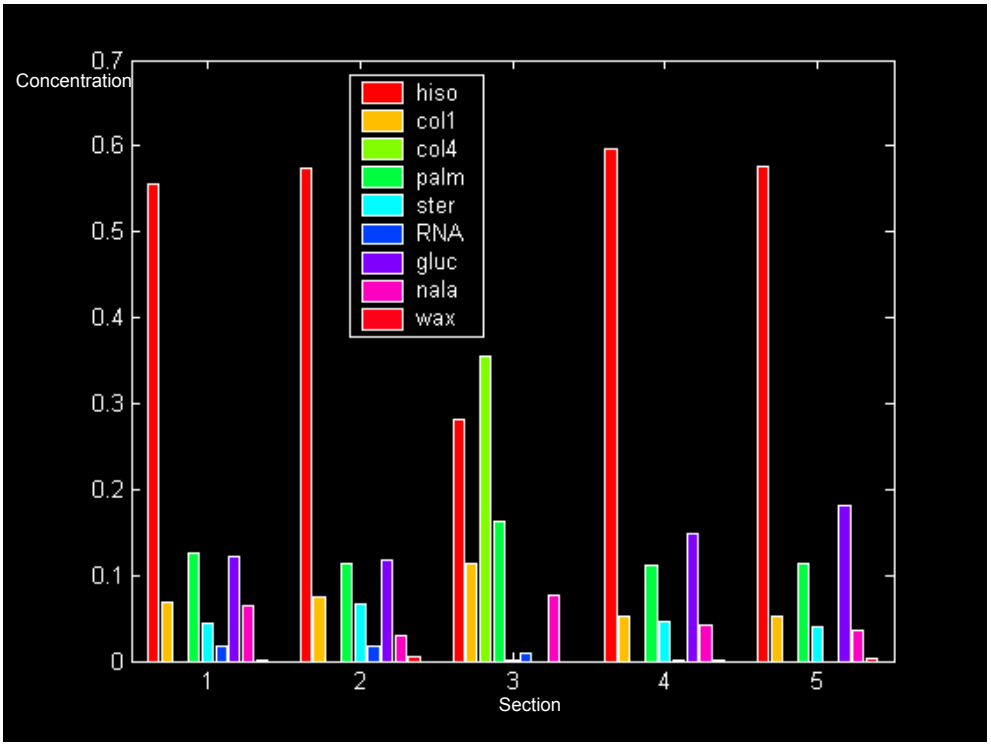

Figure 3.36 Bar chart illustrating estimated cancer relative biochemical concentrations in prostatectomy sections one to five

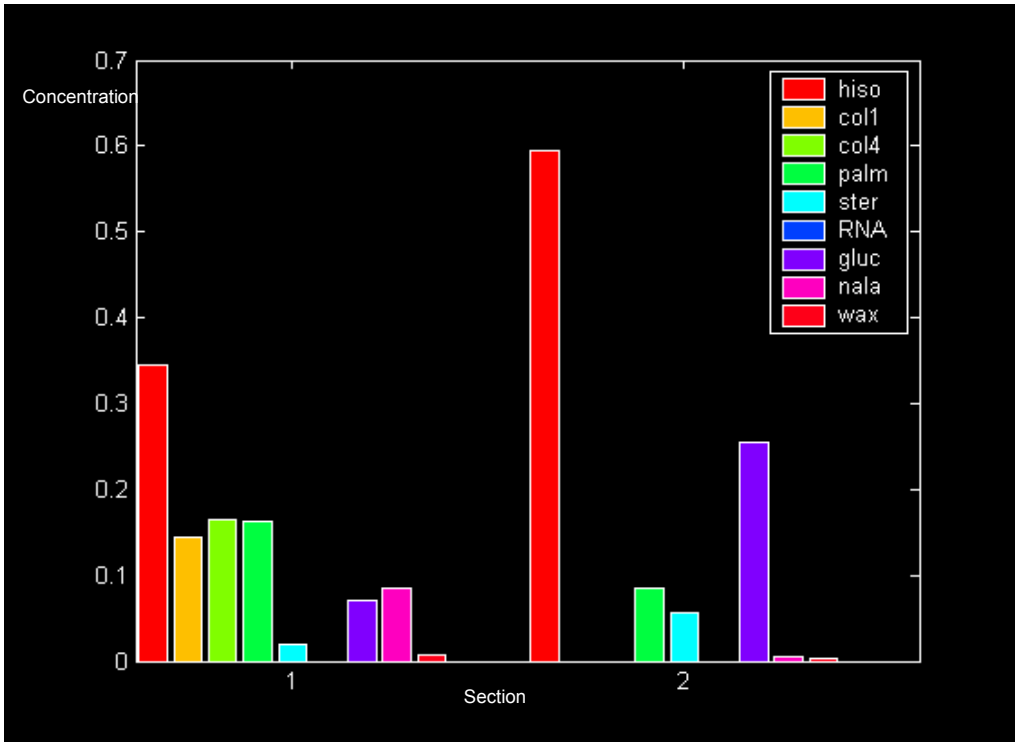

Figure 3.37 Bar chart illustrating estimated PIN relative biochemical concentrations in prostatectomy sections one and four

3.4.2 Commentary on non-negative least squares fitting study

The non-negative least squares fitting analysis of prostatectomy section one shared some similar features with biochemical relationships in the other samples however the concentration ratio results were not reproduced in all of the sections. The hypothesis that increases in nucleic acids and DNA binding protein (histone) should be seen in malignant tissue due to an increase in nuclear to cytoplasmic ratio / mitotic activity and the hypothesis of higher glycolytic rates and anaerobic metabolism in tumour cells accounting for the changes in glucose and lactate in cancerous cells has not been proven in this analysis. The black figures 3.35, 3.36 and 3.37 show the variance in relative biochemical concentrations between the prostatectomy sections for each individual pathology. Several factors may account for the lack of consistency of result: the cells of the tissue are likely to be in different stages of their cycle when analysed, and the tissue samples have different Gleason grades, which may mean that

in line with morphology the biochemistry of the tissues also changes. The major limitation of the non-negative least squares estimation method is that if one of the gross constituents in the model is unknown, the model may lead to biased estimations. In addition to this, the pure biochemical standards are not all from human sources and neither are they in the true cellular microenvironment when analysed, therefore it may be unsurprising that more conclusive findings have not been made. Future work may address this technique.

3.5 References

[1] Neviliappan NS, Kan FL, Walter TLT, Arulkumaran S, Wong PT. Infrared spectral features of exfoliated cervical cells, cervical adenocarcinoma tissue, and an adenocarcinoma cell line (SiSo). *Gynecologic Oncology* 2002, 85(1): 170-174

[2] Beleites C, Steiner G, Sowa MG, Baumgartner R, Sobottka S, Schackert G, Salzer R. Classification of human gliomas by infrared imaging spectroscopy and chemometric image processing. *Vibrational Spectroscopy* 2005, 38(1-2): 143-149

[3] Erukhimovitch V, Talyshinsky M, Souprun Y, Huleihel M. FTIR spectroscopy examination of leukemia patients plasma. *Vibrational Spectroscopy* 2006, 40(1): 40-46

[4] Jackson M, Choo LP, Watson PH, Halliday WC, Mantsch HH. Beware of connective tissue proteins: Assignment and implications of collagen absorptions in infrared spectra of human tissues. *Biochimica et Biophysica Acta* 1995, 1270(1): 1-6

[5] Diem M, Chiriboga L, Yee H. Infrared Spectroscopy of Human Cells and Tissue. VIII. Strategies for analysis of infrared tissue mapping data and applications to liver tissue. *Biopolymers* 2000, 57(5): 282-290

[6] Yang Y, Sule-Suso J, Sockalingum GD, Kegelaer G, Manfait M, El Haj AJ. Study of tumor cell invasion by Fourier transform infrared microspectroscopy. *Biopolymers* 2005, 78(6): 311-317

[7] Schultz CP, Liu KZ, Johnston JB, Mantsch HH. Study of chronic lymphocytic leukaemia cells by FT-IR spectroscopy and cluster analysis. *Leukaemia Research* 1996, 20(8): 649–655

[8] Lasch P, Chiriboga L, Yee H, Diem M. Infrared Spectroscopy of Human Cells and Tissue. IX. Detection of Disease. *Technology in Cancer Research & Treatment.* 2002, 1(1): 1-8

[9] Lasch P, Boese M, Pacifico A, Diem M. FT-IR spectroscopic investigations of single cells on the subcellular level. *Vibrational Spectroscopy*, 2002, 28(1): 147-157

[10] Sowa MG, Smith MS, Kendall C, Bock ER, Ko AC, Choo-Smith LP, Stone N. Semi-parametric estimation in the compositional modelling of multicomponent systems from Raman spectroscopic data. *Applied Spectroscopy* 2006, 60(8): 877-883

“ You see things and you say ‘why?’, I dream things that never were; and I say ‘Why not?’ ”

George Bernard Shaw 1856-1950

4 Discussion

4.1 Pilot Study Findings

4.1.1 Summary of Pilot Study Findings

Stain free FTIR imaging of snap frozen prostate tissue obtained at TURP was performed. Fourier Transform Infra Red spectra collected in imaging mode discriminated between benign and malignant prostate pathologies with high sensitivities and specificities. FTIR imaging enabled the fine detail of prostate histology to be interrogated and promising concordance was achieved between the histological diagnosis and FTIR algorithm especially in the four and six group algorithms which included ductal, glandular and stromal tissue. The differentiation between spectra from stroma associated with either benign or malignant tissue was particularly interesting because stroma is not normally utilised by the pathologist and this highlighted what FTIR could potentially add to conventional histology – total tissue analysis – this merits further investigation. Empirical analysis of the peak intensity ratios alone was not able to accurately differentiate between benign and malignant pathologies. Sophisticated multivariate analysis was used to achieve clear differentiation between pathologies and construct diagnostic algorithms. Cross validation of the two group algorithm using *leave one sample out* methodology achieved good results.

4.1.2 Pilot Study in the Context of the Literature

The studies in this thesis were conceived, planned and performed between 2005 and 2008. Prior to planning the studies, limited literature regarding the application of FTIR to prostate tissue analysis was available.

Gazi *et al* had performed a pilot study investigating the potential of FTIR to differentiate between benign and malignant prostate epithelial cells in tissue obtained at TURP and cell lines[1]. The study contained small numbers of prostate samples (five) and used approximately four highly selected spectra per pathology upon which to base the conclusion that FTIR had the potential to rapidly discriminate between prostate pathologies including Gleason grade. Table 4.1 illustrates key differences between the Gazi study and the pilot study in this thesis.

Study	Gazi *et al*	Aning
Sample number (TURP chips)	3 prostate cancer, 2 benign	4 prostate cancer, 23 benign
Primary tissue preparation	Paraffin wax embedded	Snap frozen
FTIR imaging settings	Bio-Rad FTS 6000 spectrometer. Transmission mode. Number of co-scans 513, wavenumber range 750-4000cm^{-1}, spectral resolution 16 cm^{-1}	Perkin Elmer Spotlight 300 spectrometer. Transmission mode. Number of co-scans 16, wavenumber range 720-4000cm^{-1}, spectral resolution 8 cm^{-1}
Number of spectra	<100 used for analysis	12,309 used for analysis
Peaks / peak ratios differentiating pathology	1030cm^{-1}/1080cm^{-1}	1400cm^{-1}/1450cm^{-1}

Table 4.1 The differences between the Gazi and Aning pilot studies

Gazi's pilot study was significant as its publication in the Journal of Pathology alerted clinicians and scientists to FTIR's potential application as a diagnostic clinical tool because of its ability to discriminate between prostate pathologies. The pilot study in

this thesis was designed to establish primarily whether Gazi's results were reproducible. Larger sample numbers and numbers of selected spectra were included; the sampling protocol was extended to include stromal, ductal and glandular areas within the tissue under interrogation. The results obtained in the pilot study in this thesis did not support the $1030cm^{-1}/1080cm^{-1}$ peak ratio as the key discriminating factor between benign and malignant pathologies. This may have been because the sample areas in the study were more diverse, or alternatively the peak ratio difference may be accounted for by differences in cell cycle position at the time of analysis. The peak ratio $1400cm^{-1}$ / $1450cm^{-1}$ differed between pathologies, with the ratio closer to 1.0 in malignant tissue as opposed to approximately 0.6 in benign tissue. This region corresponds to proteins and lipids (cholesterol) and may represent higher protein concentrations in cancerous cells with enlarged prominent nuclei. It has also been suggested that the amount of cholesterol in malignant tissues is lower[2,3].

Another explanation for the difference in spectra morphology between studies may be the fact that *fresh snap frozen* tissue rather than formalin fixed, archival de-paraffinated tissue was evaluated. The effect of archiving or formalin cross-linkage with proteins in prostate tissue on FTIR spectra has not been previously reported, although its effect in prostate sub-cellular studies is acknowledged[4]. Despite the differences in spectral morphology, using multivariate analysis both studies demonstrated that FTIR has the potential to discriminate between benign and malignant prostate pathology. No attempt was made in the study to sub-classify spectra by Gleason grade, as the relative number of cancer samples within the cohort was small. This was a limitation of prospective prostate sample collection at TURP at which the yield of malignant tissue is expected to be low. Difficulties were

experienced in the sectioning of small fresh frozen prostate samples, which could be compared with corresponding H&E section under histological analysis. The only conclusion of the Gazi study which was not supported was with regard to speed of analysis; imaging of relatively small areas took a considerable amount of time even with a comparatively low co-scan number.

Fernandez *et al* published work in April 2005 regarding FTIR imaging of microarrays, coupled with statistical pattern recognition techniques to differentiate benign from malignant prostate epithelium[5]. They proposed that by using this methodology, high throughput and fast classification, learning algorithms facilitated the measurement of all cell types including the least prevalent (for example nerves and lymphocytes). Each microarray contained 86 samples with up to eight samples each from 16 patients. In total the authors recorded over 9.5 million spectra from over 870 samples and reported a subset of approximately 3 million spectra from 262 samples. The paper quoted near perfect prostate pathology recognition accuracy. Whilst groundbreaking work, the results were almost too good; achieving over 95% classification accuracy in all but neural tissue. Fernandez *et al* acknowledged FTIR spectrometers may achieve high throughput and spatially resolved measurements but questioned how success in small studies would translate into practical clinical applications. if one was reliant on detecting significant biochemical changes in the form of spectral changes within small patient sets or by the examination of molecular moieties. Absence of suitable control samples has been cited as a limitation within previous FTIR studies.

The limitations of the pilot study were evident, as discussed in the commentary in the results section 3.1.6. However the promising pilot study findings merited further investigation of FTIR in tissue studies. The complex FTIR analysis proposed by Fernandez was not achievable within our laboratory and seemed to involve additional processing steps which FTIR as a technique intuitively was meant to avoid. Undoubtedly, the high throughput analysis of tissue microarrays, once validated, may represent the future in terms of evaluating large sample numbers in large phase trials however a thorough understanding of how FTIR may discriminate between pathologies is still necessary to judge its clinical niche and thus requires small scale tissue studies to continue. Prostate tissue is characteristically heterogeneous, therefore the FTIR prostate section studies were planned in the knowledge each section could act as its own intrinsic control.

4.2 FTIR Analysis of Prostatectomy Specimens

4.2.1 Summary of the Results from FTIR Analysis of Radical Prostatectomy Sections

FTIR analysis of nine radical prostatectomy sections in their entirety was performed. In knowledge of the constraints of image mapping in the pilot study, the concept of point mapping was explored. Formalin fixed prostate sections were interrogated in their paraffinated and deparaffinated forms. Interpretable spectra were obtained from both paraffinated tissue and deparaffinated tissue. The main pathologies present within the sections; benign tissue, prostate cancer and PIN were differentiated by both their spectra and multivariate analysis in paraffinated and deparaffinated corresponding sections. When the means of the total spectral data for all pathologies were examined, differentiation between pathologies was possible using the $1030cm^{-1}/1080cm^{-1}$ peak ratio proposed in Gazi's pilot study[1] however multivariate analysis was required to separate the pathologies more definitively. Superficially the three group model differentiated pathologies with reasonably good sensitivity and specificity. However when a diagnostic algorithm was constructed using the spectra from sections one to five and tested by leave one sample out validation, poor algorithm prediction was achieved. The model was then tested using a set of test spectra which had not been used to construct the model, and an even poorer performance of the diagnostic algorithm was achieved. Further investigation of the models poor performance was performed by re-analysing the individual section data. Sections which contained pathologist verified identical Gleason grade multifocal prostate tumours (without perineural invasion) were examined. It was evident from the spectra and multivariate analysis that although the pathologies may be of the same Gleason grade, their biochemical composition was different.

Technical validation studies of the FTIR microspectrometer were then performed using the pathology within the radical prostatectomy sections. The analysis of the spectrometer was reproducible over a three day period without the need to purge the atmosphere in the spectrometer with an inert gas. Optimum co-scan number and step size were also assessed. Reproducibility of FTIR analysis was confirmed the optimum settings will be utilised in future studies.

Non-negative least squares fitting was applied to the spectral dataset to attempt to classify changes in biochemical concentrations between pathologies, the findings were interesting but not robust more work is required to develop this technique.

4.2.2 Radical Prostatectomy Study Findings in the Context of the Literature

As far as the author is aware to date, the studies detailed in this thesis are the first to describe the FTIR analysis of radical prostatectomy specimens in their entirety, to follow through the concept of and the application of point mapping in prostate specimen analysis and to utilise FTIR to evaluate intra and inter patient pathologies and thus allowing for an adequate control for every FTIR measurement.

Radical prostatectomy specimens proved excellent specimens for FTIR prostate tissue analysis. The advantages observed in this study were:

- Each specimen acted as its own control
- Each specimen contained multiple pathologies for analysis
- The pathologists found it easier to clearly identify significant pathologies at which to target FTIR analysis

- The pathologists commented that radical prostatectomy specimens facilitated accurate Gleason grade allocation especially compared to the other tissues examined within this study.

The use of radical prostatectomy specimens provided a robust test of FTIR's true ability to discriminate between prostate pathologies. Multivariate analysis demonstrated good separation of benign tissue, malignant tissue and PIN, however the performance of the diagnostic algorithm was poor especially when a test spectra set was projected on the model. The poor performance is likely to be due to multiple factors: the small sample number (n=9), contaminants, the point map technique missing vital biochemical signatures between steps and potential misclassification of spectra in the model. However from the findings in this study – confirmed by follow up FTIR image mapping of specific areas, a hypothesis that the poor classification achieved by the model is due to the true heterogeneity in the biochemistry of tissue pathologies under analysis would not be unfounded. This is illustrated by the observation of biochemical differences between seemingly identical Gleason pattern tumours in this study. Although the patient numbers within this study are small, this finding supports the clinical concern that Gleason grade has significant limitations and tumours of the same Gleason grade may behave differently. Further work is required to study this finding in depth.

It is clear from the studies in this thesis that the challenges of achieving a universal FTIR classification model are significant. Studies focusing on forming diagnostic algorithms based on the flawed Gleason classification, including highly selected spectra from small prostate samples, may not have widespread clinical application if

to tissue outside of the prostate transitional zone[6,7,8]. The transitional zone has been demonstrated to express a different FTIR biochemical signature to other prostate zones[9], and the tumours which arise there may be clinically different to those that arise in the peripheral zone. In addition to this the majority of clinically significant prostate cancers are not diagnosed at TURP. Therefore in light of the findings of this thesis, broadening the horizons of specimen analysis to include radical prostatectomy specimens for all researchers in this field may in fact further enhance the credibility of FTIR analysis and its potential for automation.

FTIR imaging of tissue enables fine detail analysis of prostate tissue. However it is time consuming and produces a huge amount of data which must be processed prior to analysis. Practically, to achieve automation with current technology, a balance may have to be struck between the resolution of the technique i.e. sufficient to enable identification of pathology and analysis time. Point mapping allows larger sample areas to be examined in a reasonable period of time. The concern regarding point mapping is missing significant pathology, however it is envisaged by the author that image mapping of specific areas would complement abnormal areas identified using point mapping. The validation experiments enable the optimum characteristics to be used in future FTIR analysis. The limitation of point map techniques are acknowledged though[10].

4.3 Comparison of Study Results with Other Spectroscopic Techniques

Raman spectroscopy has achieved 89% accuracy, using leave one sample out validation, in the classification of BPH, Gleason <7, Gleason 7 and Gleason>7 when targeted at specific areas of pathology[11]. The diagnostic model in this study was constructed from 27 tissue samples and 450 spectra were recorded in total. The issue of control spectra has not been addressed in Raman studies of the prostate. The limitations of utilising Gleason grade, an imperfect standard, for the differentiation of prostate pathology has not been addressed. The potential for automation of the technique in the form of large section point map analysis has not to the authors knowledge been explored. Currently however it is not possible to measure good quality Raman spectra from paraffin embedded tissue[12]. This technology may compete in the future with FTIR as a pathological tool. OCT has yet to be applied to histological analysis of prostate tissue.

4.4 Conclusions

Prostate cancer diagnostic strategies must evolve. The stimulus for this is not only novel technologies but also a drive from department of health policy makers to achieve early diagnosis and tailored patient management strategies in all cancers[13].

FTIR microspectroscopy has demonstrated in the studies in this thesis that it is a powerful bioanalytical technique which when combined with multivariate analysis has the ability to discriminate between prostate pathologies in snap frozen, paraffinated and deparaffinated tissue. The validation studies in this thesis have established that FTIR analysis is robust and versatile. Radical prostatectomy sections have been identified as a potential gold standard specimen for FTIR prostate tissue analysis.

4.5 Summary of Contribution to Knowledge

- The studies in this thesis have demonstrated that FTIR is able to accurately identify benign, premalignant and malignant pathology in unstained snap frozen, parrifinated and deparrifinated prostate tissue.

- The studies in this thesis have validated the results of previous pilot FTIR prostate tissue studies[1] and in addition demonstrated that multivariate analysis refines the discrimination achieved between pathologies.

- The studies in this thesis were the first to evaluate radical prostatectomy sections in their entirety and highlight the importance of having an appropriate control in order to truly validate FTIR studies.

- The studies in this thesis were the first to analyse PIN and identify differences in the stroma surrounding benign and malignant glandular tissue.

- The studies in this thesis were the first to introduce and investigate the concept of utilising non-negative least squares biochemical fitting to explain hypothesised FTIR structural differences between prostate pathologies.

4.6 Future Prospects

The studies within this thesis and those performed by other groups have illustrated the potential for FTIR to be used as a pathology laboratory tool. Further work is required to increase the sample size used to construct the algorithms and the pathologies within them. This may require collaboration between different teams to achieve the large population required. Ultimately for FTIR to become established as a technique, the original work of Gleason must be replicated using FTIR instead of a pathologist and archival radical prostatectomy specimens instead of autopsy prostates.

The prostate core biopsy specimens detailed in the methodology section were collected and analysed at the end of the research period in late 2007. Due to time constraints and the necessity to share the Biophotonic Research Group facilities these specimens have been FTIR image mapped but not fully analysed. The intention was primarily to use these biopsy specimens as a test spectra group to *blind test* the TURP algorithm. The prostate cores were also to be used to investigate whether: the spectra obtained from non-malignant specimens in patients whose other prostate biopsies were also benign, were different to, the spectra obtained in non malignant specimens from patients whose other prostate biopsies were positive for prostate cancer. The next investigator will pursue this work in addition to attempting to create a FTIR spectral and hence biochemical representation of a whole prostate and including all the pathology contained within the specimen.

4.7 References

[1] Gazi E, Dwyer J, Gardner P, Ghanbari-Siahkali A, Wade AP, Miyan J, Lockyer NP, Vickerman JC, Clarke NW, Shanks JH, Scott LJ, Hart CA, Brown M. Applications of Fourier transform infrared microspectroscopy in studies of benign prostate and prostate cancer. A pilot study. *The Journal of Pathology* 2003, 201(1): 99-108

[2] Chao FC, Efron B, Wolf P. The possible prognostic usefulness of assessing serum proteins and cholesterol in malignancy. *Cancer* 1975, 35: 1223-1229

[3] Vittols S, Peterson C, Larsson O, Holm P, Aberg B. Elevated uptake of low density lipoproteins by human lung cancer tissue in vivo. *Cancer Research* 1992, 52: 6244-6247

[4] Gazi E, Dwyer J, Lockyer NP, Miyan J, Gardner P, Hart C, Brown M, Clarke NW. Fixation protocols for subcellular imaging by synchrotron-based Fourier transform infrared spectroscopy. *Biopolymers* 2005, 77(1): 18-30

[5] Fernandez DC, Bhargava R, Hewitt SM, Levin IW. Infrared spectroscopic imaging for histopathologic recognition. *Nature Biotechnology* 2005, 23(4): 469-474

[6] Gazi E, Baker M, Dwyer J, Lockyer NP, Gardner P, Shanks JH, Reeve RS, Hart CA, Clarke NW, Brown MD. A correlation of FTIR spectra derived from prostate cancer biopsies with Gleason grade and tumour stage. *European Urology* 2006, 50(4): 750-760

[7] Baker MJ, Gazi E, Brown MD, Shanks JH, Gardner P, Clarke NW. FTIR-based spectroscopic analysis in the identification of clinically aggressive prostate cancer. *British Journal of Cancer* 2008, 99: 1859-1866

[8] Baker MJ, Gazi E, Brown MD, Shanks JH, Clarke NW, Gardner P. Investigating FTIR based histopathology for the diagnosis of prostate cancer *Journal of Biophotonics* 2009, 2(1-2): 104-113

[9] German MJ, Hammiche A, Ragavan N, Tobin MJ, Cooper LJ, Matanhelia SS, Hindley AC, Nicholson CM, Fullwood NJ, Pollock HM, Martin FL. Infrared spectroscopy with multivariate analysis potentially facilitates the segregation of different types of prostate cell. *Biophysical Journal* 2006, 90(10): 3783-3795

[10] Kwiatkoski JM, Reffner JA. FT-IR microspectrometry advances. *Nature* 1987, 328: 837-838

[11] Crow P, Stone N, Kendall CA, Uff JS, Farmer JAM, Barr H, Wright MPJ. The use of Raman spectroscopy to identify and grade prostatic adenocarcinoma in vitro. *British Journal of Cancer* 2003, 89: 106-108

[12] Stone N. Raman spectroscopy of biological tissue for application in optical diagnosis of malignancy: PhD thesis: Cranfield; 2001

[13] Richards MA. The size of the prize for earlier diagnosis of cancer in England. *British Journal of Cancer* 2009, 101: S125-S129